Analysis of Hydraulic Properties of Forest Soil with Lognormal Distribution Models

Ken'ichirou Kosugi

1996

ACKNOWLEDGEMENTS

I would like to express my gratitude to Professor Sumiji Kobashi and Professor Takahisa Mizuyama for their guidance and valuable advice. Without their generous support, I could not carry out this work. Thanks are due to the member of the Dissertation Committee, Professor Goro Iwatsubo.

I am indebted to Professor Yoshihiro Fukushima for his helpful suggestions in deriving models for soil hydraulic properties. I also gratefully acknowledge helpful discussions with Professor Masakazu Suzuki and Dr. Nobuhito Ohte concerning many points in the thesis. Professor Suzuki gave me constructive criticisms of certain sections of this thesis. I did earlier laboratory experiments under Dr. Ohte's guidance.

I would like to thank Professor Takehiko Ohta and Dr. Jumpei Kubota for sharing their soils data and hydrological knowledge. Dr. Makoto Tani was always generous in sharing his hydrological knowledge. My colleague, Mr. Akihiro Nakamura, helped me in the field observations. I wish to express my gratitude to a member of my colleagues in the Laboratory of Erosion Control of Kyoto University, especially to Miss Michiko Fukuda for her helpful support, and to Mr. Hendrayanto, Mr. Yasunori Nakayama, and Mr. Hideki Yasuda, for their assistance in the observations of soil hydraulic properties.

Substantial support for this thesis was also provided by my parents. I wish to express my deep appreciation to them. My special thanks are due to my wife, Dr. Yoshiko Kosugi, who has always encouraged and assisted me in my studies.

CONTENTS

CHAPTER 1

INTRODUCTION

Modeling the water circulation process in a forestal watershed is important for the appropriate management of water resources, for the prediction of slope failure caused by heavy rainfall, and for the analysis of the energy exchange process between forest and atmosphere. Forestal hillslope is usually covered with forest soils, in which various types of water movement occur under the unsaturated condition. Water supplied by rainfall moves downward in the unsaturated soil profile to the ground water table. After rainfall ceases, some water moves upward to evaporate at the soil surface. Some water is extracted from the unsaturated soil by the root system of plants to be used for transpiration. Consequently, unsaturated soil water flow plays a significant role in the water circulation process in forestal watersheds.

Modeling unsaturated water flow in soil requires knowledge of the hydraulic properties of the soil. The hydraulic properties of unsaturated soil are represented by the relationship between the volumetric water content θ and the soil capillary pressure ψ and the relationship between the unsaturated hydraulic conductivity K and ψ. The θ-ψ relationship represents the soil moisture characteristic and is referred to as the soil water retention curve. It is based on the soil pore radius (size) distribution. The K-ψ relationship is closely related to the soil pore structure as well as to the pore radius distribution [*Kutílek and Nielsen*, 1994].

Recent studies have revealed that forest soil has peculiar pore radius distribution and hydraulic properties. *Ohta et al.* [1985] showed that the moisture characteristics of forest soils are different from those of undeveloped field soils. The θ-ψ curves of forest soils determined by *Ohte and Suzuki* [1990] indicated that many macropores exist in forest soils. *Kosugi and Ohte* [1992] computed pore radius distributions from observed θ-ψ curves and showed that forest soils have many macropores whose radii are greater than 0.1 mm. It has been reported that the existence of macropores increases the permeability of forest soil and reduces the surface flow on forestal hillslope [*Kirkby*, 1978; *Tsukamoto*, 1992].

In recent years, many observations of the moisture characteristics of forest soils have been made for the purpose of evaluating the soil pore radius distribution. In order to estimate the effective pore volume for water holding, *Kumlung and Takeda* [1991] and *Ohnuki et al.* [1994] measured water retention curves of forest soils. Some works on the

relationship between the amount of forest soil pores and the water discharge from forestal watersheds have been published [e.g., *Takeshita*, 1985; *Arimitsu et al.*, 1995; *Kato and Hotta*, 1995]. Since soil moisture characteristics significantly affect the plant growth, many forest soil scientists have observed water retention curves of forest soils and evaluated the soil pore radius distribution. *Mashimo* [1960] analyzed the observed θ-ψ curves of soil samples collected from 10 different forests, and suggested a soil pore classification system in which coarse and fine pores are divided by the pore capillary pressure value of -500 cm. This definition has been widely used to observe pore radius distribution of forest soils [e.g., *Arimitsu*, 1970; *Kobayashi*, 1982; *Ogasiwa et al.*, 1991].

However, the knowledge accumulated by these measurements of soil pore radius distribution has not been effectively used in physical analyses of water flow in forest soils. One reason is that the observed moisture characteristics of forest soils have not been analyzed using functional models for soil water retention.

Many mathematical expressions have been proposed by soil scientists and hydrologists to describe the θ-ψ and K-ψ relationships. *King* [1965] suggested a water retention model in order to solve the equation of unsaturated soil water flow numerically. *Klute and Heermann* [1974] modified the King model for expressing the hysteretic phenomena found in the θ-ψ relationship. *Tani* [1982] proposed a retention model with a relatively simple functional form, which has been widely used for modeling water movement in soils. *Leibenzon* [1947] derived a model for soil hydraulic conductivity, in which the unsaturated hydraulic conductivity is expressed as a power function with respect to the soil water content. *Gardner*'s [1958] exponential model for the hydraulic conductivity has been frequently used in analytical solutions of soil water flow.

Several models for water retention [e.g., *Brooks and Corey*, 1964; *van Genuchten*, 1980; *Russo*, 1988] have been developed to be compatible with models by *Burdine* [1953] and *Mualem* [1976] for the purpose of deriving analytical expressions that can be used to predict the hydraulic conductivity of soil. The sets of the water retention model and the derived model for hydraulic conductivity are referred to as the combined water-retention-hydraulic-conductivity models, and have been widely used for modeling purposes [e.g., *Russo et al.*, 1994; *Letha and Elango*, 1994]. These models are also useful for the inverse method to determine the soil hydraulic properties from transient data associated with unsaturated soil water flow [e.g., *Russo et al.*, 1991; *Toorman et al.*, 1992].

In recent years, these combined water-retention-hydraulic-conductivity models have been widely used for theoretical studies on soil hydraulic properties. Some models have been used for expressing the hysteretic phenomena found in the θ-ψ and K-ψ relationships [e.g., *Luckner et al.*, 1989; *Stauffer et al.*, 1992]. Works on statistical analysis of spatial variability in parameters of these models have been published by *Wierenga et al.* [1991] and *Russo and Bouton* [1992], and scaling methods of soil water

retention and hydraulic conductivity, based on these combined models, have been proposed by *Hopmans* [1987], *Ahuja and Williams* [1991] and *Clausnitzer et al.* [1992]. Parameters of these models have been related to the soil texture and other soil properties such as bulk density and percentage of organic matter by *Clapp and Hornberger* [1978], *McCuen et al.* [1981], *Carsel and Parrish* [1988] and *Wösten and van Genuchten* [1988].

Forest hydrologists have done physical analyses of soil water flow on forestal hillslope by using the models for water retention and hydraulic conductivity. *Kubota et al.* [1987] analyzed the θ-ψ relationship of forest soil by using the soil water retention model proposed by *Klute and Heermann* [1974]. They combined the Klute and Heermann model with the hydraulic conductivity model proposed by *Leibenzon* [1947] for analyzing the downslope flow on forestal hillslope. The set of the Klute and Heermann model and the Leibenzon model was adopted by *Ohta et al.* [1983] for modeling vertical unsaturated flow in a forest soil profile. *Ohte* [1992] determined the θ-ψ curves of undisturbed forest soils taken with large-size samplers, and analyzed vertical soil water flow using the combined water-retention-hydraulic-conductivity model developed by *Brooks and Corey* [1964]. Moreover, *Tani*'s [1982] retention model was combined with the Leibenzon model and used for analyzing the properties of one-dimensional unsaturated flow in a soil column [*Tani*, 1985]. The set of the Tani model and the Leibenzon model has been widely used to analyze water flow on forestal hillslope [*Suzuki*, 1984; *Tsuboyama and Sammori*, 1989]. *Sammori and Tsuboyama* [1990] and *Sammori* [1994] adopted the combined water-retention-hydraulic-conductivity model developed by *van Genuchten* [1980] to analyze slope stability taking the phenomena of infiltration into consideration.

Despite their usefulness, these combined models use empirical curve-fitting equations for the soil water retention curve. They are not derived based on soil pore radius distribution, nor do they emphasize the physical significance of their empirical parameters. Hence, these combined models cannot be effectively used to analyze moisture characteristics of forest soils in connection with the soil pore radius distribution. They are not necessarily suitable models for evaluating the effect of the soil pore radius distribution on the water movement in the soil.

On the other hand, several attempts have been made to derive models for the pore radius distribution for the purpose of analyzing the soil hydraulic properties on the basis of soil pore structure. *Brutsaert* [1966] applied several distribution laws such as the incomplete gamma distribution, the lognormal distribution, and his own original distribution form, to the model for the pore radius distribution, and derived expressions for the soil water retention. By combining some of these water retention models with the model for predicting the hydraulic conductivity suggested by *Childs and Collis-George* [1950], *Brutsaert* [1968] obtained some models for the saturated and unsaturated hydraulic conductivities. However, rather complicated forms of the derived conductivity

models limited their usefulness for modeling purposes. Although *Laliberte* [1969] suggested his own distribution form for the soil pore radius distribution and derived a water retention model, the corresponding model for hydraulic conductivity was not developed. *Tyler and Wheatcraft* [1990] derived a water retention model by assuming that soil pore structure is based on the concept of fractal geometry. However, the model is applicable only to specific media and does not have sufficient flexibility.

The objectives of this study are (a) to propose for soil water retention a general model which performs as well as any existing empirical model and which was developed by applying a distribution law available in general probability theory, (b) to derive a model for hydraulic conductivity from the proposed retention model, (c) to characterize the pore radius distribution and hydraulic properties of forest soils by application of the proposed models, and (d) to evaluate the effects of the pore radius distribution of forest soil on the water movement phenomena on forestal hillslope. Figure 1.1 shows the structure of this study.

The objective of **Chapter 2** is to review some of the widely used water retention models and to compare the parameters of the models. The functions for expressing hydraulic conductivity, which are derived by combining the widely used retention models with *Mualem*'s [1976] model for predicting hydraulic conductivity, are also summarized.

In **Chapter 3**, a water retention model (the LN model) is developed by applying a three-parameter lognormal distribution law to the soil pore radius distribution. The accuracy and the parameters of the widely used retention models are analyzed in comparison with those of the LN model.

The purpose of **Chapter 4** is to analyze the moisture characteristics of different forest soils using the LN model. The typical θ-ψ curve of forest soil is compared to the typical θ-ψ curves of loamy soil, sandy soil, and undeveloped field soil by analyzing the parameters of the LN model.

The LN model is modified in **Chapter 5** to have a relatively simple functional form and to have parameters which are related directly to the statistics of the soil pore radius distribution. Using the parameters of the resulting model (the LN2 model), the effects of forest soil structure on the soil pore radius distribution and the soil moisture characteristic are analyzed.

In **Chapter 6**, the parameters of the LN2 model are related to the soil pore ratios derived from the widely used soil pore classification systems. A new diagram to evaluate the soil pore radius distribution in connection with the retention characteristic is proposed. Simple means of estimating the parameters of the model are also suggested.

In **Chapter 7**, the LN2 model is combined with *Mualem*'s [1976] model in order to derive a model for soil hydraulic conductivity. The accuracy of the resulting combined water-retention-hydraulic-conductivity model (C-LN2 model) is verified for observed data sets for some soils having widely varying hydraulic properties.

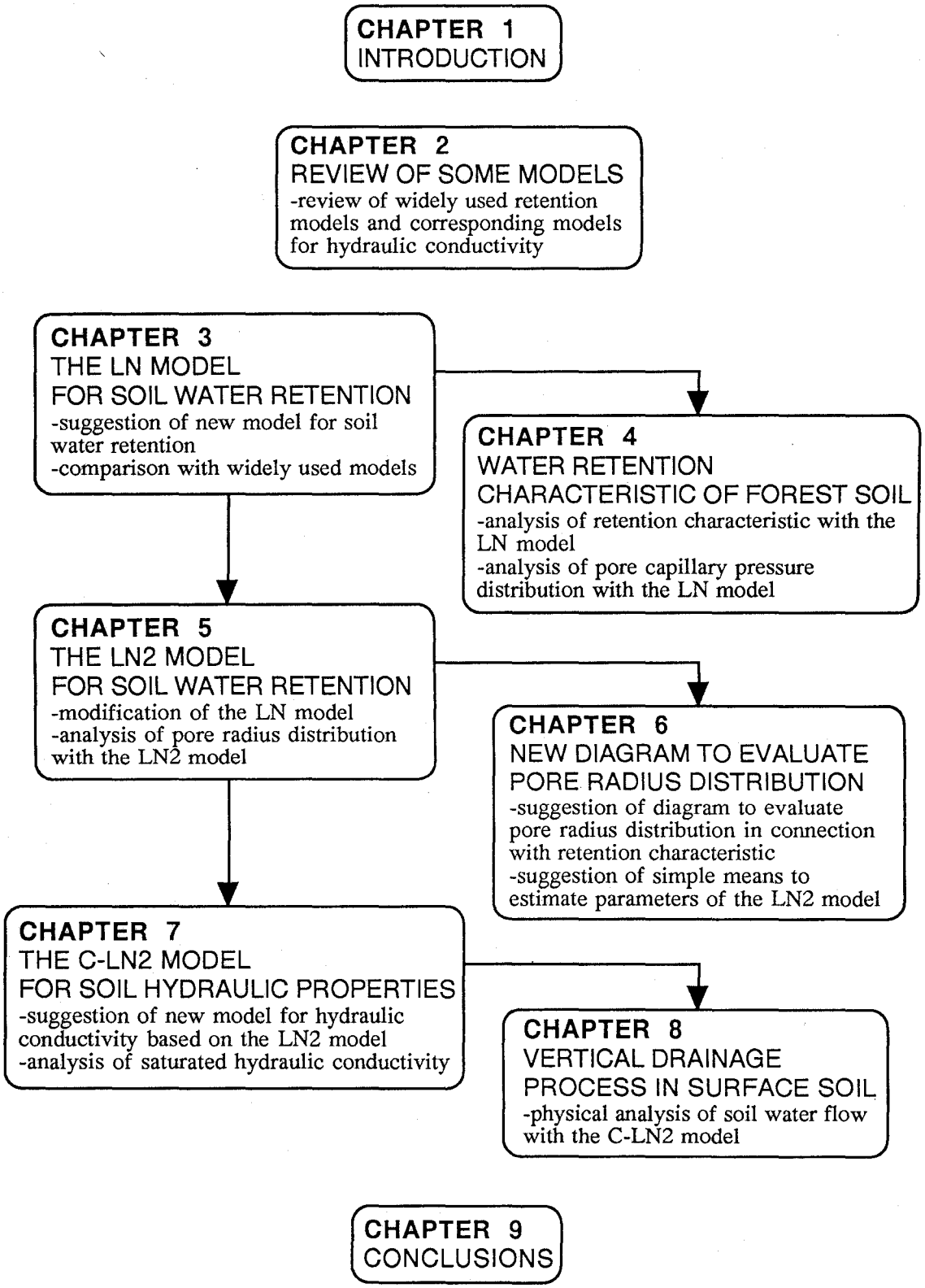

Figure 1.1 Structure of this study.

In **Chapter 8**, the C-LN2 model is adopted for physical analyses of unsaturated soil water flow. The effect of the pore radius distribution of forest soil on the water movement phenomena on forestal hillslope is clarified.

Chapter 9 summarizes the conclusions derived in each chapter. The general conclusions of this study are presented.

REFERENCES

Ahuja, L. R., and R. D. Williams, Scaling water characteristic and hydraulic conductivity based on Gregson-Hector-McGowan approach, *Soil Sci. Soc. Am. J.*, *55*(2), 308-319, 1991.

Arimitsu, K., Analysis of soil pore radius distribution using a suction plate (in Japanese*), *Jpn. J. For. Environment*, *12*(1), 31-35, 1970.

Arimitsu, K., M. Araki, K. Miyakawa, S. Kobayashi, and M. Kato, Water holding capacities estimated by soil pore capacities of Takaragawa Experiment Station: Comparison of No. 1 and No. 2 experimental watersheds (in Japanese with English summary), *Jpn. J. For. Environment*, *37*, 49-58, 1995.

Brooks, R. H., and A. T. Corey, Hydraulic properties of porous media, *Hydrol. Pap. 3*, Civil Eng. Dept., Colo. State Univ., Fort Collins, 1964.

Brutsaert, W., Probability laws for pore-size distributions, *Soil Sci.*, *101*, 85-92, 1966.

Brutsaert, W., The permeability of a porous medium determined from certain probability laws for pore size distribution, *Water Resour. Res.*, *4*(2), 425-434, 1968.

Burdine, N. T., Relative permeability calculation from size distribution data, *Trans. Am. Inst. Min. Metall. Pet. Eng.*, *198*, 71-78, 1953.

Carsel, R. F., and R. S. Parrish, Developing joint probability distribution of soil water retention characteristics, *Water Resour. Res.*, *24*(5), 755-769, 1988.

Childs, E. C., and N. Collis-George, The permeability of porous materials, *Proc. Roy. Soc., Ser. A*, *201*, 392-405, 1950.

Clapp, R. B., and G. M. Hornberger, Empirical equations for some soil hydraulic properties, *Water Resour. Res.*, *14*(4), 601-604, 1978.

Clausnitzer, V., J. W. Hopmans, and D. R. Nielsen, Simultaneous scaling of soil water retention and hydraulic conductivity curves, *Water Resour. Res.*, *28*(1), 19-31, 1992.

Gardner, W. R., Some steady state solutions of unsaturated moisture flow equations with application to evaporation from a water table, *Soil Sci.*, *85*, 228-232, 1958.

Hopmans, J. W., A comparison of various methods to scale soil hydraulic properties, *J. Hydrol.*, *93*, 241-256, 1987.

Kato, M., and I. Hotta, Estimation of the water holding capacity of the catchments by the runoff analysis (in Japanese with English summary), *Jpn. J. For. Environment*, *37*, 77-88, 1995.

King, L. G., Description of soil characteristics for partially saturated flow, *Soil Sci. Soc. Am. Proc.*, *29*, 359-362, 1965.

Kirkby, M. J., *Hillslope Hydrology*, John Wiley, New York, 1978.

Klute, A., and D. F. Heermann, Soil water profile development under a periodic boundary condition, *Soil Sci.*, *117*, 265-271, 1974.

Kobayashi, S., Changes in soil caused by forest clear-cutting (in Japanese), *Pedologist*, *26*, 150-163, 1982.

Kosugi, K., and N. Ohte, Analysis of soil-pore connection properties affecting the permeability

of forest soils (in Japanese with English Summary), *J. Jpn. For. Soc.*, *74*, 373-382, 1992.

Kubota, J., Y. Fukushima, and M. Suzuki, Observation and modeling of the runoff process on a hillslope (in Japanese with English Summary), *J. Jpn. For. Soc.*, *69*, 258-269, 1987.

Kumlung, A., and Y. Takeda, Changes of soil properties in relation to lapsed years of hillside works on a granite area, *J. Jpn. For. Soc.*, *73*, 327-338, 1991.

Kutílek, M., and D. R. Nielsen, *Soil Hydrology*, Catena Verlag, Cremlingen, Germany, 1994.

Laliberte, G. E., A mathematical function for describing capillary pressure-desaturation data, *Bull. Int. Ass. Sci. Hydrol.*, *14*(2), 131-149, 1969.

Leibenzon, L. S., *Flow of Natural Liquids and Gases in Porous Medium* (in Russian), Gostekhizdat, Moscow, 1947.

Letha, J., and K. Elango, Simulation of mildly unsaturated flow, *J. Hydrol.*, *154*, 1-17, 1994.

Luckner, L., M. Th. van Genuchten, and D. R. Nielsen, A consistent set of parametric models for the two-phase flow of immiscible fluids in the subsurface, *Water Resour. Res.*, *25*(10), 2187-2193, 1989.

Mashimo, Y., Studies on the physical properties of forest soil and their relation to the growth of sugi (*Cryptomeria japonica*) and hinoki (*Chamaecyparis obtusa*) (in Japanese with English Summary), *Forest Soils Jpn.*, *11*, 1-182, 1960.

McCuen, R. H., W.J. Rawls, and D. L. Brakensiek, Statistical analysis of the Brooks-Corey and the Green-Ampt parameters across soil textures, *Water Resour. Res.*, *17*(4), 1005-1013, 1981.

Mualem, Y., A new model for predicting the hydraulic conductivity of unsaturated porous media, *Water Resour. Res.*, *12*(3), 513-522, 1976.

Ogasiwa, K., T. Kondou, and Y. Mashimo, An analysis of factors affecting coarse pore volume of forest soil with the quantification-I method, I, Coarse pore volume of soil at various depth in sugi (*Cryptomeria japonica*) stands (in Japanese), *J. Jpn. For. Soc.*, *73*, 393-395, 1991.

Ohnuki, Y., R. Terazono, H. Ikuzawa, and I. Hirata, Distribution and physical properties of surficial soils in Minami-Meijiyama experimental watershed in Okinawa Island, Japan (in Japanese), *J. Jpn. For. Soc.*, *76*, 355-360, 1994.

Ohta, T., Y. Fukushima, and M. Suzuki, Research on runoff from hillsides by one-dimensional transient saturated-unsaturated flow (in Japanese with English Summary), *J. Jpn. For. Soc.*, *65*, 125-134, 1983.

Ohta, T., Y. Tsukamoto, and M. Hiruma, The behavior of rainwater on a forested hillslope, I, The properties of vertical infiltration and the influence of bedrock on it (in Japanese with English Summary), *J. Jpn. For. Soc.*, *67*, 311-321, 1985.

Ohte, N., *Studies on Pore Structure and Hydraulic Properties of Forest Soils* (in Japanese*), A doctor thesis, Kyoto Univ., 1992.

Ohte, N., and M. Suzuki, Hydraulic properties of forest soils, II, Method of determining the volumetric water content-pressure head relationship by the saturated-unsaturated hydraulic conductivity test using a large-size soil sample (in Japanese with English Summary), *J. Jpn. For. Soc.*, *72*, 468-477, 1990.

Russo, D., Determining soil hydraulic properties by parameter estimation: On the selection of a model for the hydraulic properties, *Water Resour. Res.*, *24*(3), 453-459, 1988.

Russo, D., E. Bresler, U. Shani, and J. C. Parker, Analyses of infiltration events in relation to determining soil hydraulic properties by inverse problem methodology, *Water Resour. Res.*, *27*(6), 1361-1373, 1991.

Russo, D., J. Zaidel, and A. Laufer, Stochastic analysis of solute transport in partially saturated heterogeneous soil, I, Numerical experiments, *Water Resour. Res.*, *30*(3), 769-779, 1994.

Russo, D., and M. Bouton, Statistical analysis of spatial variability in unsaturated flow parameters, *Water Resour. Res.*, *28*(7), 1911-1925, 1992.

Sammori, T., *Numerical Analysis of Sensitivity of Slope Failure to Various Factors* (in Japanese*), A doctor thesis, Kyoto Univ., 1994.

Sammori, T., and Y. Tsuboyama, Study on method of slope stability considering infiltration phenomenon (in Japanese with English Summary), *J. Jpn. Soc. Erosion Control Eng.*, *43*(4), 14-21, 1990.

Stauffer, F., H. J. Franke, and T. Dracos, Hysteretic storativity concept for aquifer simulation, *Water Resour. Res.*, *28*(9), 2307-2314, 1992.

Suzuki, M., The properties of a base-flow recession on small mountainous watersheds, I, Numerical analysis using the saturated-unsaturated flow model (in Japanese with English summary), *J. Jpn. For. Soc.*, *66*, 174-182, 1984.

Takeshita, K., Some considerations on the relation between forest soil and control function to river discharge (in Japanese), *Jpn. J. For. Environment*, *27*(2), 19-26, 1985.

Tani, M., The properties of a water-table rise produced by a one-dimensional, vertical, unsaturated flow (in Japanese with English summary), *J. Jpn. For. Soc.*, *64*, 409-418, 1982.

Tani, M., Analysis of one-dimensional, vertical, unsaturated flow in consideration of runoff properties of a mountainous watershed (in Japanese with English summary), *J. Jpn. For. Soc.*, *67*, 449-460, 1985.

Toorman, A. F., P. J. Wierenga, and R. G. Hills, Parameter estimation of hydraulic properties from one-step outflow data, *Water Resour. Res.*, *28*(11), 3021-3028, 1992.

Tsuboyama, Y., and T. Sammori, Numerical simulation of seepage in a forested hillslope by finite element method (in Japanese with English Summary), *J. Jpn. Soc. Hydrol. Water Resour.*, *2*(2), 49-56, 1989.

Tsukamoto, Y., *Forest Hydrology* (in Japanese*), Buneido, Tokyo, Japan, 1992.

Tyler, S. W., and S. W. Wheatcraft, Fractal processes in soil water retention, *Water Resour. Res.*, *26*(5), 1047-1054, 1990.

van Genuchten, M. Th., A closed-form equation for predicting the hydraulic conductivity of unsaturated soils, *Soil Sci. Soc. Am. J.*, *44*(5), 892-898, 1980.

Wierenga, P. J., R. G. Hills, and D. B. Hudson, The Las Cruces trench site: Characterization, experimental results, and one-dimensional flow predictions, *Water Resour. Res.*, *27*(10), 2695-2705, 1991.

Wösten, J. H. M., and M. Th. van Genuchten, Using texture and other soil properties to predict the unsaturated soil hydraulic functions, *Soil Sci. Soc. Am. J.*, *52*, 1762-1770, 1988.

* The title is tentative translation from the original Japanese title by the author of this thesis.

CHAPTER 2

REVIEW OF SOME MODELS FOR SOIL WATER RETENTION AND HYDRAULIC CONDUCTIVITY

2.1 INTRODUCTION

Modeling unsaturated water flow in soil requires knowledge of the hydraulic properties of the soil. The hydraulic properties of unsaturated soil are represented by the relationship between the volumetric water content θ and the soil capillary pressure ψ and the relationship between the unsaturated hydraulic conductivity K and ψ. The θ-ψ relationship represents the soil moisture characteristic and is referred to as the soil water retention curve. It is based on the soil pore radius distribution. The ratio of K to the saturated hydraulic conductivity K_s is referred to as the relative hydraulic conductivity K_r.

Many mathematical expressions that employ a small number of parameters have been proposed to describe the θ-ψ and K-ψ (or K-θ) relationships. In order to solve the equation of unsaturated soil water flow numerically, *King* [1965] suggested an equation that describes water retention characteristics of various soils. *Klute and Heermann* [1974] modified the King model for expressing the hysteretic phenomena found in the θ-ψ relationship. *Kroszynski* [1975] proposed a water retention model, in which θ is expressed as an exponential function with respect to ψ. By application of the Kozeny model for saturated hydraulic conductivity, *Leibenzon* [1947] derived a model for unsaturated hydraulic conductivity. According to his model, the relative hydraulic conductivity is expressed as a power function with respect to the soil water content. *Gardner*'s [1958] exponential model for the relative hydraulic conductivity has been frequently used in analytical solutions of soil water flow.

Other models for water retention [e.g., *Brooks and Corey*, 1964; *van Genuchten*, 1978, 1980; *Russo*, 1988] have been developed to be compatible with models by *Burdine* [1953] and *Mualem* [1976] for the purpose of deriving analytical expressions that can be used to predict the relative hydraulic conductivity of soil. The sets of the water retention model and the derived model for relative hydraulic conductivity are referred to as the combined water-retention-hydraulic-conductivity models, and have been widely used for modeling purposes [e.g., *Russo et al.*, 1994; *Letha and Elango*, 1994]. These models are also useful for the inverse method to determine the soil hydraulic properties

from transient data associated with unsaturated soil water flow [e.g., *Russo et al.*, 1991; *Toorman et al.*, 1992].

The objective of this chapter is to review some of the widely used water retention models and to compare the parameters of the models. The models for relative hydraulic conductivity, which are derived by combining the widely used retention models with *Mualem*'s [1976] model, are also summarized.

2.2 REVIEW OF SOME WATER RETENTION MODELS

Brooks and Corey [1964] suggested a water retention model (the BC model) which is frequently used by soil scientists and hydrologists. According to their model, the effective saturation, S_e, is expressed as a power function with respect to ψ:

$$\begin{aligned} S_e &= (\psi_{cB}/\psi)^{\lambda} \qquad \psi < \psi_{cB} \\ S_e &= 1 \qquad\qquad\quad \psi \geq \psi_{cB} \end{aligned} \tag{2.1}$$

where ψ_{cB} and λ are estimated parameters and S_e is defined as

$$S_e = (\theta - \theta_r)/(\theta_s - \theta_r) \tag{2.2}$$

where θ_s and θ_r are the saturated and residual water contents, respectively. Here θ_r is defined as the water content at which ψ is infinitely small and the soil water conductivity is assumed to be zero. However, θ_r is commonly regarded as an empirical parameter. It is treated as one of the fitted parameters in this study. The difference between θ_s and θ_r (that is, θ_s - θ_r) is called the effective porosity. The parameter ψ_{cB} is the bubbling pressure (or the air entry value of ψ) and is assumed to be a measure of the maximum sizes of pores forming a continuous network of flow channels within a soil. The parameter λ is dimensionless, characterizes the pore radius distribution, and is referred to as the pore size distribution index [*Brooks and Corey*, 1964]. By supposing that soil pore structure is based on the concept of fractal geometry, *Tyler and Wheatcraft* [1990] showed that λ is related to fractal dimension. *Milly* [1987] has pointed out that the presence of the distinct bubbling pressure ψ_{cB} and the absence of an inflection point on the θ-ψ curve in this model cause discrepancies with field-measured moisture characteristics.

An alternative *S*-shaped model was suggested by *van Genuchten* [1978, 1980]:

$$S_e = 1/\left\{1 + (\alpha_V|\psi|)^n\right\}^m \tag{2.3}$$

where α_V and n ($n > 1$) represent empirical parameters which are reportedly related to the inverse of the bubbling pressure and the pore size distribution index ($n = \lambda + 1$), respectively, and m is related to n by $m = 1 - 1/n$ [*van Genuchten*, 1980]. The θ-ψ curve expressed by (2.3) does not account for the bubbling pressure but does have an inflection point, allowing the van Genuchten model to perform better than the BC model for many

Table 2.1 Parameters of the van Genuchten (VG) Model, the Brooks and Corey (BC) Model, and the Modified Tani (TA) Model

Model	P1	P2	P3
VG	...	ψ_{0V}	m
BC	ψ_{cB}	...	λ
TA	ψ_{cT}	ψ_{0T}	...

P1 is the bubbling pressure, P2 is the capillary pressure at the inflection point on the θ-ψ curve, and P3 is a dimensionless parameter. Each model contains the saturated and residual water contents.

soils, particularly for data near saturation [*van Genuchten and Nielsen*, 1985]. While *Powers et al.* [1992] regarded α_V as a measure of pore throat size and *Russo* [1988] assumed that n is related to the width of the pore radius distribution, strict definitions of these parameters have not yet been proposed. *Van Genuchten* [1978] differentiated (2.3) twice with respect to ψ to obtain

$$\psi_{0V} = -m^{1-m}/\alpha_V \tag{2.4}$$

where ψ_{0V} represents the capillary pressure at the inflection point on the θ-ψ curve. Inverting (2.4) with respect to α_V and substituting into (2.3) yields

$$S_e = \left\{1 + m(\psi/\psi_{0V})^{1/1-m}\right\}^{-m} \tag{2.5}$$

where $m = 1 - 1/n$; m $(0 < m < 1)$ is also related to the width of the pore radius distribution. Equation (2.5) is referred to as the VG model. The value of S_e at the inflection point is derived by substituting $\psi = \psi_{0V}$ into (2.5):

$$S_e(\psi_{0V}) = (1+m)^{-m} \tag{2.6}$$

Equation (2.6) indicates that $S_e(\psi_{0V})$ depends only on m. By considering that m can only take on values between 0 and 1, $S_e(\psi_{0V})$ has the restriction:

$$0.5 < S_e(\psi_{0V}) < 1 \tag{2.7}$$

The third retention model is based on the model suggested by *Tani* [1982]; that is,

$$S_e = (1+\psi/\psi_{0T})\exp(-\psi/\psi_{0T}) \tag{2.8}$$

where ψ_{0T} corresponds to the capillary pressure at the inflection point on the θ-ψ curve. Because of its simplicity, (2.8) has been widely used for modeling water movement in

soils [e.g., *Suzuki*, 1984; *Tani*, 1985]. For consistency to be maintained with other two-parameter models (BC and VG), (2.8) is modified to include the bubbling pressure ψ_{cT} while conserving the nature of ψ_{0T}:

$$S_e = \left(1+\frac{\psi_{cT}-\psi}{\psi_{cT}-\psi_{0T}}\right)\exp\left(-\frac{\psi_{cT}-\psi}{\psi_{cT}-\psi_{0T}}\right) \qquad \psi < \psi_{cT} \tag{2.9}$$

$$S_e = 1 \qquad \psi \geq \psi_{cT}$$

Equation (2.9) is called the TA model.

Table 2.1 summarizes the parameters for the three retention models. It is clear from the table that the VG, BC, and TA models all have two parameters other than the saturated and residual water contents. The VG model does not use the bubbling pressure, the BC model does not use the capillary pressure at the inflection point, and the TA model does not use a dimensionless parameter which is related to the width of the pore radius distribution.

2.3 MODELS FOR RELATIVE HYDRAULIC CONDUCTIVITY

Many models for predicting the relative hydraulic conductivity K_r from soil water retention curve have been proposed [e.g., *Childs and Collis-George*, 1950; *Burdine*, 1953; *Marshall*, 1958; *Mualem*, 1976; *Nishimura et al.*, 1985]. These models were developed by characterizing the macroscopic flux in a soil using the microscopic soil pore radius distribution [*Kutílek and Nielsen*, 1994]. It has been reported that the model proposed by *Mualem* [1976] performs relatively well in comparison with other models such as *Burdine*'s [1953] model [*van Genuchten and Nielsen*, 1985].

The Mualem model is similar to the *Childs and Collis-George* [1950] model which computes the probability of the connection of pairs of pores, but uses a modified assumption concerning the hydraulic conductivity of the pore sequence. He assumed an empirical power function with respect to the effective saturation S_e (suggested by *Burdine* [1953]) for the pore tortuosity factor. Derived model for the relative hydraulic conductivity K_r is written in the form

$$K_r = K/K_s = S_e^{\,l}\left\{\int_0^{S_e}\frac{dS_e}{|\psi|}\Big/\int_0^1\frac{dS_e}{|\psi|}\right\}^2 \tag{2.10}$$

where K_s is the saturated hydraulic conductivity. The exponent l in the tortuosity factor ($S_e^{\,l}$) was decided to be 1/2 by *Mualem* [1976] as an average for some 45 soils. The factor of $\int_0^{S_e}|\psi|^{-1}dS_e / \int_0^1|\psi|^{-1}dS_e$ is computed using the microscopic pore radius distribution derived from the soil water retention curve.

Combining the BC model expressed as (2.1) with (2.10) gives the functional relationships between K_r and S_e, and K_r and ψ:

$$K_r(S_e) = S_e^{2+l+2/\lambda} \tag{2.11}$$

$$\begin{aligned} K_r(\psi) &= (\psi_{cB}/\psi)^{2+(2+l)\lambda} \qquad \psi < \psi_{cB} \\ K_r(\psi) &= 1 \qquad\qquad\qquad\qquad \psi \geq \psi_{cB} \end{aligned} \tag{2.12}$$

The K_r model expressed as (2.11) is identical to the model proposed by *Leibenzon* [1947].

Van Genuchten [1978, 1980] substituted (2.3) into (2.10) and integrated to yield

$$K_r(S_e) = S_e^l \left\{1 - \left(1 - S_e^{1/m}\right)^m\right\}^2 \tag{2.13}$$

$$K_r(\psi) = \frac{\left[1 - (\alpha_V|\psi|)^{n-1}\left\{1 + (\alpha_V|\psi|)^n\right\}^{-m}\right]^2}{\left\{1 + (\alpha_V|\psi|)^n\right\}^{ml}} \tag{2.14}$$

where $m = 1 - 1/n$. The combination of the water retention model expressed as (2.3) and the hydraulic conductivity model expressed as (2.13) or (2.14) has been used extensively in numerical modeling of unsaturated soil water flow [e.g., *Jury et al.*, 1991].

By combining *Tani*'s [1982] water retention model expressed as (2.8) with (2.10), the following expression of K_r is derived:

$$K_r(\psi) = (1 + \psi/\psi_{0T})^l \exp\{-(2+l)\psi/\psi_{0T}\} \tag{2.15}$$

With the restriction of $l = 0$, (2.15) is identical to the K_r model suggested by *Gardner* [1958] in which K_r is expressed as an exponential function with respect to ψ.

2.4 SUMMARY AND CONCLUSIONS

This chapter summarized three water retention models, all of which have been used widely by soil scientists and hydrologists. According to the model suggested by *Brooks and Corey* [1964] (the BC model), the effective saturation is expressed as a power function with respect to the capillary pressure. *Van Genuchten*'s [1978, 1980] model (the VG model) was transformed to include the capillary pressure at the inflection point on the θ-ψ curve instead of the parameter α_V which is reportedly related to the inverse of the bubbling pressure. The retention model suggested by *Tani* [1982] was modified to include the bubbling pressure. The derived model was referred to as the TA model. By comparison of the parameters of the three water retention models, it was shown that the VG, BC, and TA models all have two parameters other than the saturated and residual water contents. The VG model does not use the bubbling pressure, the BC model does not use the capillary pressure at the inflection point, and the TA model does not use a dimensionless parameter which is related to the width of the pore radius distribution.

The VG, BC, and TA models were combined with *Mualem*'s [1976] model for predicting the relative hydraulic conductivity of soil. The relative hydraulic conductivity is defined as the ratio of the unsaturated hydraulic conductivity to the saturated hydraulic conductivity. Resulting analytical expressions for the relative hydraulic conductivity were summarized.

REFERENCES

Brooks, R. H., and A. T. Corey, Hydraulic properties of porous media, *Hydrol. Pap. 3*, Civil Eng. Dept., Colo. State Univ., Fort Collins, 1964.

Burdine, N. T., Relative permeability calculation from size distribution data, *Trans. Am. Inst. Min. Metall. Pet. Eng., 198*, 71-78, 1953.

Childs, E. C., and N. Collis-George, The permeability of porous materials, *Proc. Roy. Soc., Ser. A, 201*, 392-405, 1950.

Gardner, W. R., Some steady state solutions of unsaturated moisture flow equations with application to evaporation from a water table, *Soil Sci., 85*, 228-232, 1958.

Jury, W. A., W. R. Gardner, and W. H. Gardner, *Soil Physics*, Wiley, New York, 1991.

King, L. G., Description of soil characteristics for partially saturated flow, *Soil Sci. Soc. Am. Proc., 29*, 359-362, 1965.

Klute, A., and D. F. Heermann, Soil water profile development under a periodic boundary condition, *Soil Sci., 117*, 265-271, 1974.

Kroszynski, U., Flow in a vertical porous column drained at its bottom at constant flux, *J. Hydrol., 24*, 135-153, 1975.

Kutílek, M., and D. R. Nielsen, *Soil Hydrology*, Catena Verlag, Cremlingen, Germany, 1994.

Leibenzon, L. S., *Flow of Natural Liquids and Gases in Porous Medium* (in Russian), Gostekhizdat, Moscow, 1947.

Letha, J., and K. Elango, Simulation of mildly unsaturated flow, *J. Hydrol., 154*, 1-17, 1994.

Marshall, T. J., A relation between permeability and size distribution of pores, *J. Soil Sci., 9*(1), 1-8, 1958.

Milly, P. C. D., Estimation of Brooks-Corey parameters from water retention data, *Water Resour. Res., 23*(6), 1085-1089, 1987.

Mualem, Y., A new model for predicting the hydraulic conductivity of unsaturated porous media, *Water Resour. Res., 12*(3), 513-522, 1976.

Nishimura, N., T. Mitsuno, and T. Maruyama, A unified model for predicting unsaturated hydraulic conductivity, Relationship between the soil water characteristic curve and unsaturated hydraulic conductivity, I (in Japanese with English summary), *Trans. JSIDRE, 116*, 1-8, 1985.

Powers, S. E., L. M. Abriola, and W. J. Weber, Jr., An experimental investigation of nonaqueous phase liquid dissolution in saturated subsurface system: Steady state mass transfer rates, *Water Resour. Res., 28*(10), 2691-2705, 1992.

Russo, D., Determining soil hydraulic properties by parameter estimation: On the selection of a model for the hydraulic properties, *Water Resour. Res., 24*(3), 453-459, 1988.

Russo, D., E. Bresler, U. Shani, and J. C. Parker, Analyses of infiltration events in relation to determining soil hydraulic properties by inverse problem methodology, *Water Resour. Res., 27*(6), 1361-1373, 1991.

Russo, D., J. Zaidel, and A. Laufer, Stochastic analysis of solute transport in partially saturated heterogeneous soil, I, Numerical experiments, *Water Resour. Res.*, *30*(3), 769-779, 1994.

Suzuki, M., The properties of a base-flow recession on small mountainous watersheds, I, Numerical analysis using the saturated-unsaturated flow model (in Japanese with English summary), *J. Jpn. For. Soc.*, *66*, 174-182, 1984.

Tani, M., The properties of a water-table rise produced by a one-dimensional, vertical, unsaturated flow (in Japanese with English summary), *J. Jpn. For. Soc.*, *64*, 409-418, 1982.

Tani, M., Analysis of one-dimensional, vertical, unsaturated flow in consideration of runoff properties of a mountainous watershed (in Japanese with English summary), *J. Jpn. For. Soc.*, *67*, 449-460, 1985.

Toorman, A. F., P. J. Wierenga, and R. G. Hills, Parameter estimation of hydraulic properties from one-step outflow data, *Water Resour. Res.*, *28*(11), 3021-3028, 1992.

Tyler, S. W., and S. W. Wheatcraft, Fractal processes in soil water retention, *Water Resour. Res.*, *26*(5), 1047-1054, 1990.

van Genuchten, M. Th., A closed-form equation for predicting the hydraulic conductivity of unsaturated soils, *Soil Sci. Soc. Am. J.*, *44*(5), 892-898, 1980.

van Genuchten, M. Th., and D. R. Nielsen, On describing and predicting the hydraulic properties of unsaturated soils, *Ann. Geophys.*, *3*(5), 615-628, 1985.

van Genuchten, R., Calculating the unsaturated hydraulic conductivity with a new closed-form analytical model, *Res. Rep. 78-WR-08*, Dept. of Civil Eng., Princeton, N. J., 1978.

CHAPTER 3

THREE-PARAMETER LOGNORMAL DISTRIBUTION MODEL FOR SOIL WATER RETENTION

3.1 INTRODUCTION

The moisture characteristic of soil is represented by the relationship between the volumetric water content θ and the soil capillary pressure ψ and is referred to as the soil water retention curve. It is based on the soil pore radius (size) distribution. As summarized in Chapter 2, many functions for expressing the θ-ψ curve have been proposed for modeling water flow in unsaturated soil and for deriving analytical expressions that can be used to predict the relative hydraulic conductivity of soil.

In recent years, these retention models have been popularly used in various analyses of the moisture characteristic. *McCuen et al.* [1981] and *Carsel and Parrish* [1988] have done statistical studies of the relationships between the parameters of retention models and the soil texture. Some of these retention models have been used for expressing the hysteretic phenomena found in the moisture characteristic [e.g., *Klute and Heermann*, 1974; *Luckner et al.*, 1989; *Stauffer et al.*, 1992]. Works on statistical analysis of spatial variability in parameters of retention models have been published by *Wierenga et al.* [1991] and *Russo and Bouton* [1992], and scaling methods of soil water retention, based on retention models, have been proposed by *Ahuja and Williams* [1991] and *Clausnitzer et al.* [1992]. Despite their usefulness, most of these models are empirical curve-fitting equations and do not emphasize the physical significance of their empirical parameters.

On the other hand, several attempts have been made to derive models for the pore radius distribution for the purpose of analyzing the moisture characteristic on the basis of soil pore structure. *Brutsaert* [1966] applied several distribution laws, such as the incomplete gamma distribution, the lognormal distribution, and his own original distribution form, to the model for the pore radius distribution. *Laliberte* [1969] also suggested his own distribution form. In recent years, fractal scaling has received renewed interest. *Tyler and Wheatcraft* [1990], for instance, derived a pore radius distribution form by assuming that soil pore structure is based on the concept of fractal geometry. These models are acceptable only for specific media, and the water retention equations

derived from them do not have sufficient flexibility. This chapter proposes for water retention a general model which performs as well as any existing empirical model and which was developed by applying a distribution law available in general probability theory.

The water capacity function is defined as the slope of the θ-ψ curve and is necessary for modeling water movement in unsaturated soil. The water capacity function is related to the pore radius distribution function by transforming variables under the assumption that there is a direct correspondence between the pore radius and the capillary pressure. In this chapter, the water capacity function is regarded as the pore capillary pressure distribution function. Because of the well-known fact that particle size distributions of many soils are approximately lognormal [*Aitchison and Brown*, 1957; *Shirazi and Boersma*, 1984], it seems reasonable to use the lognormal distribution to describe the pore radius distribution. By Application of a three-parameter lognormal distribution to the pore radius distribution, an expression for the pore capillary pressure distribution which has an alternative three-parameter lognormal distribution form is obtained. From this expression, a new model for water retention that has parameters that are closely related to the statistics of the pore capillary pressure distribution and that exhibits great flexibility for determining retention curves of various soils is proposed. The accuracy and the parameters of the widely used retention models (the VG, BC, and TA models summarized in Chapter 2) are analyzed in comparison with those of the proposed model.

3.2 THEORY

3.2.1 Definition of the Pore Capillary Pressure Distribution Function

The pore radius distribution function $g(r)$ is defined by

$$g(r) = d\theta / dr \tag{3.1}$$

where r is the pore radius. Consequently, $g(r)dr$ represents the volume of full pores of radii $[r, r + dr]$ per unit volume of medium. Here r is assumed to be related to ψ for a given saturation by the capillary pressure function

$$\psi = -2\gamma_w \cos\beta_c / \varrho_w g r = A / r \tag{3.2}$$

where γ_w is the surface tension between water and air, β_c is the contact angle, ϱ_w is the density of water, and g is the acceleration of gravity. The constant value of -2 $\gamma_w \cos\beta_c/\varrho_w g = A$ = -0.149 cm^2 [*Brutsaert*, 1966] is used in this study. On the basis of this direct correspondence of r and ψ, the distribution $g(r)$ is transformed into the distribution $f(\psi)$ by the following equation:

$$f(\psi) = g(r)dr / d\psi \tag{3.3}$$

Substituting (3.1) into (3.3) yields

$$f(\psi) = d\theta / d\psi \tag{3.4}$$

Hence, $f(\psi)d\psi$ represents the volume of full pores in which water is retained by capillary pressure ψ to $\psi + d\psi$ per unit volume of medium. Therefore $f(\psi)$ can be regarded as the pore capillary pressure distribution function. From (3.4), it is evident that $f(\psi)$ is identical to the water capacity function, which is defined as the slope of the θ-ψ curve.

The relationship between θ and ψ can be obtained by integrating (3.4) with the knowledge that $\theta = \theta_r$ when $\psi = -\infty$:

$$\theta(\psi) = \int_{-\infty}^{\psi} f(\psi)d\psi + \theta_r \tag{3.5}$$

Furthermore, the relationship between the effective saturation S_e and ψ is

$$S_e(\psi) = \frac{1}{\theta_s - \theta_r}\int_{-\infty}^{\psi} f(\psi)d\psi \tag{3.6}$$

It should be noted here that $f(\psi)$ is not a probability density function but a function whose definite integral from $-\infty$ to 0 equals the effective porosity (θ_s - θ_r). The same is true of $g(r)$.

3.2.2 Proposed Model for Water Retention

Many models have already been proposed for $g(r)$. Here, the author proposes a new model for $g(r)$ such that

$$g(r) = \frac{(\theta_s - \theta_r)r_{\max}}{\sqrt{2\pi}\sigma r(r_{\max} - r)} \exp\left[-\frac{\left\{ \ln\left(\frac{r}{r_{\max} - r} \right) - \mu \right\}^2}{2\sigma^2} \right] \tag{3.7}$$

where $r_{\max}$ represents the maximum pore radius in the medium and σ and μ are dimensionless parameters ($\sigma > 0$; $\mu > 0$). Equation (3.7) is derived by applying the normal distribution to the distribution of $\ln(r/(r_{\max} - r))$, which is given by a transformation of $g(r)$. Here, μ and σ^2 are the first moment about the origin (i.e., the mean) and the second moment about the mean (i.e., the variance, with σ as the standard deviation) of the distribution of $\ln(r/(r_{\max} - r))$, respectively. Equation (3.7) has a three-parameter lognormal distribution form. In comparison with *Brutsaert*'s [1966] model for $g(r)$, which is based on a simple two-parameter lognormal distribution, (3.7), which also contains the maximum pore radius $r_{\max}$, is relatively complicated.

By substituting (3.2) and (3.7) into (3.3) and differentiating, the pore capillary pressure distribution function $f(\psi)$ can be obtained:

$$f(\psi) = \frac{\theta_s - \theta_r}{\sqrt{2\pi}\sigma(\psi_c - \psi)} \exp\left[-\frac{\left\{ \ln\left(\frac{\psi_c}{\psi - \psi_c} \right) - \mu \right\}^2}{2\sigma^2} \right] \qquad \psi < \psi_c \qquad (3.8)$$

$$f(\psi) = 0 \qquad \psi \geq \psi_c$$

where ψ_c, which is related to r_{max} by (3.2), is the bubbling pressure. Differentiating (3.8) with respect to ψ and setting $f'(\psi) = 0$, the capillary pressure at the peak of $f(\psi)$, that is, the mode of $f(\psi)$, can be derived as a function of ψ_c, σ, and μ :

$$\psi_0 = \psi_c \left\{ 1 + \exp\left(-\mu - \sigma^2 \right) \right\} \qquad (3.9)$$

where ψ_0 represents the mode of $f(\psi)$. Inverting (3.9) with respect to μ and substituting into (3.8) gives

$$f(\psi) = \frac{\theta_s - \theta_r}{\sqrt{2\pi}\sigma(\psi_c - \psi)} \exp\left[-\frac{\left\{ \ln\left(\frac{\psi_c - \psi}{\psi_c - \psi_0} \right) - \sigma^2 \right\}^2}{2\sigma^2} \right] \qquad \psi < \psi_c \qquad (3.10)$$

$$f(\psi) = 0 \qquad \psi \geq \psi_c$$

Equation (3.10) has an alternative three-parameter lognormal distribution form because the distribution of $\ln\{(\psi_c\text{-}\psi)/(\psi_c\text{-}\psi_0)\}$ obeys the normal distribution $N(\sigma^2, \sigma^2)$. Figure 3.1a shows a plot of (3.10) for θ_s = 0.6, θ_r = 0.1, ψ_c = -10 cm, ψ_0 = -30 cm, and σ = 0.6. As can be seen, the distribution expressed by (3.10) is not symmetrical and is similar to the typical water capacity function [see *Jury et al.*, 1991]. The mean ψ_a, the median ψ_m, and the variance σ_ψ^2, (where σ_ψ is the standard deviation) of $f(\psi)$ are expressed by the following functions with respect to ψ_c, ψ_0, and σ :

$$\psi_a = \psi_c - (\psi_c - \psi_0) \exp\left(3\sigma^2 / 2 \right) \qquad (3.11)$$

$$\psi_m = \psi_c - (\psi_c - \psi_0) \exp\left(\sigma^2 \right) \qquad (3.12)$$

$$\sigma_\psi^2 = (\psi_c - \psi_0)^2 \exp\left(3\sigma^2 \right) \left\{ \exp\left(\sigma^2 \right) - 1 \right\} \qquad (3.13)$$

It should be noted that $S_e(\psi_m)$ is equal to 0.5 because the definite integral of $f(\psi)$ from -∞ to ψ_m is equal to that from ψ_m to 0.

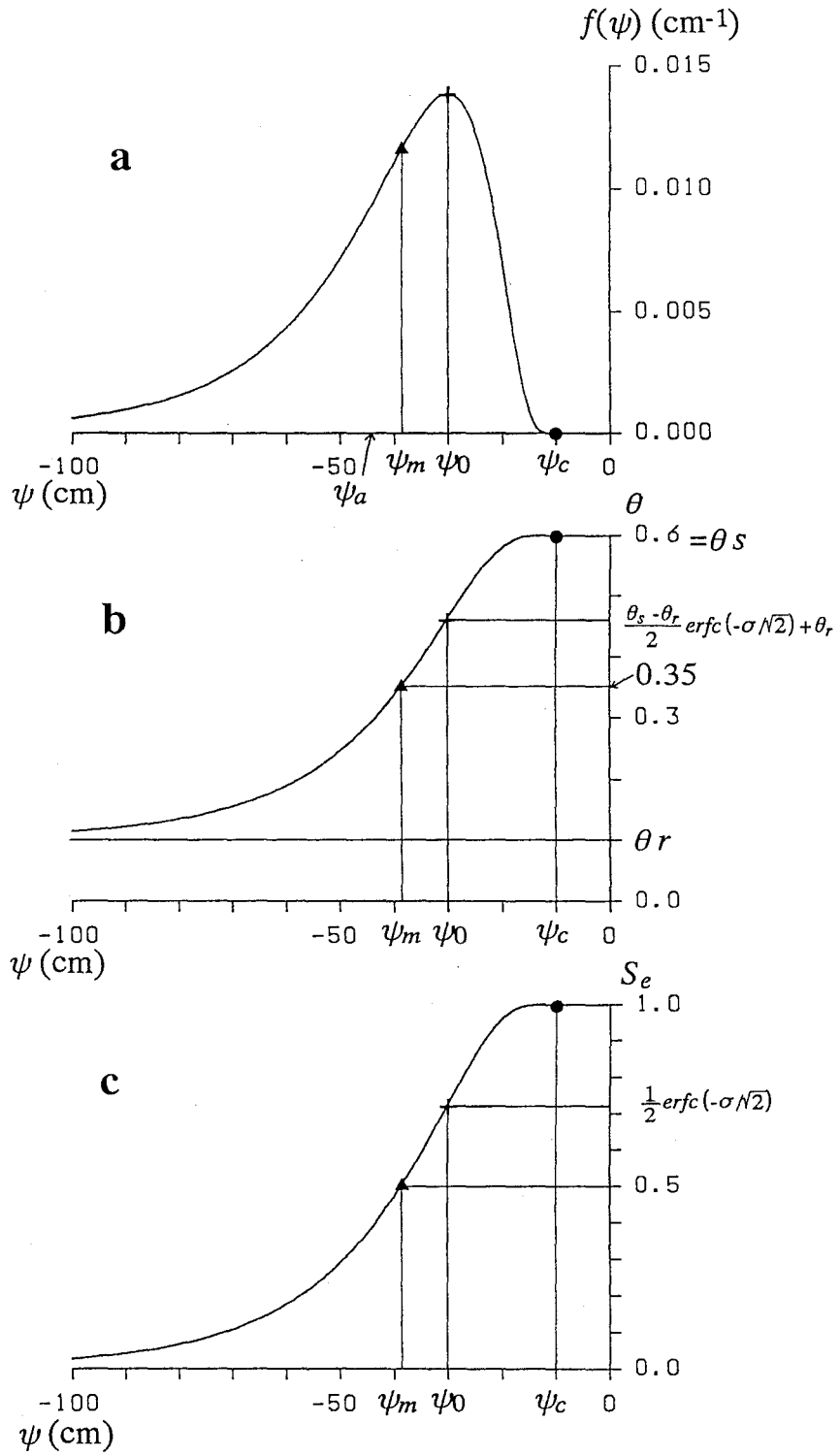

Figure 3.1 Curves for (a) $f(\psi)$, (b) θ-ψ, and (c) S_e-ψ based on the LN model, showing plots of (3.10) and (3.14) for $\theta_s = 0.6$, $\theta_r = 0.1$, $\psi_c = -10$ cm, $\psi_0 = -30$ cm, and $\sigma = 0.6$.

Table 3.1 Parameters of the van Genuchten (VG) Model, the Brooks and Corey (BC) Model, the Modified Tani (TA) Model, the Proposed LN Model, and the Proposed VK Model

Model	P1	P2	P3
VG	···	ψ_{0V}	m
BC	ψ_{cB}	···	λ
TA	ψ_{cT}	ψ_{0T}	···
LN	ψ_c	ψ_0	σ
VK	ψ_{cK}	ψ_{0K}	m_K

P1 is the bubbling pressure, P2 is the capillary pressure at the inflection point on the θ-ψ curve, and P3 is a dimensionless parameter. Each model contains the saturated and residual water contents.

Substituting (3.10) into (3.6) and integrating yields an expression for water retention:

$$S_e = \frac{1}{2}\operatorname{erfc}\left(\frac{\ln\{(\psi_c-\psi)/(\psi_c-\psi_0)\}-\sigma^2}{\sqrt{2}\sigma}\right) \qquad \psi < \psi_c$$
$$S_e = 1 \qquad \psi \geq \psi_c \tag{3.14}$$

where erfc denotes the complementary error function. Figures 3.1b and 3.1c show functional relationships between θ and ψ, and between S_e and ψ, both of which were generated by (3.14) (referred to as the LN model) with the same parameters as those used for $f(\psi)$ in Figure 3.1a. Notice that ψ_c and ψ_0 correspond to the bubbling pressure (the air entry suction) and the capillary pressure at the inflection point on the θ-ψ curve, respectively. The parameters of the LN model are compared with those of the other three models (the VG, BC, and TA models) in Table 3.1. The VG, BC, and TA models are expressed as (2.5), (2.1), and (2.9), respectively. Other than θ_s and θ_r, only the LN model contains three parameters: the bubbling pressure ψ_c, the capillary pressure at the inflection point ψ_0, and a dimensionless parameter σ, which is the standard deviation of the transformed pore capillary pressure distribution and which is related to the width of the pore radius distribution. The value of S_e at the inflection point is found by substituting $\psi = \psi_0$ into (3.14):

$$S_e(\psi_0) = \frac{1}{2}\operatorname{erfc}\left(-\sigma/\sqrt{2}\right) \tag{3.15}$$

Consequently, σ determines the value of $S_e(\psi_0)$. By considering that σ can only take on positive values, the following restriction applies:

$$0.5 < S_e(\psi_0) < 1 \tag{3.16}$$

This restriction is identical to the restriction for the S_e value at the inflection point in the VG model (see (2.7)).

3.3 RESULTS OF MODEL VALIDATION TESTS

For verification of the accuracy of the LN model and for comparison of the parameters of the LN model with the parameters of the other three retention models (VG, BC and TA), a nonlinear least squares optimization procedure based on Marquardt's maximum neighborhood method [*Marquardt*, 1963] was used to analyze observed retention data sets. Retention data sets for 50 soils were taken from the catalogue by *Mualem* [1976]. By applying Marquardt's method, θ_r was treated as one of the fitted parameters, and the θ_s values were taken from the catalogue. As with *van Genuchten and Nielsen* [1985], the residual sum of squares (RSS) of the fitted versus observed water contents was used to compare the accuracies of the four retention models.

In Figure 3.2, the RSS for the LN model (RSS_{LN}) are compared with those for the VG model (RSS_{VG}), the BC model (RSS_{BC}), and the TA model (RSS_{TA}) for 50 sets of data. Figure 3.2a indicates that RSS_{LN} were much lower than RSS_{VG} for many data sets, whereas for some data sets, particularly those for which the parameter ψ_c was estimated

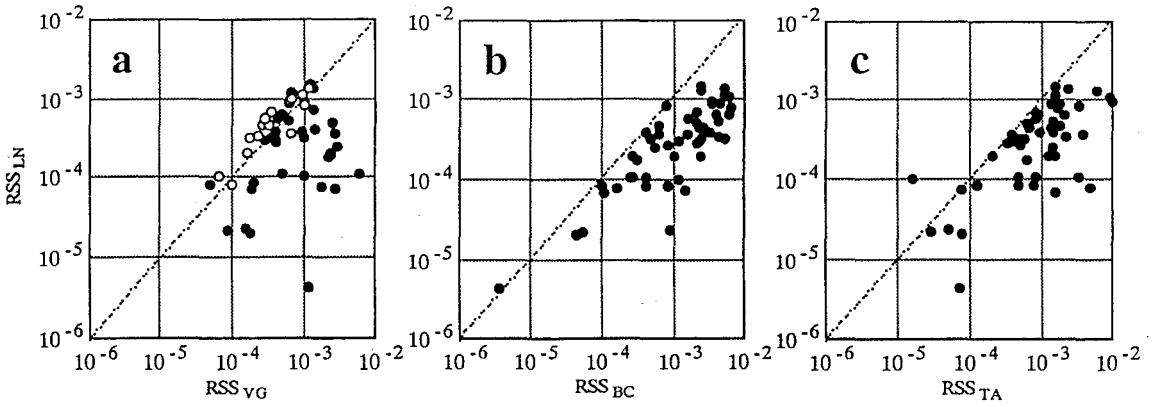

Figure 3.2 Comparison among computed residual sum of squares (RSS) for the LN model (RSS_{LN}) and those for (a) the VG model (RSS_{VG}), (b) the BC model (RSS_{BC}), and (c) the TA model (RSS_{TA}), for 50 sets of observed retention data. Open circles in Figure 3.2a indicate data sets for which the parameter ψ_c was estimated to be zero.

to be zero (shown as open circles in Figure 3.2a), RSS_{LN} were a little higher than RSS_{VG}. Figures 3.2b and 3.2c show that RSS_{LN} were lower than RSS_{BC} and RSS_{TA} for most data sets. Average RSS values for the 50 sets of data were 4.41×10^{-4}, 9.95×10^{-4}, 20.23×10^{-4}, and 16.05×10^{-4} for RSS_{LN}, RSS_{VG}, RSS_{BC}, and RSS_{TA}, respectively. Thus, the LN model provides the best fit with measured observations. Among two-parameter models, the VG model, on average, showed the best fit. RSS_{VG} values were the lowest values for 26 data sets of 50, RSS_{BC} were the lowest for 16 data sets, and RSS_{TA} were the lowest for eight data sets.

3.4 COMPARISON OF THE PROPOSED MODEL WITH WIDELY USED MODELS

3.4.1 The VG Model Versus the LN Model

For illustration of a typical retention data set for which the VG model performed best of all the two-parameter models, the observed data set for Touchet silt loam [*King*, 1965] (Mualem's soil index 3308 [*Mualem*, 1976]), is compared with the fitted curves generated by the VG and LN models in Figure 3.3a. Estimated parameters, including those of the other two models, are shown in Table 3.2. Although the RSS_{LN} for this example is a little higher than the RSS_{VG}, one can see from Figure 3.3a that the LN model also produces an acceptable fit.

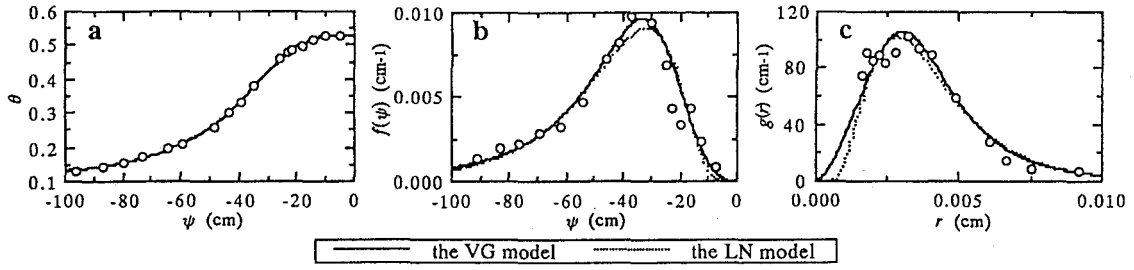

Figure 3.3 Observed and fitted (a) θ-ψ curves, (b) $f(\psi)$ curves, and (c) $g(r)$ curves for Touchet silt loam. Circles in Figure 3.3b indicate $f(\psi)$ values derived by numerically differentiating observed θ-ψ data, and circles in Figure 3.3c indicate $g(r)$ values derived by substituting $f(\psi)$ values together with (3.2), with the constant $A = -0.149$ cm^2, into (3.3).

Table 3.2 Fitted Values for Parameters of the Respective Water Retention Models and the Residual Sum of Squares (RSS) of the Curve Fittings for the Retention Curves Plotted in Figures 3.3, 3.7, and 3.11

Soil Name and Type of Model	θ_s *1	θ_r	P1, cm	P2, cm	P3	RSS × 10^5
Touchet silt loam	0.528					
VG		0.100	···	-33.3	0.7177	18.2
BC		0.000	-21.1	···	0.8500	523.5
TA		0.116	-12.5	-29.5	···	58.6
LN		0.117	0.0	-31.8	0.5024	32.4
VK		0.100	0.0	-33.3	0.7177	18.2
Rubicon sandy loam	0.381					
VG		0.176	···	-85.6	0.8508	248.7
BC		0.155	-67.6	···	2.296	27.6
TA		0.176	-58.5	-77.3	···	158.9
LN		0.146	-66.7	-70.6	1.377	20.6
VK		0.106	-66.3	-72.1	0.3594	18.6
Fragmented Fox Hill sandstone	0.503					
VG		0.165	···	-25.3	0.7563	40.0
BC		0.115	-17.6	···	1.206	215.8
TA		0.171	-11.4	-22.1	···	32.3
LN		0.168	-6.3	-22.8	0.5850	30.1
VK		0.158	-5.4	-24.0	0.6959	33.1

P1 is the bubbling pressure (ψ_{cB}, ψ_{cT}, ψ_c, and ψ_{cK} of the BC, TA, LN, and VK models, respectively), P2 is the capillary pressure at the inflection point on the θ-ψ curve (ψ_{0V}, ψ_{0T}, ψ_0, and ψ_{0K} of the VG, TA, LN, and VK models, respectively), and P3 is a dimensionless parameter (m, λ, σ, and m_K of the VG, BC, LN, and VK models, respectively).

*1 Taken from Mualem's catalogue [*Mualem*, 1976].

Figure 3.3b shows a comparison between the observed $f(\psi)$ curve, which was derived by numerically differentiating the retention data shown in Figure 3.3a, and fitted curves obtained by use of the LN and VG models with the parameters shown in Table 3.2. The function $f(\psi)$ based on the VG model is derived by differentiating (2.5) with respect to ψ to obtain

$$f(\psi) = \frac{(\theta_s - \theta_r)m^2}{(1-m)(-\psi_{0V})}\left(\frac{\psi}{\psi_{0V}}\right)^{m/(1-m)}\left\{1+m\left(\frac{\psi}{\psi_{0V}}\right)^{1/(1-m)}\right\}^{-1-m} \tag{3.17}$$

In Figure 3.3b, the observed $f(\psi)$ takes on a positive value as soon as ψ becomes less than zero. As ψ becomes small, $f(\psi)$ rises to a peak and then gradually declines. Each fitted curve produces an acceptable match with the observed $f(\psi)$. Table 3.2 shows that for this example, ψ_c was estimated to be zero, and ψ_0 (-31.8 cm) was estimated to be similar to ψ_{0V} (-33.3 cm). In the VG model, the bubbling pressure is absent, and ψ_{0V} is the mode of $f(\psi)$ and is therefore analogous to ψ_0 in the LN model. This can be confirmed by differentiating (3.17) and substituting $\psi = \psi_{0V}$ to show that indeed $f'(\psi_{0V}) = 0$. Consequently, it seems reasonable to assume that the VG model is analogous to the LN model under the restriction $\psi_c = 0$.

The accuracy of the LN model with the restriction $\psi_c = 0$ was tested with the 50 sets of retention data. The model contains two parameters ψ_0 and σ. In Figure 3.4, RSS_{VG} are compared with the RSS for the LN model with the restriction $\psi_c = 0$ (RSS_{LN2}). As expected, RSS_{VG} and RSS_{LN2} were similar. More precisely, the former values were a little lower than the latter values for most data sets. As shown in Figure 3.5, ψ_{0V} took on nearly the same value as ψ_0 of the LN model with the restriction $\psi_c = 0$ for most data sets. Figure 3.6 indicates that there is a negative correlation between the estimated m value and σ of the LN model with the restriction $\psi_c = 0$. In the VG or the LN model, the effective saturation at the inflection point on the θ-ψ curve depends only on m or σ. In the LN model with the restriction $\psi_c = 0$, $S_e(\psi_0)$ is also given by (3.15). Assuming that $S_e(\psi_0)$ and $S_e(\psi_{0V})$ expressed by (2.6) are the same, the relationship between m and σ is

$$\operatorname{erfc}\left(-\sigma/\sqrt{2}\right) = 2(1+m)^{-m} \tag{3.18}$$

A plot of (3.18), shown in Figure 3.6 by the solid line, predicts the estimated m-σ relationship well. The other expression for the m-σ relationship is obtained by assuming that the median of $f(\psi)$ based on the LN model with the restriction $\psi_c = 0$ (which is derived by substituting $\psi_c = 0$ into (3.12)) is the same as that based on the VG model (ψ_{mV}); ψ_{mV} is given by substituting $S_e = 0.5$ into (2.5):

$$\psi_{mV} = \psi_{0V}\left\{\left(2^{1/m}-1\right)/m\right\}^{1-m} \tag{3.19}$$

Hence the other expression is

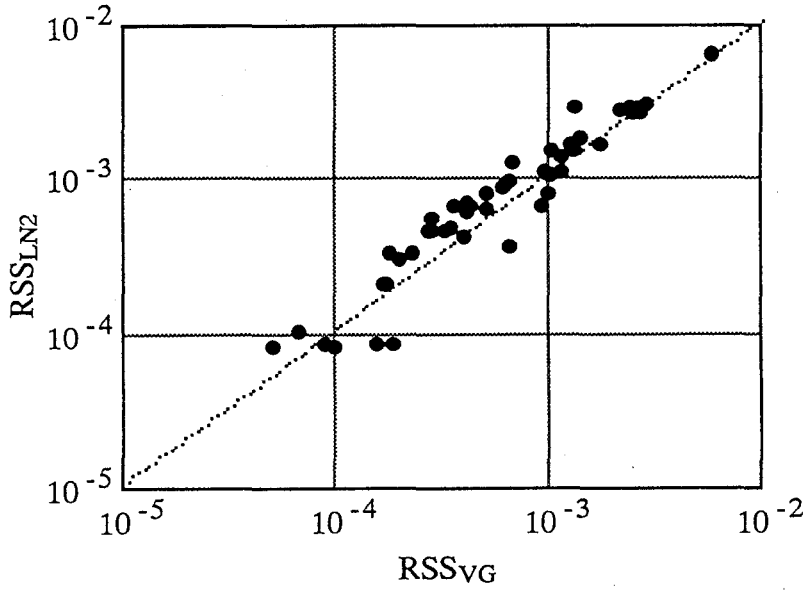

Figure 3.4 Comparison between computed residual sum of squares for the VG model (RSS_{VG}) and the LN model restricted to $\psi_c = 0$ (RSS_{LN2}).

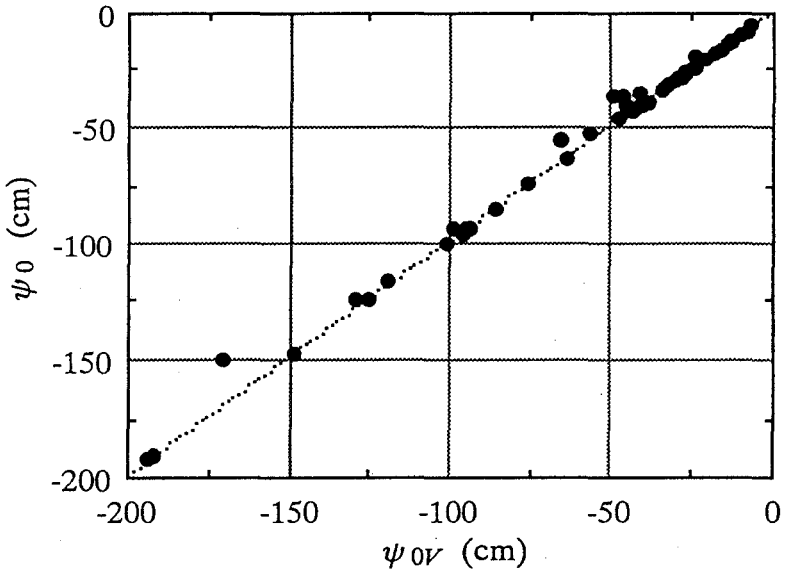

Figure 3.5 Comparison between estimated parameter ψ_{0V} of the VG model and ψ_0 of the LN model restricted to $\psi_c = 0$. Both ψ_{0V} and ψ_0 represent the capillary pressure at the inflection point on the fitted θ-ψ curve.

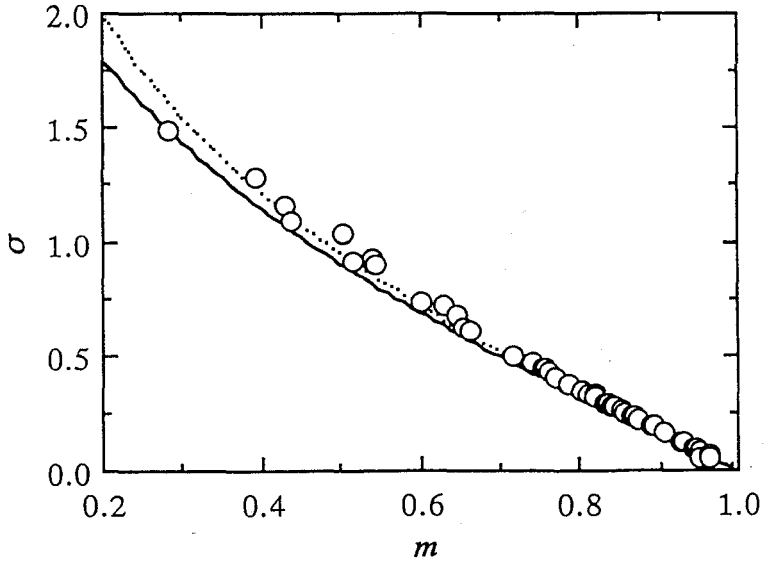

Figure 3.6 Relationship between estimated parameter m of the VG model and σ of the LN model restricted to $\psi_c = 0$. The solid line indicates the analytical m-σ relationship expressed as (3.18), and the dotted line indicates the analytical m-σ relationship expressed as (3.20).

$$\sigma^2 = (1-m)\ln\left\{\left(2^{1/m}-1\right)/m\right\} \tag{3.20}$$

A plot of (3.20), shown in Figure 3.6 by the dotted line, exhibits a slightly better fit than a plot of (3.18) at larger σ values. As a result, both (3.18) and (3.20) can be used for expressing the correlation between m and σ. Figures 3.4, 3.5, and 3.6 clearly show that the VG model is analogous to the LN model with the restriction $\psi_c = 0$.

Figure 3.3c shows a comparison between the observed $g(r)$ curve and fitted curves based on the VG and LN models using the parameters shown in Table 3.2. The observed $g(r)$ curve was derived by substituting into (3.3) both the observed $f(\psi)$ values shown in Figure 3.3b and (3.2) using the constant value of A = -0.149 cm^2. With the restriction $\psi_c = 0$ (i.e., $r_{max} \rightarrow \infty$), (3.7) is transformed as follows:

$$g(r) = \frac{\theta_s - \theta_r}{\sqrt{2\pi}\sigma r}\exp\left[-\frac{\left\{\ln r - \left(\ln r_0 - \sigma^2\right)\right\}^2}{2\sigma^2}\right] \tag{3.21}$$

where r_0 is the pore radius, which is related to ψ_0 by (3.2). Equation (3.21) represents a

simple two-parameter lognormal distribution since $\ln(r)$ obeys $N(\ln(r_0) - \sigma^2, \sigma^2)$. It can be seen from Figure 3.3c that the $g(r)$ curve based on the VG model, obtained by substituting (3.2) and (3.17) into (3.3), is similar to the lognormal distribution.

3.4.2 The BC Model Versus the LN Model

In Figure 3.7a the observed retention data set for Rubicon sandy loam [*Topp*, 1969] (Mualem's soil index 3501 [*Mualem*, 1976]) is compared with the fitted curves obtained by the BC and LN models. Estimated parameters are shown in Table 3.2. It can be seen that both the BC and the LN models match the observed curve equally well. In this example, the observed $f(\psi)$ curve shown in Figure 3.7b contrasts with the $f(\psi)$ curve shown in Figure 3.3b: $f(\psi)$ remains near zero when ψ is greater than the bubbling pressure, and then there is an immediate sharp increase followed by a gradual decline. Consequently, the bubbling pressure is nearly the same as the mode of $f(\psi)$. The expression for $f(\psi)$ based on the BC model, which performs quite well in Figure 3.7b, is given by differentiating (2.1) with respect to ψ to obtain

$$f(\psi) = \frac{(\theta_s - \theta_r)\lambda}{-\psi_{cB}}\left(\frac{\psi_{cB}}{\psi}\right)^{1+\lambda} \qquad \psi < \psi_{cB} \tag{3.22}$$

$$f(\psi) = 0 \qquad \psi \geq \psi_{cB}$$

A plot of (3.22) culminates at the bubbling pressure ψ_{cB} (in this example, ψ_{cB} = -67.6

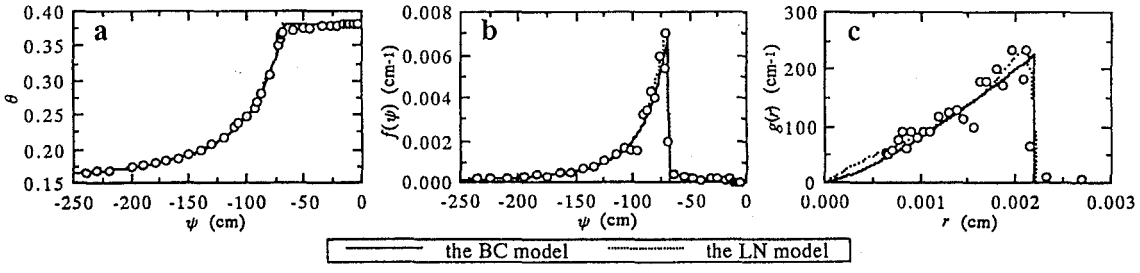

Figure 3.7 Observed and fitted (a) θ-ψ curves, (b) $f(\psi)$ curves, and (c) $g(r)$ curves for Rubicon sandy loam. Circles in Figures 3.7b and 3.7c are as defined in Figure 3.3.

cm). Figure 3.7b shows that (3.10) also produced acceptable results with an estimated ψ_c (-66.7 cm) that is nearly the same as the estimated ψ_0 (-70.6 cm). It therefore seems reasonable to conclude that the LN model corresponds to the BC model when $\psi_c \rightarrow \psi_0$.

Considering that the VG model is analogous to the LN model under the restriction $\psi_c = 0$, the ratio of ψ_c to ψ_0 can be used as an index to evaluate the relative accuracy of the VG and BC models. This ratio will be expressed as a dimensionless number ζ (i.e., $\zeta = \psi_c/\psi_0$). The VG model is expected to perform better than the BC model for a data set for which ζ is estimated to be about zero (i.e., $\psi_c \approx 0$), whereas the BC model is expected to perform better than the VG model for a data set for which ζ is estimated to be nearly 1 (i.e., $\psi_c \approx \psi_0$). The relationship between ζ and the ratio of RSS_{BC} to RSS_{VG} for the 50 sets of retention data is shown in Figure 3.8. As expected, the ratio decreases as ζ approaches 1. RSS_{VG} are lower than RSS_{BC} when ζ is less than about 0.7, and for most data sets, RSS_{BC} are lower than RSS_{VG} when $\zeta > 0.7$.

For the 18 retention data sets for which RSS_{BC} are lower than RSS_{VG}, the estimated ψ_{cB} and ψ_c values are mostly the same, whereas there is no apparent correlation between λ and σ, as shown in Figure 3.9. Figure 3.10 shows the correlation between λ and the standard deviation σ_ψ of $f(\psi)$, which is given by substituting estimated ψ_c, ψ_0, and σ values into (3.13). There is a negative correlation between λ and $\log(\sigma_\psi)$. By use of (3.11), (3.12), and (3.13), σ_ψ^2 is expressed as a function of ψ_c, ψ_a, and ψ_m:

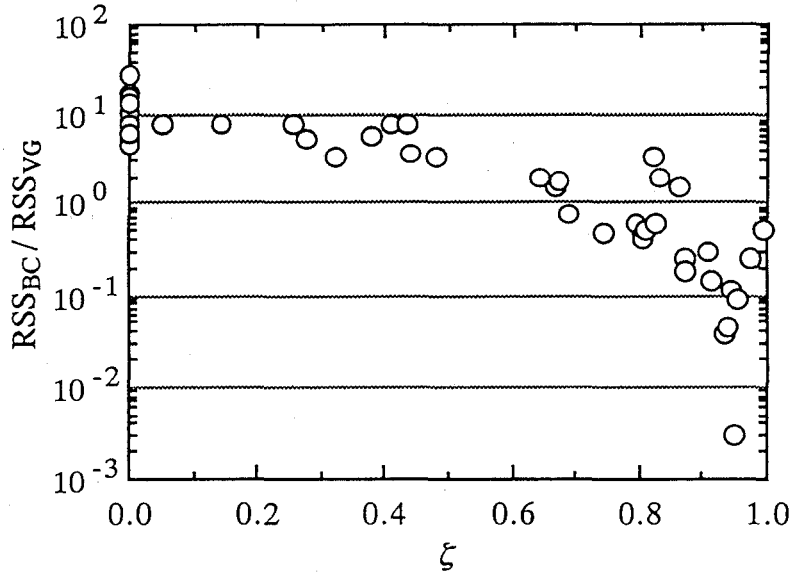

Figure 3.8 Relationship between computed ζ (= ψ_c/ψ_0) and the ratio of residual sum of squares (RSS) for the BC model (RSS_{BC}) to those for the VG model (RSS_{VG}).

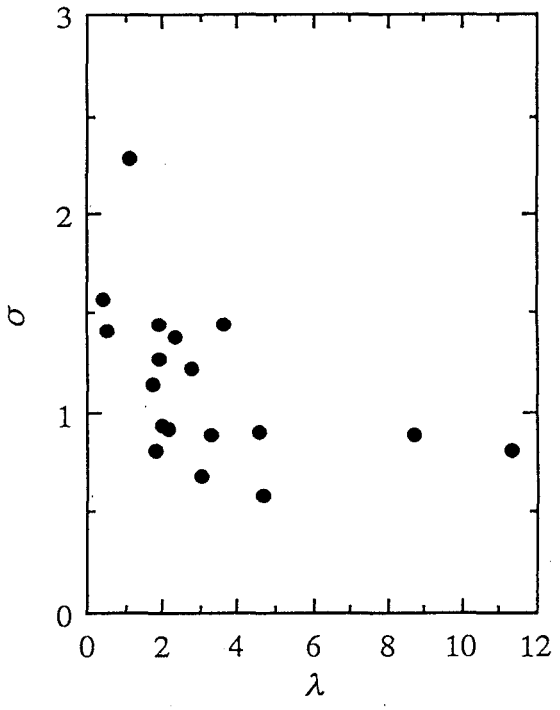

Figure 3.9 Relationship between estimated λ of the BC model and σ of the LN model for 18 retention data sets for which the BC model exhibited a better fit than the VG model.

$$\sigma_{\psi}^2 = (\psi_c - \psi_a)^2 \left\{ \left(\frac{\psi_c - \psi_a}{\psi_c - \psi_m} \right)^2 - 1 \right\} \tag{3.23}$$

The mean ψ_{aB} and the median ψ_{mB} of $f(\psi)$ expressed by (3.22) are

$$\begin{aligned} \psi_{aB} &= \psi_{cB}\lambda/(\lambda - 1) \qquad \lambda > 1 \\ \psi_{aB} &= -\infty \qquad\qquad\qquad 0 < \lambda \le 1 \end{aligned} \tag{3.24}$$

$$\psi_{mB} = 2^{1/\lambda}\psi_{cB} \tag{3.25}$$

Assuming that ψ_{cB}, ψ_{aB}, and ψ_{mB} are equal to ψ_c, ψ_a, and ψ_m, respectively, the following formula is obtained by substituting (3.24) and (3.25) into (3.23) when $\lambda > 1$:

$$\log(\sigma_{\psi}) = \log(-\psi_{cB}) + 0.5\log\left[(\lambda - 1)^{-1} \left\{ (\lambda - 1)^{-2} \left(1 - 2^{1/\lambda}\right)^{-2} - 1 \right\} \right] \tag{3.26}$$

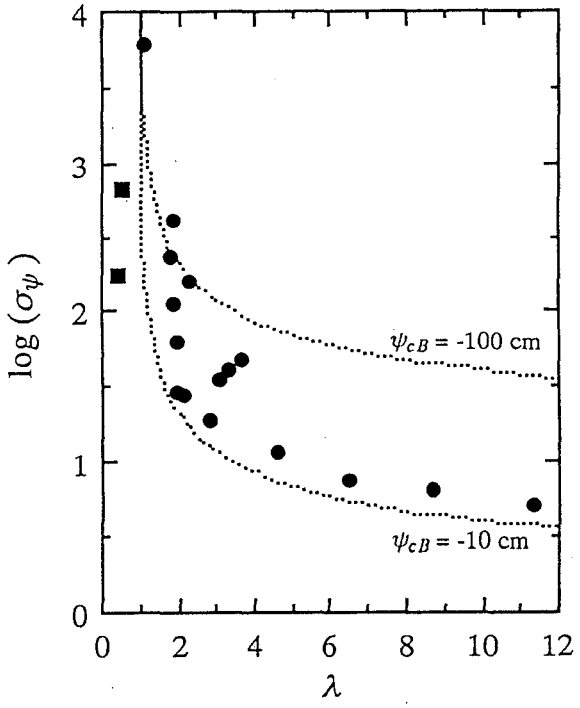

Figure 3.10 Relationship between estimated λ of the BC model and the standard deviation σ_ψ of $f(\psi)$ derived by substituting estimated ψ_c, ψ_0, and σ into (3.13). Squares and circles indicate data sets for which $\lambda \leq 1$ and $\lambda > 1$, respectively. Dotted lines indicate the analytical relationship expressed by (3.26) with ψ_{cB} = -10 cm and -100 cm.

Hence σ_ψ is related to both ψ_{cB} and λ. Plots of (3.26) for ψ_{cB} = -10 cm and ψ_{cB} = -100 cm are indicated by the dotted lines in Figure 3.10. Plots of the λ-log(σ_ψ) relationship for the 16 data sets (represented by circles in Figure 3.10) in which estimated λ values were greater than 1 and estimated ψ_{cB} values were in the range of about -10 to -100 cm are distributed between the two analytical curves. These results show that (3.26) is acceptable. As shown in Figure 3.10, the rate of change of σ_ψ with respect to λ is quite large when λ is in the range of 1 to 4.

Figure 3.7c shows a comparison of the observed $g(r)$ curve and fitted curves based on the BC and LN models with the parameters shown in Table 3.2. The $g(r)$ curve generated from the BC model is a power function, as already suggested by *Taylor et al.* [1990]. Figure 3.7c shows that the $g(r)$ curve corresponding to the LN model, which is expressed as (3.7), is similar to the power function in this example.

3.4.3 The TA Model Versus the LN Model

In Figure 3.11a, a typical retention data set for which the TA model performed best of all the two-parameter models (fragmented Fox Hill sandstone [*Brooks and Corey*, 1964]; Mualem's soil index 4132 [*Mualem*, 1976]) is compared with fitted curves generated by the TA and LN models. Both models performed quite well. On the basis of the TA model, the following expression for $f(\psi)$ is derived:

$$f(\psi) = \frac{(\theta_s - \theta_r)(\psi_{cT} - \psi)}{(\psi_{cT} - \psi_{0T})^2} \exp\left(-\frac{\psi_{cT} - \psi}{\psi_{cT} - \psi_{0T}}\right) \qquad \psi < \psi_{cT} \tag{3.27}$$

$$f(\psi) = 0 \qquad \psi \geq \psi_{cT}$$

Figure 3.11b shows that a plot of (3.27) using the parameters shown in Table 3.2 matches the observed $f(\psi)$ curve just as well as a plot of (3.10).

Equation (3.27) has two parameters, ψ_{cT} and ψ_{0T}, which correspond to the bubbling pressure ψ_c and the mode ψ_0 of the LN model, respectively. However, (3.27) has no dimensionless parameter corresponding to σ. Figure 3.12 shows the computed relationship between estimated σ and the ratio of RSS_{TA} to RSS_{LN} for the 50 sets of retention data. The ratio falls to a minimum of about 1 around $\sigma = 0.6$. That is, the TA model performs just as well as the LN model for the retention data set for which σ is estimated to be about 0.6. In the LN model, the effective saturation at the inflection point ($S_e(\psi_0)$) is a function of σ, whereas in the TA model, $S_e(\psi_{0T})$ takes on the constant value

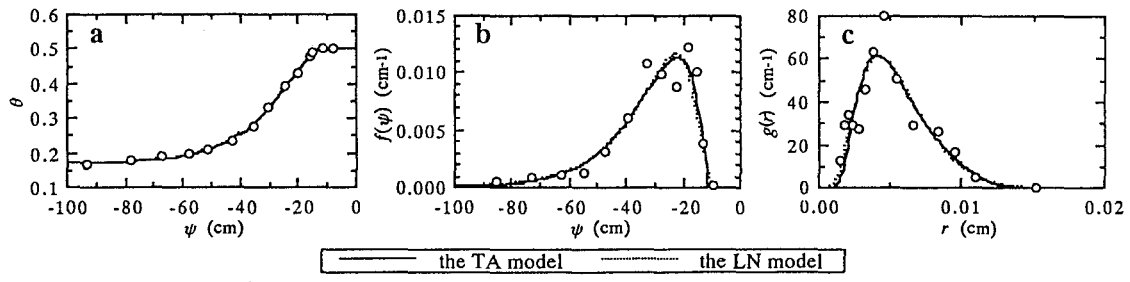

Figure 3.11 Observed and fitted (a) θ-ψ curves, (b) $f(\psi)$ curves, and (c) $g(r)$ curves for Fox Hill sandstone. Circles in Figures 3.11b and 3.11c are as defined in Figure 3.3.

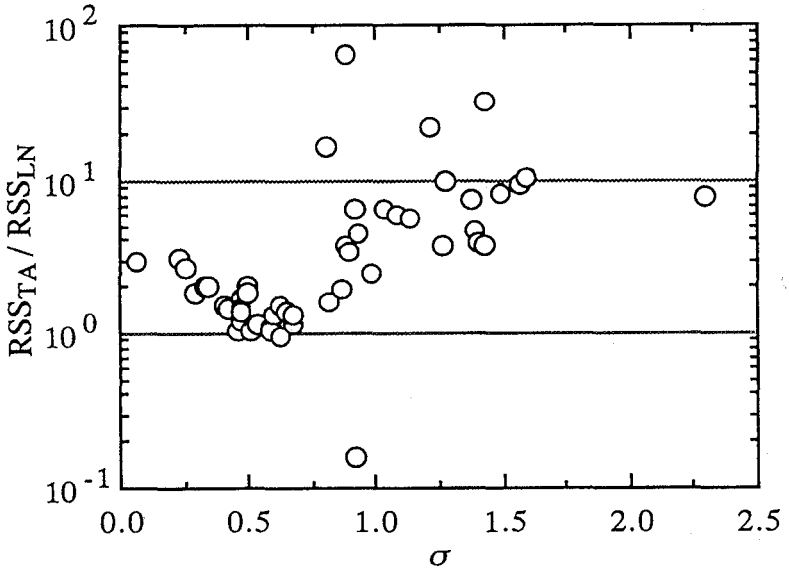

Figure 3.12 Relationship between estimated σ of the LN model and the ratio of residual sum of squares (RSS) for the TA model (RSS_{TA}) to those for the LN model (RSS_{LN}).

of $2e^{-1}$. Assuming that $S_e(\psi_{0T})$ is equal to $S_e(\psi_0)$,

$$\operatorname{erfc}\left(-\sigma/\sqrt{2}\right) = 4e^{-1} \tag{3.28}$$

The value of σ that satisfies (3.28) is about 0.62, at which the ratio RSS_{TA}/RSS_{LN} falls to almost the lowest point, as shown in Figure 3.12. In conclusion, it appears that the TA model is analogous to the LN model under the restriction $\sigma \approx 0.62$.

Figure 3.11c shows the observed $g(r)$ curve and two fitted curves based on the TA and LN models, both of which performed equally well.

3.4.4 Residual Water Content

In models for water retention, the concept of residual water content θ_r is an essential but problematic element. The nature of θ_r is still controversial: *Luckner et al.* [1989] suggested a physically based definition of θ_r, which was not widely accepted because it is not supported by observation [*Nimmo*, 1991]. Since most studies using θ_r treat it as a fitted parameter, its value depends on observed retention data (as has been pointed out by *Nimmo* [1991]) and on the adopted retention model itself.

In Figure 3.13, the difference between the estimated θ_r value for each two-parameter model and that for the LN model is related to the relative accuracy (expressed by the ratio of RSS) of each model. In Figure 3.13, the estimated θ_r for the VG, BC, TA, and LN models are called θ_{rVG}, θ_{rBC}, θ_{rTA}, and θ_{rLN}, respectively. It can be seen from Figure 3.13a that θ_{rVG} is similar to θ_{rLN} for the data sets for which the VG model performs well, although there are some exceptions. As RSS_{VG}/RSS_{LN} becomes higher, θ_{rVG} becomes greater than θ_{rLN}. On the other hand, Figure 3.13b shows that θ_{rBC} is smaller than θ_{rLN} for the data sets for which the BC model performs poorly, whereas θ_{rBC} takes on similar values to θ_{rLN} in the data sets for which the model produces a good fit. The relationship between θ_{rTA} - θ_{rLN} and the ratio RSS_{TA}/RSS_{LN} shown in Figure 3.13c is the same as that shown in Figure 3.13a: θ_{rTA} is similar to θ_{rLN} for the data sets for which RSS_{TA}/RSS_{LN} is lower, and θ_{rTA} becomes greater than θ_{rLN} as RSS_{TA}/RSS_{LN} increases. That is, when each two-parameter model produces a good fit with the observed data, the estimated θ_r for the model is similar to the estimated θ_r for the LN model. As a result, a general θ_r value can be estimated from observed retention data by using the LN model.

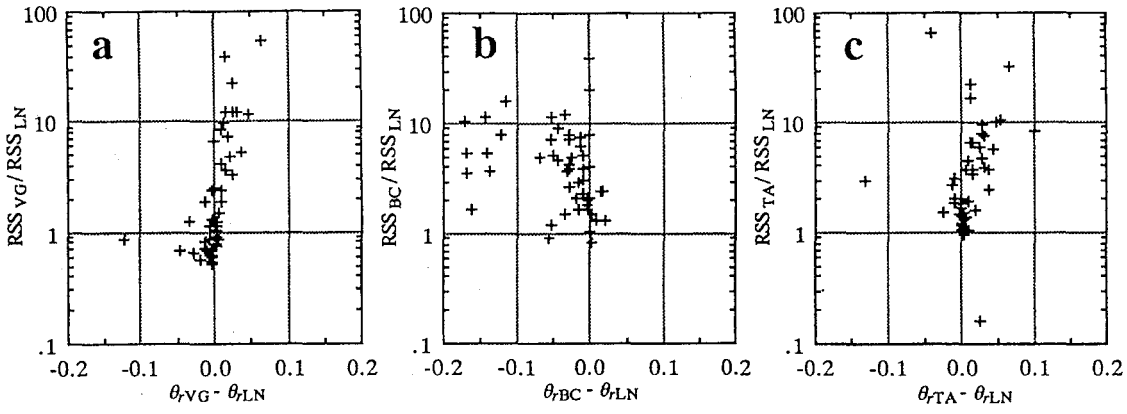

Figure 3.13 Ratios of residual sum of squares for each two-parameter retention model (RSS_{VG}, RSS_{BC}, and RSS_{TA}) to those for the LN model (RSS_{LN}) versus the difference between the estimated residual water content for each tow-parameter model and that for the LN model (θ_{rVG} - θ_{rLN}, θ_{rBC} - θ_{rLN}, and θ_{rTA} - θ_{rLN}). The parameters θ_{rVG}, θ_{rBC}, θ_{rTA}, and θ_{rLN} indicate estimated residual water contents for the VG, BC, TA, and LN models, respectively.

3.5 ESSENTIAL PARAMETERS FOR A GENERAL RETENTION MODEL

Figure 3.14 shows a scatterplot of the relationship between ζ, which was computed from estimated ψ_c and ψ_0 values, and the estimated σ value for each retention data set. Each plot symbol represents the two-parameter model that performed best of the three (VG, BC, and TA) for each data set. Most of the 26 points representing data sets for which the VG model presented the best fit are in the range $\zeta < 0.7$ and are widely scattered with respect to the σ axis. All 16 points representing data sets for which the BC model performed best are located in the region in which ζ is greater than about 0.7. Points associated with the data sets for which the TA model showed the best match are distributed along the line $\sigma = 0.62$ and take on ζ values from 0 to nearly 0.9. Both ζ and σ appear to be indexes for evaluating the relative accuracy of the existing two-parameter retention models.

On the basis of the LN model, the expression for the scaled retention curve is

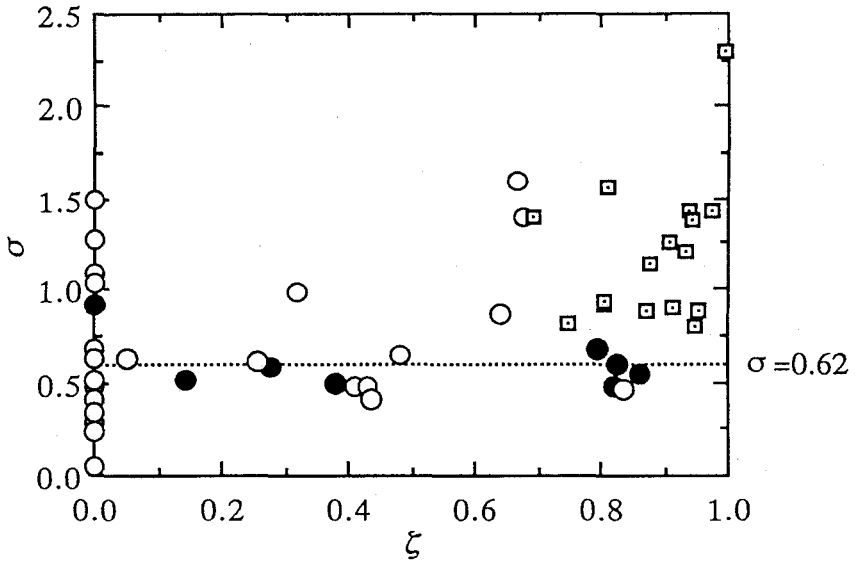

Figure 3.14 Relationship between computed ζ (= ψ_c/ψ_0) and estimated σ of the LN model. Open circles, squares, and solid circles indicate data sets for which the VG, BC, and TA models, respectively, exhibited the best fit of the two-parameter retention models.

$$S_e = \frac{1}{2}\mathrm{erfc}\left(\frac{\ln\{(\psi^* - \zeta)/(1-\zeta)\} - \sigma^2}{\sqrt{2}\sigma}\right) \qquad \psi^* > \zeta$$
$$S_e = 1 \qquad \psi^* \le \zeta \tag{3.29}$$

where ψ^* is the ratio of ψ to ψ_0 (i.e., $\psi^* = \psi/\psi_0$). It is clear that ζ and σ are parameters which characterize the scaled retention curve. The LN model presents great flexibility because it utilizes both variables ζ and σ. In each two-parameter model, there is a certain restriction on ζ or σ, which limits the flexibility of the model. Three parameters, the bubbling pressure, the mode of the pore capillary pressure distribution (identical to the capillary pressure at the inflection point on the θ-ψ curve), and the dimensionless parameter related to the width of the pore radius distribution, must be included in a general water retention model.

Despite its great flexibility, the LN model is not expressed as an elementary function and will therefore be limited in its use in models for processes in soils. Another expression for water retention, which has the same parameters as the LN model and can be expressed as an elementary function, is derived by modifying the VG model to include the bubbling pressure while conserving the nature of both ψ_{0v} and m:

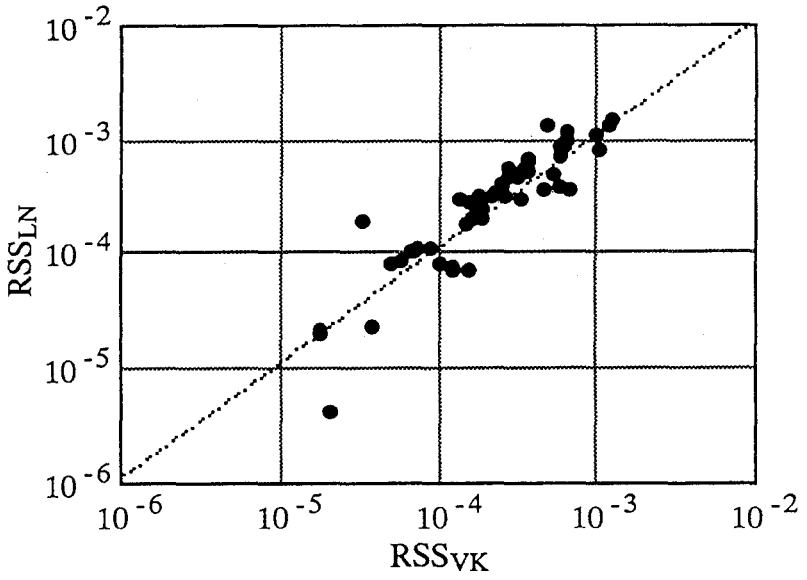

Figure 3.15 Comparison between computed residual sum of squares (RSS) for the VK model (RSS_{VK}) and those for the LN model (RSS_{LN}).

$$S_e = \left\{1 + m_K \left(\frac{\psi_{cK} - \psi}{\psi_{cK} - \psi_{0K}} \right)^{1/(1-m_K)} \right\}^{-m_K} \qquad \psi < \psi_{cK} \tag{3.30}$$

$$S_e = 1 \qquad \psi \geq \psi_{cK}$$

Equation (3.30) (referred to as the VK model) is identical to the VG model when the bubbling pressure, ψ_{cK}, is equal to 0. The ψ_{cK}, ψ_{0K}, and m_K of the VK model correspond to the above mentioned three parameters that are essential for a general retention model (see Table 3.1). In Figure 3.15, RSS for the VK model (RSS_{VK}) matched with the 50 sets of retention data are compared with RSS_{LN}. Figure 3.15 shows that the VK model performs as well as the LN model. The average RSS_{VK} value for 50 sets of data was 3.39 $\times 10^{-4}$, a little lower than that for RSS_{LN} (4.41×10^{-4}). Estimated parameters of the VK model for the retention curves plotted in Figures 3.3, 3.7, and 3.11 are shown in Table 3.2. The VK model was quite similar to the LN model for these curves. It should be noted that estimated θ_r values for the VK model were similar to those for the LN model, with the former values being a little lower than the latter ones in most data sets. Expressed as an elementary function, the VK model can be effectively used for modeling water movement in soils [e.g., *Kosugi and Fukushima*, 1994].

3.6 SUMMARY AND CONCLUSIONS

In this chapter, the water capacity function was regarded as the pore capillary pressure distribution function $f(\psi)$, which is related to the pore radius distribution function $g(r)$ by the capillary pressure function. By application of a three-parameter lognormal distribution to $g(r)$, an expression for $f(\psi)$ which has an alternative three-parameter lognormal distribution form was obtained. A new expression for the θ-ψ relationship was then derived which contains three parameters other than the saturated water content θ_s and the residual water content θ_r. These three parameters are the bubbling pressure ψ_c, the mode (ψ_0) of $f(\psi)$ (identical to the capillary pressure at the inflection point on the θ-ψ curve), and the standard deviation σ (dimensionless) of transformed $f(\psi)$, which describes the effective saturation at the inflection point and is related to the width of the pore radius distribution.

The accuracies of the proposed retention model (LN), the existing models of *van Genuchten* [1978, 1980] (VG) and *Brooks and Corey* [1964] (BC), and the modified *Tani* [1982] model (TA) were tested for 50 sets of observed retention data for various soils. Results showed the LN model to be very flexible. By comparing the estimated parameters of the LN model with those of the existing models, it was shown that the VG model is analogous to the LN model under the restriction $\psi_c = 0$, the BC model is similar to the LN model when $\psi_c \rightarrow \psi_0$, and the TA model is analogous to the LN model when σ is restricted to $\sigma \approx 0.62$. As a result, it was concluded that the three parameters corresponding to ψ_c, ψ_0, and σ must be included in a general retention model.

By comparison of the estimated θ_r for each existing model with the estimated θ_r for the LN model, it was shown that the former value is approximately the same as the latter one when the existing model performs as well as the LN model. Hence a general θ_r value can be estimated by using the LN model.

On the basis of the LN model, an expression for the scaled retention curve was proposed. The scaled retention curve is characterized by two dimensionless parameters, σ and ζ, which is the ratio of ψ_c to ψ_0. These parameters are indexes for evaluating the relative accuracies of the existing models.

Another retention model (VK), which contains the three essential parameters and performs as well as the LN model, was derived by modifying the VG model. Expressed as an elementary function, the VK model is useful for models for processes in soils.

In summary, this chapter proposed an expression for water retention which performs as well as any existing empirical model by applying a theoretical probability law. The proposed LN model produces acceptable results, and its parameters are directly related to the statistics of $f(\psi)$. This model and its parameters are analyzed in the following chapters connected to soil structure, texture, hydraulic conductivity, and water movement in unsaturated soil.

REFERENCES

Ahuja, L. R., and R. D. Williams, Scaling water characteristic and hydraulic conductivity based on Gregson-Hector-McGowan approach, *Soil Sci. Soc. Am. J.*, *55*(2), 308-319, 1991.

Aitchison, J., and J. A. C. Brown., *The Lognormal Distribution*, Cambridge University Press, Cambridge, England, 1957.

Brooks, R. H., and A. T. Corey, Hydraulic properties of porous media, *Hydrol. Pap. 3*, Civil Eng. Dept., Colo. State Univ., Fort Collins, 1964.

Brutsaert, W., Probability laws for pore-size distributions, *Soil Sci., 101*, 85-92, 1966.

Carsel, R. F., and R. S. Parrish, Developing joint probability distribution of soil water retention characteristics, *Water Resour. Res., 24*(5), 755-769, 1988.

Clausnitzer, V., J. W. Hopmans, and D. R. Nielsen, Simultaneous scaling of soil water retention and hydraulic conductivity curves, *Water Resour. Res., 28*(1), 19-31, 1992.

Jury, W. A., W. R. Gardner, and W. H. Gardner, *Soil Physics*, Wiley, New York, 1991.

King, L. G., Description of soil characteristics for partially saturated flow, *Soil Sci. Soc. Am. Proc., 29*, 359-362, 1965.

Klute, A., and D. F. Heermann, Soil water profile development under a periodic boundary condition, *Soil Sci., 117*, 265-271, 1974.

Kosugi, K., and Y. Fukushima, Estimation of evapotranspiration at alfalfa field on irrigated land in arid district, *J. Jpn. Soc. Hydrol. Water Resour., 7*(5), 420-429, 1994.

Laliberte, G. E., A mathematical function for describing capillary pressure-desaturation data, *Bull. Int. Ass. Sci. Hydrol., 14*(2), 131-149, 1969.

Luckner, L., M. Th. van Genuchten, and D. R. Nielsen, A consistent set of parametric models for the two-phase flow of immiscible fluids in the subsurface, *Water Resour. Res., 25*(10), 2187-2193, 1989.

Marquardt, D. W., An algorithm for least-squares estimation on non-linear parameters, *J. Soc. Ind. Appl. Math.*, *11*, 431-441, 1963.

McCuen, R. H., W.J. Rawls, and D. L. Brakensiek, Statistical analysis of the Brooks-Corey and the Green-Ampt parameters across soil textures, *Water Resour. Res.*, *17*(4), 1005-1013, 1981.

Mualem, Y., A catalogue of the hydraulic properties of unsaturated soils, *Proj. 442*, 100 pp., Technion-Israel Inst. of Technol., Haifa, Israel, 1976.

Nimmo, J. R., Comment on the treatment of residual water content in "A consistent set of parametric models for the two-phase flow of immiscible fluids in the subsurface" by L. Luckner et al., *Water Resour. Res.*, *27*(4), 661-662, 1991.

Russo, D., and M. Bouton, Statistical analysis of spatial variability in unsaturated flow parameters, *Water Resour. Res.*, *28*(7), 1911-1925, 1992.

Shirazi, M. A., and L. Boersma, A unifying quantitative analysis of Soil Texture, *Soil Sci. Soc. Am. J.*, *48*., 142-147, 1984.

Stauffer, F., H. J. Franke, and T. Dracos, Hysteretic storativity concept for aquifer simulation, *Water Resour. Res.*, *28*(9), 2307-2314, 1992.

Tani, M., The properties of a water-table rise produced by a one-dimensional, vertical, unsaturated flow (in Japanese with English summary), *J. Jpn. For. Soc.*, *64*, 409-418, 1982.

Taylor, S. W., P. C. D. Milly, and P. R. Jaffe, Biofilm growth and the related changes in the physical properties of a porous medium, 2., permeability, *Water Resour. Res.*, *26*(9), 2161-2169, 1990.

Topp, G. C., Soil-water hysteresis measured in a sandy loam and compared with the hysteretic domain model, *Soil Sci. Soc. Am. Proc.*, *33*, 645-651, 1969.

Tyler, S. W., and S. W. Wheatcraft, Fractal processes in soil water retention, *Water Resour. Res.*, *26*(5), 1047-1054, 1990.

van Genuchten, M. Th., A closed-form equation for predicting the hydraulic conductivity of unsaturated soils, *Soil Sci. Soc. Am. J.*, *44*(5), 892-898, 1980.

van Genuchten, M. Th., and D. R. Nielsen, On describing and predicting the hydraulic properties of unsaturated soils, *Ann. Geophys.*, *3*(5), 615-628, 1985.

van Genuchten, R., Calculating the unsaturated hydraulic conductivity with a new closed-form analytical model, *Res. Rep. 78-WR-08*, Dept. of Civil Eng., Princeton, N. J., 1978.

Wierenga, P. J., R. G. Hills, and D. B. Hudson, The Las Cruces trench site: Characterization, experimental results, and one-dimensional flow predictions, *Water Resour. Res.*, *27*(10), 2695-2705, 1991.

CHAPTER 4

ANALYSIS OF WATER RETENTION CHARACTERISTIC OF FOREST SOIL WITH THREE-PARAMETER LOGNORMAL DISTRIBUTION MODEL

4.1 INTRODUCTION

In recent years, many observations of the moisture characteristics of forest soils have been made for the purpose of evaluating the soil pore radius (size) distribution. *Mashimo* [1960] observed the relationship between the volumetric water content θ and the capillary pressure ψ of soil samples collected from 10 forests, and proposed that soil pores be classified as either coarse or fine. He defined coarse pores as those in which water is retained by a capillary pressure greater than -500 cm (that is, pF 2.7). This definition has been used widely in analyses of forest soil pore radius distribution [e.g., *Kumlung and Takeda*, 1991; *Ogasiwa et al.*, 1991a, 1991b]. By comparing observed θ-ψ curves, *Ohta et al.* [1985] showed that the moisture characteristics of forest soils are different from those of undeveloped field soils. *Ohte and Suzuki* [1990] proposed a method for determining the θ-ψ curve using a large-size sample of undisturbed forest soil. The θ-ψ curves obtained with this method revealed that many macropores exist in forest soils. *Kosugi and Ohte* [1992] computed pore radius distributions from observed θ-ψ curves and showed that forest soil has many macropores whose radii are greater than 0.1 mm.

The moisture characteristic is one of the fundamental relations in the physical analysis of water flow in unsaturated soil. As reviewed in Chapter 2, many functions for expressing the θ-ψ curve have been proposed for modeling purposes. Recently, some of these water retention models have been used to analyze water-related phenomena on mountainous watersheds. *Ohte* [1992] analyzed vertical unsaturated flow in a forest soil column using a retention model developed by *Brooks and Corey* [1964]. *Tani* [1982] developed a retention model with a relatively simple functional form. Using this model, he analyzed properties of one-dimensional unsaturated flow in a soil column [*Tani*, 1985]. The Tani model has been used to analyze water flow on forestal hillslopes [*Suzuki*, 1984; *Tsuboyama and Sammori*, 1989]. *Sammori and Tsuboyama* [1990] adopted a retention

model developed by *van Genuchten* [1980] to analyze slope stability taking infiltration phenomena into consideration.

Despite their usefulness, these retention models are empirical curve fitting equations which are applicable only to specific media. They do not emphasize the physical significance of their empirical parameters and do not have sufficient flexibility. Hence, they cannot be used for comparative analyses of the moisture characteristics of various soils. The purpose of this chapter is to analyze the moisture characteristics of different forest soils using the LN model (expressed as (3.14)), which was developed by applying a three-parameter lognormal distribution law to the soil pore radius distribution.

It was shown in the previous chapter that the LN model exhibits sufficient flexibility to accommodate retention curves of various soils taken from *Mualem*'s [1976] catalogue. Parameters of this model have physical significance on the θ-ψ curve and are related closely to the statistics of the pore capillary pressure distribution function $f(\psi)$ which is identical to the water capacity function and which is related to the pore radius distribution function $g(r)$ by the capillary pressure function. In this chapter, the accuracy of the LN model is verified for observed retention data sets of 24 forest soils and 16 undeveloped field soils as well as for data sets of 60 disturbed soils, 20 and 40 of which are loamy and sandy soils, respectively. The typical θ-ψ curve of forest soil is compared to the typical θ-ψ curves of loamy soil, sandy soil, and undeveloped field soil by analyzing estimated parameters of the LN model. From estimated parameters of this model, the standard deviation and the median of the pore capillary pressure distribution are derived. Using these two parameters, the pore capillary pressure distributions of forest soils are compared to those of loamy soils, sandy soils, and undeveloped field soils.

4.2 MATERIALS AND METHODS

Observed retention data sets of 100 soils were analyzed with the proposed LN model, which is expressed as

$$S_e = \frac{1}{2}\mathrm{erfc}\left(\frac{\ln\{(\psi_c-\psi)/(\psi_c-\psi_0)\}-\sigma^2}{\sqrt{2}\sigma}\right) \qquad \psi < \psi_c \tag{3.14}$$

$$S_e = 1 \qquad \psi \geq \psi_c$$

Table 4.1 summarizes sampling sites and soil types. Most of the retention data sets of the forest soils and the undeveloped field soils were obtained using 100 ml cylindrical samples. The sampling sites of these soils are shown in Figure 4.1.

The Kiryu watershed is situated in hills consisting of weathered granite in the southern part of Shiga Prefecture in Japan. Hillside works and planting were conducted in 1897 and 1916, so that the area now is covered with a closed forest of Japanese red pine (*Pinus densiflora* S. et Z.) and Japanese cypress (*Chamaecyparis obtusa* (S. et Z.) ENDL.). Retention data sets of 17 soils of this watershed were analyzed. Thirteen of them

Table 4.1 List of Sampling Sites and Soil Types of the 100 Soils Analyzed with the LN Model

Sampling Site	Soil Type	Number of Data Sets	Code[*1]
Kiryu	Forest soils[*2]	9	Fa1
	Forest soils[*3]	4	Fa2
	Undeveloped soils	4	Ua
Plots Nos. 12 and 14[*4]	Forest soils	7	Fb
	Undeveloped soils	6	Ub
Plot No. 17[*4]	Forest soils	2	Fc
	Undeveloped soils	6	Uc
Toinotani	Forest soils	2	Fd
Mualem's catalogue	Loamy soils[*5]	20	
	Sandy soils[*5]	40	

[*1] Used in Figures 4.2, 4.3, 4.5, 4.6, and 4.7.
[*2] Taken with 100 ml small-size samplers.
[*3] Taken with large-size samplers (diameter 19.5 cm, length 10.0 cm).
[*4] Plot (s) on the hillslope at the Rolling Land Laboratory.
[*5] Pertains to disturbed soils.

were data sets of forest soils. Nine forest soil samples of 100 ml volume were taken from top soil (10 ~ 30 cm deep from the surface). Four sets of data were obtained by *Ohte and Suzuki* [1990] using large-size forest soil samples (diameter 19.5 cm, length 10.0 cm). Four sets of data were of disturbed forest soils (presented by *Ohte and Suzuki* [1990]) including three sets of data obtained using large-size samples. On the Kiryu watershed, where there was considerable soil erosion in the 1800's, disturbed forest soils can be regarded as undeveloped field soils.

Ohta et al. [1985] presented retention data sets of 21 soils taken from a hillslope at the Rolling Land Laboratory of Tokyo University of Agriculture and Technology. This hillslope is covered with a closed forest of predominately konara (*Quercus serrata* THUNB.) and kunugi (*Quercus acutissima* CARR.). The Rolling Land Laboratory is situated in the Tama Hills in Japan (see Figure 4.1). The soil samples were taken at three plots (Nos. 12, 14, and 17) on a hillslope. Plots Nos. 12 and 14 are located on the Gotentoge gravel stratum overlaid with top soil of 40 cm depth. Seven sets of data were of forest soils taken from the top soil, and six were of undeveloped soils taken from the

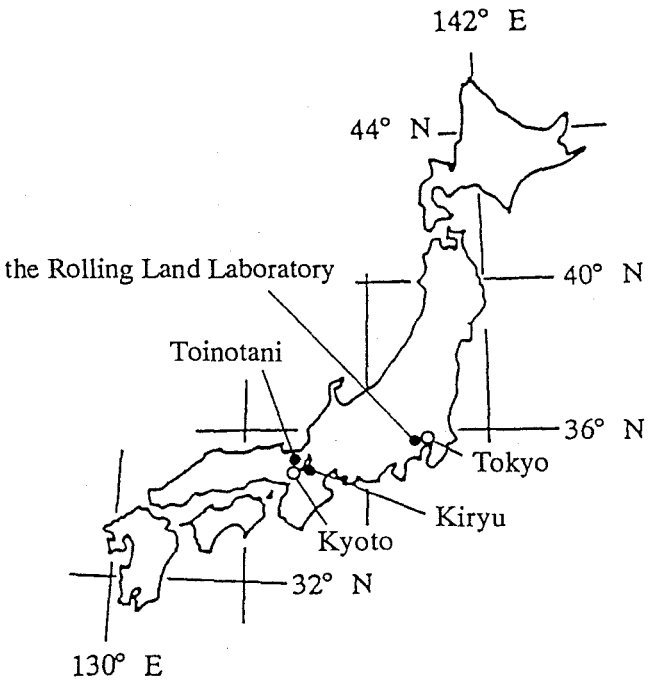

Figure 4.1 Sampling sites.

Gotentoge gravel stratum. Plot No. 17 is located on the Tama loam stratum overlaid with top soil of 20 cm depth. Two sets of data were of forest soils taken from the top soil, and six were of undeveloped soils taken from the Tama loam stratum.

Retention data sets of two forest soils on the Toinotani watershed of the Kyoto University Forest in Ashu were analyzed. This forest is situated in the northeastern part of Kyoto Prefecture in Japan (see Figure 4.1). The Toinotani watershed is covered with a closed forest of predominately sugi (*Cryptomeria japonica* D. DON) and mizume (*Betula grossa* S. et Z.), and is situated in the paleozoic-mesozoic hills [*Fukushima et al.*, 1979]. Two undisturbed soil samples were taken from top soil (10 cm deep from the surface).

Retention data sets of 60 soils were taken from the catalogue of *Mualem* [1976]. Most of the data sets listed in this catalogue pertain to laboratory experiments involving disturbed soils [*van Genuchten and Nielsen*, 1985]. Twenty soils were classified as loamy, and 40 soils were classified as sandy.

A nonlinear least squares optimization procedure based on Marquardt's maximum neighborhood method [*Marquardt*, 1963] was used to analyze the observed retention data sets. Applying Marquardt's method, θ_r, ψ_c, ψ_0, and σ in (3.14) were treated as the fitted parameters. Values of θ_s of the loamy and sandy soils were taken from Mualem's catalogue. Values of θ_s of the forest soils and the undeveloped field soils were obtained assuming that θ_s values are equal to porosities. Because this assumption is not always

true, especially for field soils [*Mashimo*, 1960], θ_s was treated as one of the fitted parameters for most of the data sets of the forest soils and the undeveloped field soils. Values of θ_s presented by *Ohte and Suzuki* [1990] were used for seven sets of data of soils taken with large-size samplers at Kiryu because there was a lack of near saturation data.

4.3 RESULTS

4.3.1 Model Validation Tests

To verify the accuracy of the LN model, the average residual (AR) of the fitted versus observed water contents was used. Value of AR was computed for each data set using the following equation:

$$AR = \sum_{i=1}^{N} \left| \theta_i^{fit} - \theta_i^{obs} \right| / N \qquad (4.1)$$

where θ^{fit} and θ^{obs} correspond to the fitted and observed water contents, respectively, and

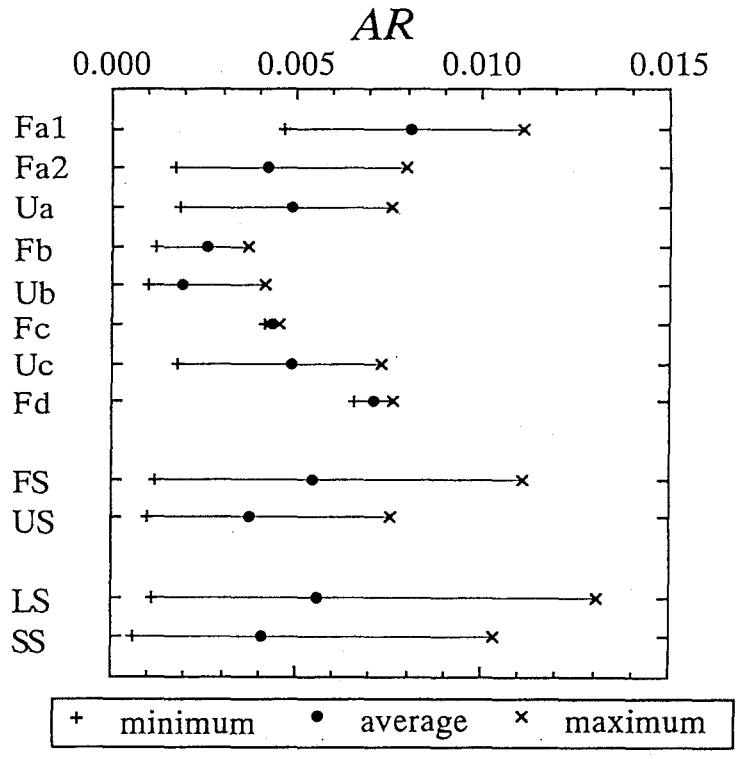

Figure 4.2 Average value and deviation of AR (average residual) for each type of soil. FS, US, LS, and SS represent forest soil, undeveloped field soil, loamy soil, and sandy soil, respectively. Other soil type codes are summarized in Table 4.1.

N is the number of data. It has been shown in Chapter 3 that the LN model performs quite well for the data sets of the loamy and sandy soils in Mualem's catalogue.

Figure 4.2 shows the computed maximum, minimum, and average AR values for each type of soil. It is clear from the figure that the loamy soils (LS) and the sandy soils (SS) have fairly small average AR values. Maximum AR values for the loamy and sandy soils are about 0.013 and 0.010, respectively, both of which appear to be sufficiently small. The forest soils taken with small-size samplers at Kiryu (Fa1) and the forest soils at Toinotani (Fd) have slightly greater average AR values than the loamy and sandy soils. Nevertheless, AR values of these forest soils are still in the small range of about 0.005 to 0.011. The forest soils taken with large-size samplers at Kiryu (Fa2) and the two types of forest soils taken at the Rolling Land Laboratory (Fb and Fc) have smaller average AR values than the loamy soils. The average AR value for all the forest soils (FS in Figure 4.2) is as small as that for the loamy soils. Every type of undeveloped field soil has an average AR value smaller than 0.005. The average AR value for all the undeveloped field soils (US in Figure 4.2) is smaller than that for the sandy soils. As a result, it can be concluded that the LN model produces acceptable matches for the retention data sets of the forest soils and the undeveloped field soils as well as for the data sets of the loamy and sandy soils.

4.3.2 Fitted Versus Observed Retention Curves

In Figure 4.3, twenty-one sets of observed retention data of the forest soils and undeveloped field soils are compared with the fitted curves generated by (3.14). It is clear that the LN model performed quite well for each data set. Note that the LN model produced acceptable results for 19 sets of data of the forest soils and undeveloped field soils which are not shown in this figure.

Figure 4.3a shows retention data sets of three forest soils taken from the top soil (10, 20, and 30 cm deep from the surface) at Kiryu. The shapes of the three θ-ψ curves resemble each other. In Figure 4.3b, the data set of the undeveloped soil at Kiryu is compared with the data set of the forest soil taken at a depth of 10 cm (the same data set as shown in Figure 4.3a). The θ-ψ curve of the undeveloped soil has a distinct bubbling pressure, whereas the θ-ψ curve of the forest soil has large changes in θ in the range of $\psi > -30$ cm. Figures 4.3c and 4.3d show four sets of data obtained using large-size samples of forest soils and undeveloped soils at Kiryu. The forest soils have rather large changes in θ when ψ is greater than -30 cm. Figures 4.3e and 4.3f show retention curves of soils on plots Nos. 12 and 14, respectively, at the Rolling Land Laboratory. The θ-ψ curves of the three forest soils, which are represented by black dots and black triangles, resemble each other. The θ-ψ curves of the four undeveloped soils taken from the Gotentoge gravel stratum have rather small changes in θ. Four sets of retention data of soils from plot No. 17 at the Rolling Land Laboratory are shown in Figure 4.3g. The θ-ψ curves of the two forest soils are similar to those of the forest soils of plots Nos. 12

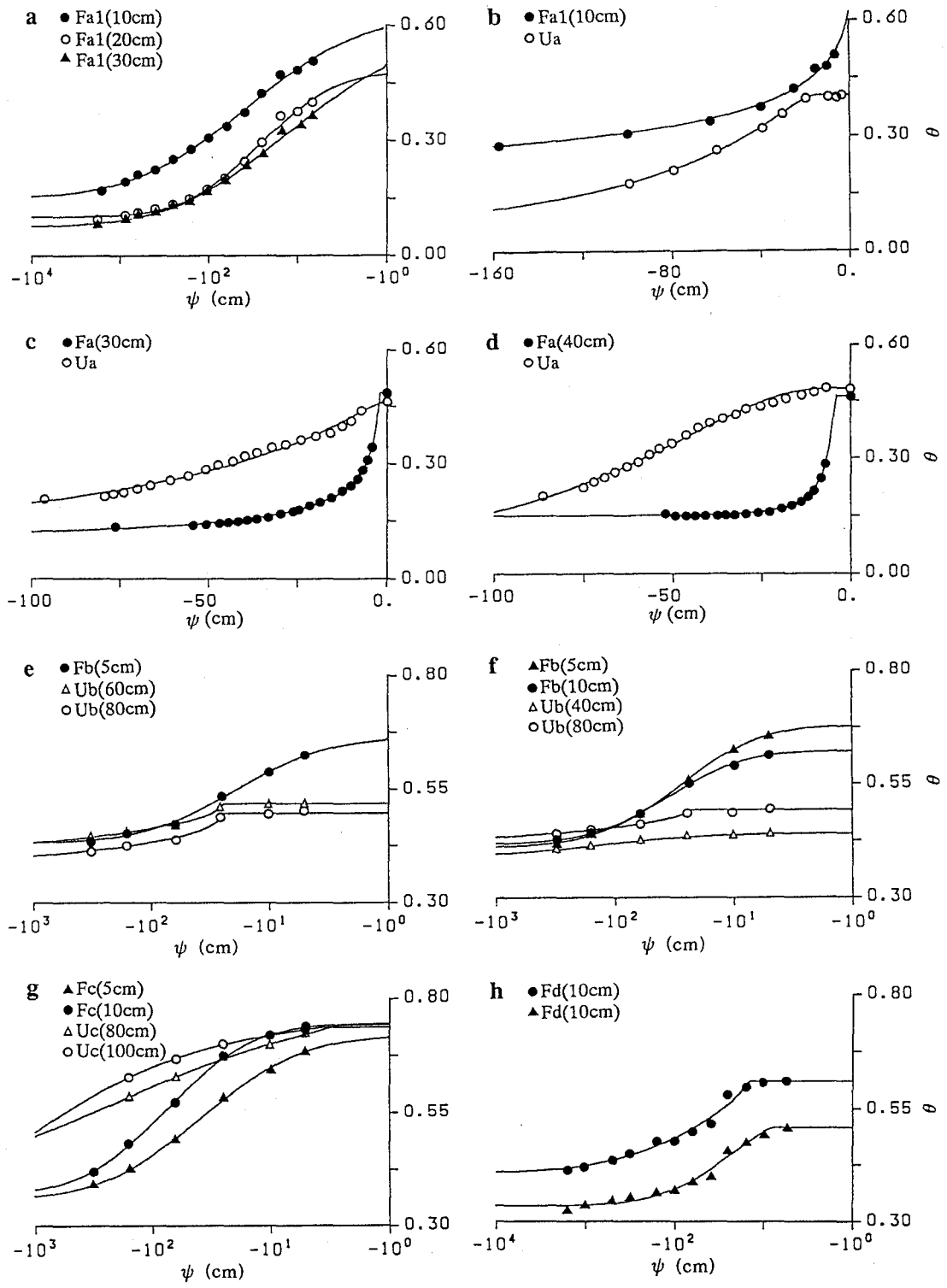

Figure 4.3 Observed and fitted θ-ψ curves of 12 forest soils and nine undeveloped field soils. Fitted curves were generated with the LN model. Soil type codes are summarized in Table 4.1. Numbers in parentheses represent depths of soil sampling.

and 14 shown in Figures 4.3e and 4.3f. Two undeveloped soils taken from the Tama loam stratum have larger θ values than the forest soils in the range of $\psi < -10^{1.5}$ cm. Retention data sets of two forest soils at Toinotani are shown in Figure 4.3h. The shapes of the two θ-ψ curves resemble each other, while the θ value corresponding to each ψ value of one sample is more than that of the other sample.

4.3.3 Estimated Parameters

Table 4.2 summarizes the average values of the estimated parameters (θ_s, θ_r, ψ_c, ψ_0, and σ) for the retention data sets of 24 forest soils, 16 undeveloped field soils, 20 loamy soils, and 40 sandy soils. Values of $S_e(\psi_0)$ in the table were obtained by substituting average σ values into (3.15). Average ψ_a, ψ_m, and σ_ψ values are included in the table. The ψ_a, ψ_m, and σ_ψ values of each retention data set were computed by substituting estimated ψ_c, ψ_0, and σ values into (3.11), (3.12), and (3.13), respectively:

$$\psi_a = \psi_c - (\psi_c - \psi_0)\exp(3\sigma^2/2) \tag{3.11}$$

$$\psi_m = \psi_c - (\psi_c - \psi_0)\exp(\sigma^2) \tag{3.12}$$

Table 4.2 Average Values of the Estimated Parameters of the LN Model

Soil Type	Forest soils		Undeveloped soils		Loamy soils		Sandy soils	
Number of Data Sets	24		16		20		40	
θ_s	0.558	(0.091)	0.570	(0.135)	0.458[*1]	(0.052[*1])	0.345[*1]	(0.083[*1])
θ_r	0.240	(0.144)	0.208	(0.192)	0.129	(0.084)	0.062	(0.053)
ψ_c, cm	-2.25	(3.56)	-9.17	(10.7)	-53.1	(58.1)	-25.6	(38.7)
ψ_0, cm	-5.03	(4.30)	-25.0	(35.1)	-82.1	(53.7)	-47.8	(42.0)
σ	1.73	(0.481)	2.22	(0.805)	1.57	(0.823)	0.758	(0.547)
$S_e(\psi_0)$[*2]	0.958	···	0.987	···	0.942	···	0.776	···
ψ_a[*3], cm	-171	(173)	-98000	(328000)	-58500	(173000)	-34700	(216000)
ψ_m[*3], cm	-27.6	(16.2)	-531	(1210)	-375	(558)	-157	(631)
$\log\sigma_\psi$[*3]	2.67	(0.826)	4.59	(1.76)	3.44	(1.84)	1.47	(1.26)

Numbers in parentheses represent standard deviation of parameter.
[*1] Obtained from θ_s values taken from Mualem's catalogue [*Mualem*, 1976].
[*2] Derived by (3.15) using average σ values.
[*3] Values of ψ_a, ψ_m, and σ_ψ were derived by (3.11), (3.12), and (3.13), respectively, using estimated ψ_c, ψ_0, and σ values.

$$\sigma_\psi{}^2 = (\psi_c - \psi_0)^2 \exp(3\sigma^2)\{\exp(\sigma^2) - 1\} \quad (3.13)$$

The table also contains the standard deviation of each parameter. It should be noted that the geometric mean was used for σ_ψ because some data sets had rather large σ_ψ values.

Table 4.2 indicates that the θ_s values of most forest soils were estimated to be more than the measured θ_s values of the loamy and sandy soils. Values of θ_r of the forest soils are more than those of the loamy and sandy soils. The sandy soils have the smallest θ_r values. The forest soils have the largest average ψ_c and ψ_0 values, and the loamy soils have the smallest values. The average σ value of the forest soils is as large as that of the loamy soils, and is more than that of the sandy soils. Consequently, average $S_e(\psi_0)$ values of the forest soils and the loamy soils are more than 0.9, whereas the sandy soils have the smaller average $S_e(\psi_0)$ value of 0.776. The forest soils have the largest average ψ_a and ψ_m values, and the sandy soils have the second largest values. The average σ_ψ value of the forest soils is more than that of the sandy soils and less than that of the loamy soils.

The average θ_s and θ_r values of the undeveloped field soils are about the same as those of the forest soils, and the average ψ_c and ψ_0 values of the former are a little smaller than those of the latter. The undeveloped field soils have the largest average σ and σ_ψ values and the smallest average ψ_a and ψ_m values. The standard deviation of every parameter of the forest soils is less than that of the undeveloped field soils. This indicates that the θ-ψ curves of the forest soils, which have been developed from soils having peculiar θ-ψ curves, resemble each other.

4.4 DISCUSSION

4.4.1 Comparison of the Water Retention Curves

Figure 4.4a shows typical θ-ψ curves of forest soil, loamy soil, and sandy soil. Each curve was generated by (3.14) using the average values of the estimated parameters shown in Table 4.2. The black dot on each curve indicates the end of the air entry region. The air entry region corresponds to the region where ψ changes but θ does not change [*Jury et al.*, 1991]. The plus sign on each curve indicates the inflection point.

Forest soil has the largest θ_s value of 0.56. Value of ψ_c of forest soil is nearly equal to zero indicating that the air entry region is quite narrow. Value of ψ_0 of forest soil is only 2.7 cm less than ψ_c. The θ value at the inflection point on the curve is nearly the same as θ_s because of the large value of σ. Hence, the inflection point is close to the end of the air entry region. Consequently, the θ-ψ curve has large changes in θ as soon as ψ becomes less than ψ_c. The rate of change of θ at the inflection point is 5.91×10^{-3} cm^{-1}. The large changes in θ continue until ψ reaches about -30 cm, then θ decreases gradually as ψ further decreases.

The θ_s value of loamy soil is 0.1 less than that of forest soil. Loamy soil has the smallest ψ_c value and the widest air entry region. Value of ψ_0 of loamy soil is about 30

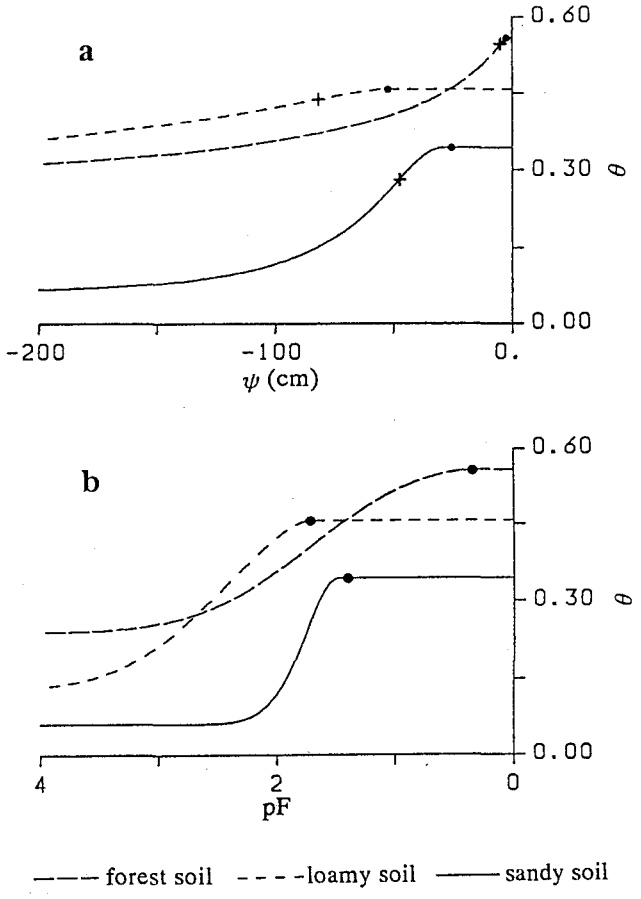

Figure 4.4 Typical (a) θ-ψ curves and (b) θ-pF curves of forest soil, loamy soil, and sandy soil. Black dot on each curve in Figures 4.4a and 4.4b indicates the end of the air entry region. Plus sign on each curve in Figure 4.4a indicates the inflection point.

cm less than ψ_c. Value of σ of loamy soil is as large as σ of forest soil, which makes the θ value at the inflection point nearly the same as θ_s. As a result, the rate of change of θ at the inflection point is quite small (8.41×10^{-4} cm^{-1}). The θ-ψ curve of loamy soil has consistently small decreases in θ as ψ decreases.

Sandy soil has the mid ψ_c value of -25.6 cm. Value of ψ_0 of sandy soil is about 22 cm less than ψ_c. The σ value of sandy soil is small compared to σ of forest soil and loamy soil. It results in a small θ value at the inflection point, which is about 0.1 less than θ_s. The rate of change of θ at the inflection point is 5.03×10^{-3} cm^{-1} which is as great as that of forest soil and is much greater than that of loamy soil. Decreases in θ are small when ψ is less than -150 cm.

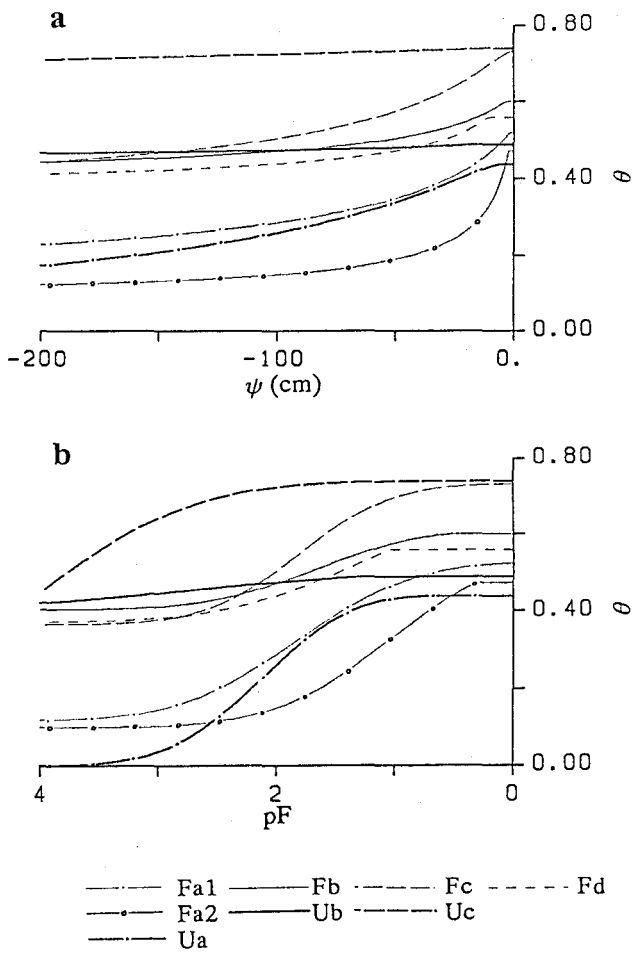

Figure 4.5 Typical (a) θ-ψ curves and (b) θ-pF curves of five types of forest soils and three types of undeveloped field soils. Soil type codes are summarized in Table 4.1.

Typical θ-pF curves of forest soil, loamy soil, and sandy soil are shown in Figure 4.4b. The pF value is defined as the common logarithm of $|\psi|$. The black dot on each curve indicates the end of the air entry region. With forest soil, θ begins to decrease when pF reaches 0.35. With loamy soil, θ is equal to θ_s when pF is smaller than 1.7. Value of θ decreases gradually when pF > 1.7. With sandy soil, θ decreases rapidly when 2.0 > pF > 1.5. Value of θ is nearly the same as θ_r at pF = 2.5. Forest soil has the largest θ_r value. The θ_r value of loamy soil is 0.11 less than that of forest soil and 0.07 more than that of sandy soil.

In Figure 4.5a, typical θ-ψ curves of five types of forest soils are compared with typical θ-ψ curves of three types of undeveloped field soils. The eight types of soils correspond to the forest soils and undeveloped field soils that are summarized in Table

4.1. Each curve was generated with the LN model using the average values of the estimated parameters for each type of soil. The forest soils taken with small-size samplers at Kiryu (Fa1) have larger θ values and greater changes in θ than the undeveloped soils at Kiryu (Ua) when ψ is greater than -30 cm. When ψ < -50 cm, the rate of change of θ for the former is less than that for the latter. The forest soils taken with large-size samplers at Kiryu (Fa2) have rather large changes in θ in the region where ψ is greater than -30 cm. The rates of change of θ for the undeveloped soils on plots Nos. 12 and 14 at the Rolling Land Laboratory (Ub) are quite small, whereas the forest soils on the same plots (Fb) have larger θ values and greater changes in θ when ψ > -60 cm. The undeveloped soils on plot No. 17 at the Rolling Land Laboratory (Uc) have constant θ values of about 0.7, whereas the forest soils on the same plot (Fc) have rapid decreases in θ. The typical θ-ψ curve of the forest soils at Toinotani (Fd) is similar to that of the forest soils on plots Nos. 12 and 14 at the Rolling Land Laboratory. All θ-ψ curves of the five types of forest soils resemble the typical θ-ψ curve of forest soil shown in Figure 4.4a: the curves have quite narrow air entry regions, rapid decreases in θ when ψ > -30 cm, and gradual changes in θ as ψ further decreases.

The typical θ-pF curves of the forest soils and undeveloped field soils are shown in Figure 4.5b. It is clear that all of the curves of the five types of forest soils are similar to the typical θ-pF curve of forest soil shown in Figure 4.4b. Three types of undeveloped field soils have peculiar typical θ-pF curves. The undeveloped soils at Kiryu (Ua) have large changes in θ when 3 > pF > 1. With the undeveloped soils on plots Nos. 12 and 14 at the Rolling Land Laboratory (Ub), the rate of change of θ is small. With the undeveloped soils on plot No. 17 (Uc), θ decreases rapidly in the region where pF is greater than 2.5.

4.4.2 Comparison of the Pore Capillary Pressure Distributions

By analyzing a soil water retention curve with the LN model, four parameters can be derived to evaluate the pore capillary pressure distribution $f(\psi)$ of the soil: the mode ψ_0, mean ψ_a, median ψ_m, and standard deviation σ_ψ of $f(\psi)$. Parameter σ_ψ is related to the width of $f(\psi)$. Parameters ψ_0, ψ_a, and ψ_m are related to the representative ψ value of $f(\psi)$. Here, ψ_0 and ψ_m correspond to the capillary pressure at the inflection point on the θ-ψ curve and the capillary pressure at S_e = 0.5, respectively, whereas ψ_a has no physical significance on the θ-ψ curve (see Figure 3.1). The pore radius, which is related to ψ_m by the capillary pressure function expressed as (3.2), is the median of the pore radius distribution $g(r)$. The pore radii, which are related to ψ_0 and ψ_a by (3.2), have no statistical significance for $g(r)$. Hence the two parameters, ψ_m and σ_ψ, were used to evaluate the $f(\psi)$ of the 100 soils.

Figure 4.6 shows a scatterplot of the relationships between ψ_m and σ_ψ for 84 sets of retention data of the forest soils, the loamy soils, and the sandy soils. Values of ψ_m and σ_ψ of each data set were computed using (3.12) and (3.13), respectively, from estimated

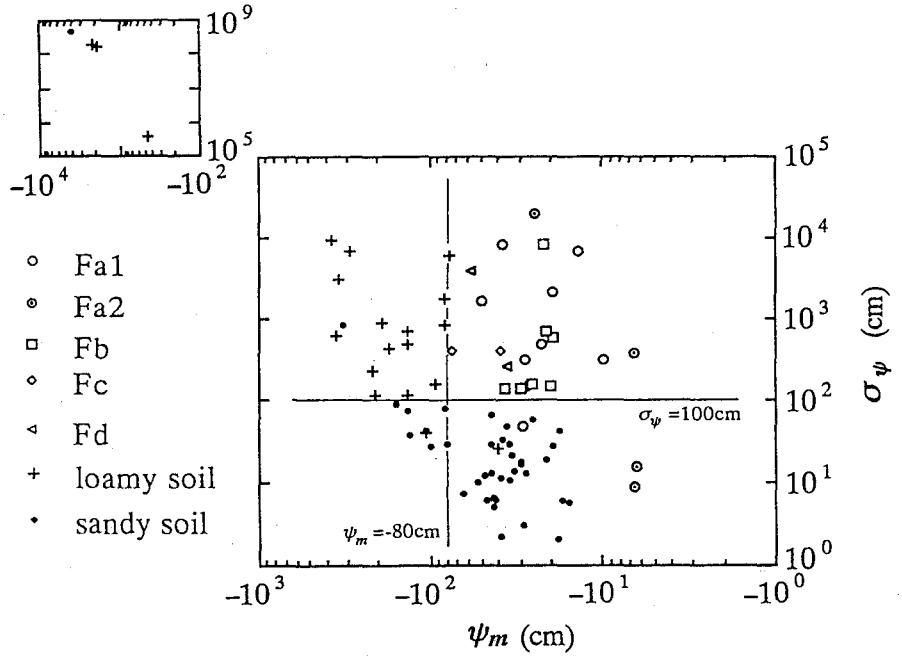

Figure 4.6 Relationship between ψ_m and σ_ψ for 24 forest soils, 20 loamy soils, and 40 sandy soils. Soil type codes are summarized in Table 4.1.

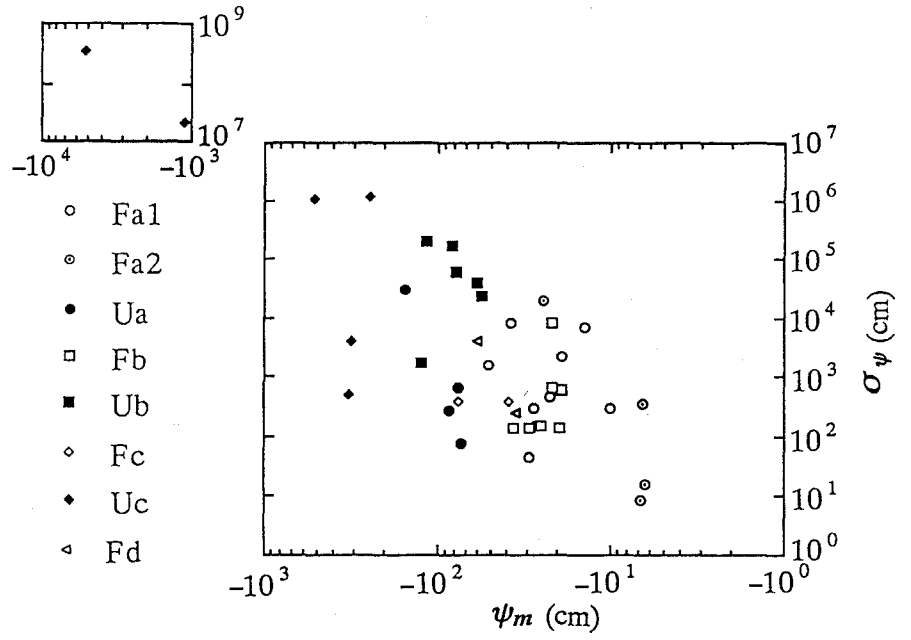

Figure 4.7 Relationship between ψ_m and σ_ψ for 24 forest soils and 16 undeveloped field soils. Soil type codes are summarized in Table 4.1.

ψ_c, ψ_0, and σ values. Most of the 20 points representing the data sets of the loamy soils are in the range of ψ_m < -80 cm, and σ_ψ > 100 cm. Thirty-one out of the 40 points representing the data sets of the sandy soils are in the range of ψ_m > -80 cm, and 37 out of the 40 are located in the region in which σ_ψ is smaller than 100 cm. Consequently, σ_ψ (that is, the width of $f(\psi)$) of the loamy soils is greater than that of the sandy soils, and ψ_m, which has a positive correlation with the median of $g(r)$, of the loamy soils is smaller than that of the sandy soils. Most of the 24 points representing the data sets of the forest soils are in the range of ψ_m > -80 cm and σ_ψ > 100 cm regardless of the soil sampling site. Figure 4.6 shows that the forest soils have larger $f(\psi)$ widths than the sandy soils, and have greater ψ_m values (that is, medians of $g(r)$ are greater) than the loamy soils. It should be noted that the ψ_m values of three forest soils taken with large-size samplers at Kiryu are quite large. One of the forest soils taken with large-size samplers has the largest σ_ψ value.

In Figure 4.7, the relationships between ψ_m and σ_ψ for the retention data sets of the 16 undeveloped field soils are compared with those for the 24 forest soils. It is clear that the undeveloped field soils have smaller ψ_m values than the forest soils. Three out of the four points representing data sets of the undeveloped soils at Kiryu (Ua) have ψ_m values of about -80 cm and σ_ψ values from 10^2 to 10^3 cm. Five out of the six points, which are associated with data sets of the undeveloped soils on plots Nos. 12 and 14 at the Rolling Land Laboratory (Ub), lie within -120 < ψ_m < -60 cm and $10^4 < \sigma_\psi < 10^{5.5}$ cm. Six points representing data sets of the undeveloped soils on plot No. 17 at the Rolling Land Laboratory (Uc) are located in the region in which ψ_m is smaller than -200 cm and are widely scattered with respect to the σ_ψ axis ($10^{2.5} < \sigma_\psi < 10^{8.5}$ cm). Most of the 22 points representing data sets of the forest soils at Kiryu (Fa), on plots Nos. 12 and 14 (Fb) and plot No. 17 (Fc) at the Rolling Land Laboratory lie in the range about -80 < ψ_m < -10 cm and $10^2 < \sigma_\psi < 10^4$ cm. That is, $f(\psi)$ of the forest soils, which were developed from soils having different types of $f(\psi)$, resemble each other. The forest soils at Kiryu have greater ψ_m values than the undeveloped soils at Kiryu, whereas the σ_ψ values of the former are about the same as those of the latter. The forest soils on plots Nos. 12 and 14 at the Rolling Land Laboratory have greater ψ_m values and smaller σ_ψ values than the undeveloped soils on the same plots. It appears that the process of developing $f(\psi)$ is different for soils at Kiryu and soils on plots Nos. 12 and 14 at the Rolling Land Laboratory. Value of ψ_m of the forest soils at Kiryu increases whereas σ_ψ does not change appreciably. Both ψ_m and σ_ψ of the forest soils on plots Nos. 12 and 14 change: ψ_m becomes greater and σ_ψ becomes smaller.

4.5 SUMMARY AND CONCLUSIONS

In this chapter, retention data sets of 24 forest soils, 16 undeveloped field soils, 20 disturbed loamy soils, and 40 disturbed sandy soils were analyzed using the LN model.

Based on a comparison of the average residuals of the fitted versus observed water contents, it was shown that the LN model produces acceptable matches for retention data sets of the forest soils and the undeveloped field soils as well as for data sets of the disturbed loamy and sandy soils.

The LN model contains five parameters that have physical significance on the θ-ψ curve: the saturated water content θ_s, the residual water content θ_r, the bubbling pressure (that is, the capillary pressure at the end of the air entry region) ψ_c, the capillary pressure at the inflection point ψ_0, and a dimensionless σ which determines the effective saturation at the inflection point. Using the average values of the estimated parameters, typical θ-ψ curves of forest soil, loamy soil, and sandy soil were generated. The typical θ-ψ curve of forest soil has large θ_s and θ_r values, and a rather narrow air entry region. Because of large ψ_0 and σ values, the inflection point on the θ-ψ curve is close to the end of the air entry region. As a result, the typical θ-ψ curve of forest soil has rapid decreases in θ when $\psi > -30$ cm. The typical θ-ψ curve of loamy soil has a wide air entry region and a gradual decrease in θ at the inflection point. The typical θ-ψ curve of sandy soil has more rapid decreases in θ around the inflection point than the typical θ-ψ curve of loamy soil. The θ-ψ curves of five types of forest soils resemble each other, whereas the θ-ψ curves of three types of undeveloped field soils were different from each other.

The water capacity function, which is defined as the slope of the θ-ψ curve, is related to the pore radius distribution function, and can be regarded as the pore capillary pressure distribution function $f(\psi)$. Using parameters of the LN model, the standard deviation σ_ψ, and the median ψ_m, of $f(\psi)$ were computed for each retention data set. Parameter σ_ψ represents the width of $f(\psi)$ and ψ_m is related to the median of the pore radius distribution. Results showed that the forest soils have larger $f(\psi)$ widths than the sandy soils and have greater ψ_m values (that is, medians of the pore radius distribution are greater) than the loamy soils. The undeveloped field soils have smaller ψ_m values than the forest soils.

The LN model exhibited sufficient flexibility to accommodate retention curves of various soils and could be used for comparative analyses of θ-ψ curves and pore capillary pressure distributions. With this retention model, knowledge of the moisture characteristics and the pore structure of forest soils will be used adequately for analyses of water-related phenomena on mountainous watersheds.

REFERENCES

Brooks, R. H., and A. T. Corey, Hydraulic properties of porous media, *Hydrol. Pap. 3*, Civil Eng. Dept., Colo. State Univ., Fort Collins, 1964.

Fukushima, Y., M. Suzuki, M. Tani, H. Kato, and T. Ohta, The hydrological observations in the two small catchments in palaeozoic hilly mountains in Ashiu experimental forest (in Japanese with English Summary), *Bull. Kyoto Univ. Forests, 51*, 152-163, 1979.

Jury, W. A., W. R. Gardner, and W. H. Gardner, *Soil Physics*, Wiley, New York, 1991.

Kosugi, K., and N. Ohte, Analysis of soil-pore connection properties affecting the permeability

of forest soils (in Japanese with English Summary), *J. Jpn. For. Soc.*, *74*, 373-382, 1992.

Kumlung, A., and Y. Takeda, Changes of soil properties in relation to lapsed years of hillside works on a granite area, *J. Jpn. For. Soc.*, *73*, 327-338, 1991.

Marquardt, D. W., An algorithm for least-squares estimation on non-linear parameters, *J. Soc. Ind. Appl. Math.*, *11*, 431-441, 1963.

Mashimo, Y., Studies on the physical properties of forest soil and their relation to the growth of sugi (*Cryptomeria japonica*) and hinoki (*Chamaecyparis obtusa*) (in Japanese with English Summary), *Forest Soils Jpn.*, *11*, 1-182, 1960.

Mualem, Y., A catalogue of the hydraulic properties of unsaturated soils, *Proj. 442*, 100 pp., Technion-Israel Inst. of Technol., Haifa, Israel, 1976.

Ogasiwa, K., T. Kondou, and Y. Mashimo, An analysis of factors affecting coarse pore volume of forest soil with the quantification-I method, I, Coarse pore volume of soil at various depth in sugi (*Cryptomeria japonica*) stands (in Japanese), *J. Jpn. For. Soc.*, *73*, 393-395, 1991a.

Ogasiwa, K., T. Kondou, and Y. Mashimo, An analysis of factors affecting coarse pore volume of forest soil with the quantification-I method, II, Relationship between coarse pore volume of surface soil and stand density in sugi (*Cryptomeria japonica*) stands (in Japanese), *J. Jpn. For. Soc.*, *73*, 396-400, 1991b.

Ohta, T., Y. Tsukamoto, and M. Hiruma, The behavior of rainwater on a forested hillslope, I, The properties of vertical infiltration and the influence of bedrock on it (in Japanese with English Summary), *J. Jpn. For. Soc.*, *67*, 311-321, 1985.

Ohte, N., *Studies on Pore Structure and Hydraulic Properties of Forest Soils* (in Japanese*), A doctor thesis, Kyoto Univ., 1992.

Ohte, N., and M. Suzuki, Hydraulic properties of forest soils, II, Method of determining the volumetric water content-pressure head relationship by the saturated-unsaturated hydraulic conductivity test using a large-size soil sample (in Japanese with English Summary), *J. Jpn. For. Soc.*, *72*, 468-477, 1990.

Sammori, T., and Y. Tsuboyama, Study on method of slope stability considering infiltration phenomenon (in Japanese with English Summary), *J. Jpn. Soc. Erosion Control Eng.*, *43*(4), 14-21, 1990.

Suzuki, M., The properties of a base-flow recession on small mountainous watersheds, I, Numerical analysis using the saturated-unsaturated flow model (in Japanese with English summary), *J. Jpn. For. Soc.*, *66*, 174-182, 1984.

Tani, M., The properties of a water-table rise produced by a one-dimensional, vertical, unsaturated flow (in Japanese with English summary), *J. Jpn. For. Soc.*, *64*, 409-418, 1982.

Tani, M., Analysis of one-dimensional, vertical, unsaturated flow in consideration of runoff properties of a mountainous watershed (in Japanese with English summary), *J. Jpn. For. Soc.*, *67*, 449-460, 1985.

Tsuboyama, Y., and T. Sammori, Numerical simulation of seepage in a forested hillslope by finite element method (in Japanese with English Summary), *J. Jpn. Soc. Hydrol. Water Resour.*, *2*(2), 49-56, 1989.

van Genuchten, M. Th., A closed-form equation for predicting the hydraulic conductivity of unsaturated soils, *Soil Sci. Soc. Am. J.*, *44*(5), 892-898, 1980.

van Genuchten, M. Th., and D. R. Nielsen, On describing and predicting the hydraulic properties of unsaturated soils, *Ann. Geophys.*, *3*(5), 615-628, 1985.

* The title is tentative translation from the original Japanese title by the author of this thesis.

CHAPTER 5

TWO-PARAMETER LOGNORMAL DISTRIBUTION MODEL FOR ANALYZING WATER RETENTION CHARACTERISTIC OF FOREST SOIL

5.1 INTRODUCTION

Since soil moisture characteristics significantly affect the plant growth, many soil scientists have observed water retention curves of forest soils and evaluated the soil pore radius distribution. *Mashimo* [1960] analyzed the observed θ-ψ curves of soil samples collected from 10 different forests, and suggested that the soil pores can be classified into two types, the coarse and fine pores. He defined coarse pores as those in which water is retained by capillary pressures greater than -500 cm (that is, pF 2.7). This definition has been widely used to observe pore radius distribution of forest soils [e.g., *Arimitsu*, 1970; *Kobayashi*, 1982; *Ogasiwa et al.*, 1991]. In order to estimate water holding capacity of forest soils, *Takeshita* [1985] proposed that soil pores can be classified into four types according to the pore capillary pressure values, and measured pore radius distribution of forest soils. He analyzed the relationship between the obtained water holding capacity of forest soils and the water discharge from forestal watersheds. Measurements of pore radius distribution of forest soils have been carried out many times in similar manners [e.g., *Kumlung and Takeda*, 1991; *Ohnuki et al.*, 1994]. However, the knowledge accumulated by these measurements of soil pore radius distribution has not been effectively used in physical analyses of water flow in forest soils. One reason is that the observed moisture characteristics of forest soils have not been analyzed using functional models for soil water retention.

On the other hand, forest hydrologists have measured water retention characteristics of forest soils for modeling water movement in forestal watersheds. In the physical analyses of soil water flow, some models for soil water retention have been proposed and used. *Ohta et al.* [1985] discussed the properties of vertical infiltration of rainwater in forest soil profiles in connection with the observed soil water retention curves. *Kubota et al.* [1987] analyzed the θ-ψ relationship of forest soil obtained by field observations using the soil water retention model proposed by *Klute and Heermann* [1974]. The Klute and Heermann model was adopted by *Ohta et al.* [1983] for modeling vertical

unsaturated flow in a forest soil profile. *Ohte* [1992] determined the θ-ψ curves of undisturbed forest soils taken with large-size samplers, and analyzed vertical soil water flow using a retention model developed by *Brooks and Corey* [1964]. Moreover, *Tani* [1982] suggested a retention model with a relatively simple functional form. Using this model, he analyzed properties of one-dimensional unsaturated flow in a soil column [*Tani*, 1985]. The Tani model has been used to analyze water flow on forestal hillslopes [*Suzuki*, 1984; *Tsuboyama and Sammori*, 1989]. *Sammori and Tsuboyama* [1990] adopted a retention model developed by *van Genuchten* [1980] to analyze slope stability taking the phenomena of infiltration into consideration. Despite their usefulness for numerical modeling of soil water flow, these retention models are empirical curve fitting equations. They are not derived based on soil pore radius distribution, nor do they emphasize the physical significance of their empirical parameters. Hence, these retention models cannot be effectively used for analyzing moisture characteristics of forest soils in connection with the soil pore radius distribution.

The LN model for soil water retention (expressed as (3.14)) was developed by applying three-parameter lognormal distribution laws to both the soil pore radius distribution function and the water capacity function, which is regarded as the pore capillary pressure distribution function. Parameters of the LN model have physical significance on the θ-ψ curve and are related closely to the statistics of the pore capillary pressure distribution. It was shown in Chapters 3 and 4 that the LN model performs as well as any existing empirical model for determining retention curves of various soils and is effectively used for comparative analyses of the moisture characteristics of various soils, while at the same time, the model has a relatively complicated functional form in comparison with widely used retention models. Applying a restriction to one of the parameters, the LN model is modified in this chapter to have a relatively simple functional form and to have parameters which are related directly to the statistics of the soil pore radius distribution. The resulting water retention model is applied to observed retention data sets of 282 forest soils. Then, the effects of forest soil structure, as well as the soil texture, type, and horizon on the soil pore radius distribution and the soil moisture characteristic are analyzed using the parameters of the proposed model.

5.2 TWO-PARAMETER LOGNORMAL DISTRIBUTION MODEL FOR SOIL WATER RETENTION

Based on the LN model, the pore capillary pressure distribution function $f(\psi)$ and the soil water retention curve (that is, the relationship between the effective saturation S_e and the soil capillary pressure ψ) are expressed as

$$f(\psi)=\frac{\theta_s-\theta_r}{\sqrt{2\pi}\sigma(\psi_c-\psi)}\exp\left[-\frac{\left\{\ln\left(\frac{\psi_c-\psi}{\psi_c-\psi_0}\right)-\sigma^2\right\}^2}{2\sigma^2}\right] \qquad \psi<\psi_c \qquad (3.10)$$

$$f(\psi)=0 \qquad \psi\geq\psi_c$$

$$S_e=\frac{1}{2}\mathrm{erfc}\left(\frac{\ln\{(\psi_c-\psi)/(\psi_c-\psi_0)\}-\sigma^2}{\sqrt{2}\sigma}\right) \qquad \psi<\psi_c \qquad (3.14)$$

$$S_e=1 \qquad \psi\geq\psi_c$$

The other expression for (3.14) is

$$S_e=Q\left(\ln\{(\psi_c-\psi)/(\psi_c-\psi_0)\}/\sigma-\sigma\right) \qquad \psi<\psi_c \qquad (5.1)$$

$$S_e=1 \qquad \psi\geq\psi_c$$

where Q is the complementary normal distribution function defined as

$$Q(x)=\int_x^\infty\frac{1}{\sqrt{2\pi}}\exp\left(-\frac{x^2}{2}\right)dx \qquad (5.2)$$

In Chapter 4, it was shown that values of ψ_c of (3.14) are nearly equal to zero for many forest soils. According to the results derived in Subsections 3.4.1 and 3.4.2, (3.14) with the restriction of ψ_c = 0 still produces acceptable matches with retention curves of soils which have no distinct bubbling pressures. When the restriction of ψ_c = 0 is applied, (3.10) and (5.1) are transformed as follows:

$$f(\psi)=\frac{\theta_s-\theta_r}{\sqrt{2\pi}\sigma(-\psi)}\exp\left[-\frac{\left\{\ln(\psi/\psi_0)-\sigma^2\right\}^2}{2\sigma^2}\right] \qquad (5.3)$$

$$S_e=Q\left(\ln(\psi/\psi_0)/\sigma-\sigma\right) \qquad (5.4)$$

Figures 5.1a and 5.1b show plots of (5.3) and (5.4), respectively, for ψ_0 = -50 cm, σ = 0.6, θ_s = 0.4 and θ_r = 0.1. The distribution expressed by (5.3) is not symmetrical. Notice that ψ_0 corresponds to the capillary pressure at the inflection point on the S_e-ψ curve. The value of S_e at the inflection point is derived by substituting $\psi=\psi_0$ into (5.4):

$$S_e(\psi_0)=Q(-\sigma) \qquad (5.5)$$

Equation (5.5) is identical to (3.15). Consequently, σ is the parameter which determines the value of $S_e(\psi_0)$. Small σ value reduces $S_e(\psi_0)$ value and makes the retention curve steep at the inflection point. The median of $f(\psi)$ expressed as (5.3) (ψ_m) is given by substituting S_e = 0.5 into (5.4):

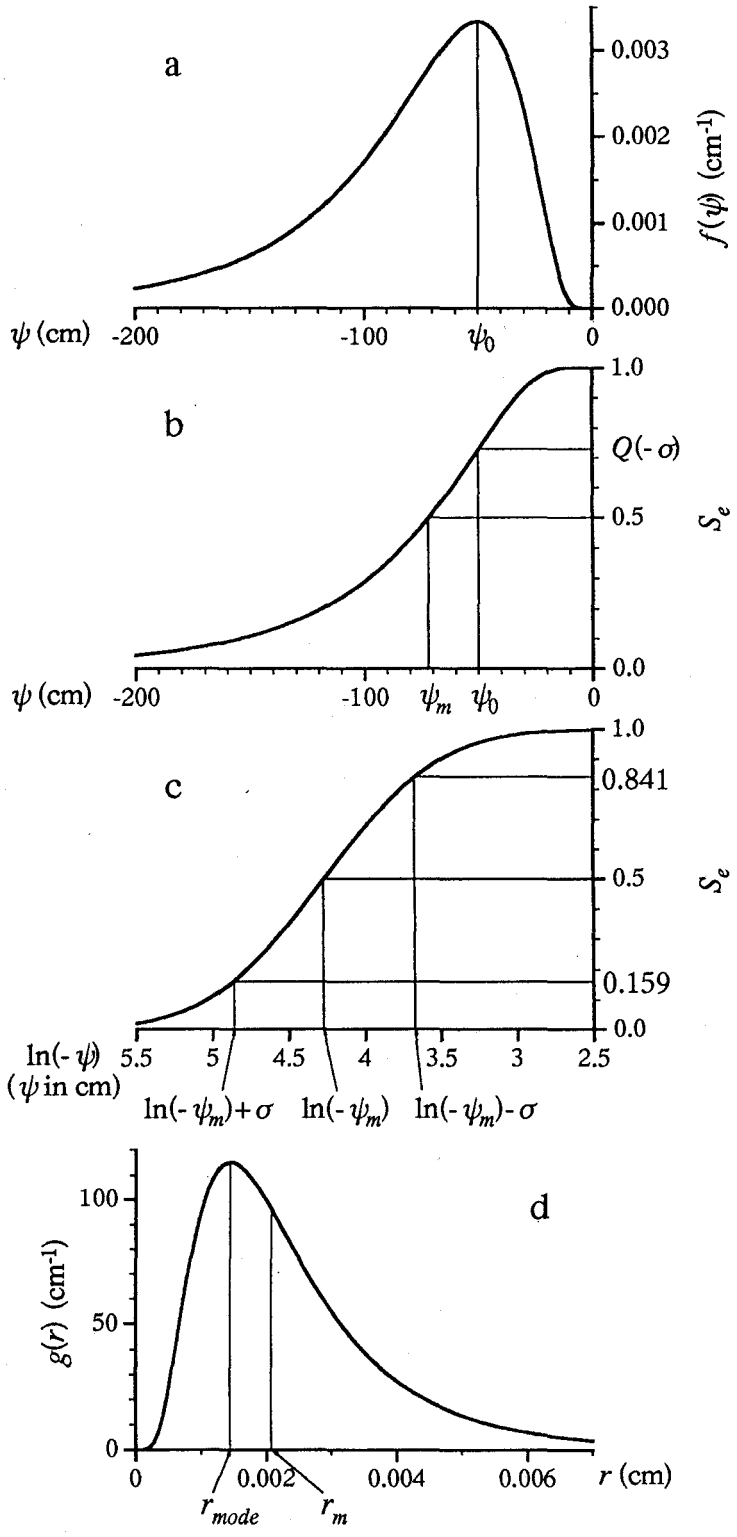

Figure 5.1 Curves for (a) $f(\psi)$, (b) S_e-ψ, (c) S_e-ln(-ψ), and (d) $g(r)$ based on the LN2 model, showing plots of (5.3), (5.4), (5.8), and (5.9) for $\theta_s = 0.4$, $\theta_r = 0.1$, $\sigma = 0.6$, $\psi_0 = -50$ cm, $\psi_m = -71.7$ cm ($\ln(-\psi_m) = 4.27$), $r_m = 2.08 \times 10^{-3}$ cm, and $r_{mode} = 1.45 \times 10^{-3}$ cm.

$$\psi_m = \psi_0 \exp(\sigma^2) \tag{5.6}$$

Inverting (5.6) with respect to ψ_0 and substituting into (5.3) and (5.4) yields

$$f(\psi) = \frac{\theta_s - \theta_r}{\sqrt{2\pi}\sigma(-\psi)} \exp\left[-\frac{\{\ln(\psi/\psi_m)\}^2}{2\sigma^2}\right] \tag{5.7}$$

$$S_e = Q(\ln(\psi/\psi_m)/\sigma) \tag{5.8}$$

Equation (5.7) has the lognormal distribution form since the distribution of $\ln(-\psi)$ conforms to the normal distribution $N(\ln(-\psi_m), \sigma^2)$. Consequently, ψ_m is identical to the geometric mean of $f(\psi)$. A plot of (5.8) for ψ_m = -71.7 cm (that is, $\ln(-\psi_m) = 4.27$) and $\sigma = 0.6$ is shown using a semi-logarithmic scale in Figure 5.1c. This ψ_m value is obtained from (5.6) by substituting ψ_0 = -50 cm and $\sigma = 0.6$ which are used for the $f(\psi)$ and S_e-ψ curves shown in Figures 5.1a and 5.1b, respectively. It can be seen that ψ_m is identical to the capillary pressure at the inflection point on the S_e-$\ln(-\psi)$ curve. Notice that σ is equal to the difference between $\ln(-\psi_m)$ and the $\ln(-\psi)$ value at $S_e = 0.841$, or the difference between $\ln(-\psi_m)$ and the $\ln(-\psi)$ value at S_e =0.159. Consequently, S_e-$\ln(-\psi)$ curve becomes steeper near the inflection point as σ becomes smaller. With a large σ value the curve has consistently small decreases in S_e as $\ln(-\psi)$ increases. The water retention model expressed as (5.8) is referred to as the LN2 model.

The pore radius distribution function $g(r)$ corresponding to (5.8) is derived by substituting (3.2) and (5.7) into (3.3) and differentiating:

$$g(r) = \frac{\theta_s - \theta_r}{\sqrt{2\pi}\sigma r} \exp\left[-\frac{\{\ln(r/r_m)\}^2}{2\sigma^2}\right] \tag{5.9}$$

where r_m is the pore radius which is related to ψ_m by the capillary pressure function expressed as (3.2) (that is, $r_m = A/\psi_m$). Equation (5.9) is identical to (3.21) and represents a lognormal distribution since the distribution of $\ln(r)$ conforms to $N(\ln(r_m), \sigma^2)$. Parameter r_m is equal to the median and the geometric mean of $g(r)$. Parameter σ is related to the width of $g(r)$ since it is the standard deviation of the distribution of $\ln(r)$. Value of σ is small for soil which has a narrow pore radius distribution, and is large for soil with a wide pore radius distribution. A plot of (5.9) for $r_m = 2.08 \times 10^{-3}$ cm, $\sigma = 0.6$, and $\theta_s - \theta_r = 0.3$ is shown in Figure 5.1d. This r_m value is computed from the relationship of $r_m = A/\psi_m$ by substituting ψ_m = -71.7 cm which is used for the S_e-$\ln(-\psi)$ curve shown in Figure 5.1c. As can be seen, the distribution expressed as (5.9) is not symmetrical. The mode of the pore radius distribution (r_{mode}) is expressed by the following function with respect to r_m and σ:

$$r_{mode} = r_m \exp(-\sigma^2) \tag{5.10}$$

The value of r_{mode} for $g(r)$ shown in Figure 5.1d is 1.45×10^{-3} cm.

5.3 MATERIALS AND METHODS

Observed retention data sets of 282 forest soils taken from *Mashimo* [1960] were analyzed with the LN2 model. The undisturbed soil samples were collected using 400 ml cylindrical samplers from 114 plots at 10 different forests situated in mountainous regions in the central part of Japan. The altitude of the sampling sites was between 300 and 1500 m. Samples of 200 and 79 soils pertained to brown forest soils and black soils, respectively. Samples of 165 soils were taken from A-horizon and 87 samples were taken from B-horizon. Textures of the soils ranged from heavy clay through sand according to the classification system of the International Society of Soil Science. The membrane-suction method [*Mashimo*, 1957] was adopted to measure soil water retention curves in the range of $\psi > -10^{2.5}$ cm (that is, pF 2.5).

A nonlinear least squares optimization procedure based on Marquardt's maximum neighborhood method [*Marquardt*, 1963] was used to analyze the observed retention data sets. Applying Marquardt's method ψ_m, σ, and θ_r in (5.8) were treated as the fitted parameters. Observed values of the maximum water holding capacity were used as θ_s in (5.8).

5.4 RESULTS AND DISCUSSION

5.4.1 Typical Water Retention Curves of Forest Soils

In Figure 5.2, typical θ-ψ curves of forest soils having crumb, granular, loose granular, massive, and nutty structures are compared with the fitted curves generated by (5.8). The soil structure class is based on the classification system summarized in *Kawada* [1989], which is closely related to the system according to *Soil Survey Staff* [1951]. The observed θ-ψ curves of these 17 soils are the same curves that are shown in Figure 8 of *Mashimo* [1960], and widely quoted as the typical water retention curves of forest soils [e.g., *Kawada*, 1989; *Tsukamoto*, 1992]. It is clear from the figure that the LN2 model performed quite well for each retention data set. The coefficient of determination R^2 and the estimated parameters of the model are summarized in Table 5.1. The R^2 value for every retention data set except MS2 shown in Figure 5.2d was greater than 0.97. The R^2 value for MS2 was 0.889 because of the fluctuation in the observed data. However, the LN2 model still produced an acceptable fit for this data set. It should be noted that (5.8) performed fairly well for other retention data sets which are not shown in this figure. The average R^2 value for the data sets of 282 soils was 0.993 and the minimal R^2 value was 0.889, that is the R^2 value for MS2 shown in Figure 5.2d.

Figure 5.2a shows retention data sets of four soils whose structure was classified as crumb. The θ-ψ curves have consistently gradual decreases in θ as ψ decreases. Table

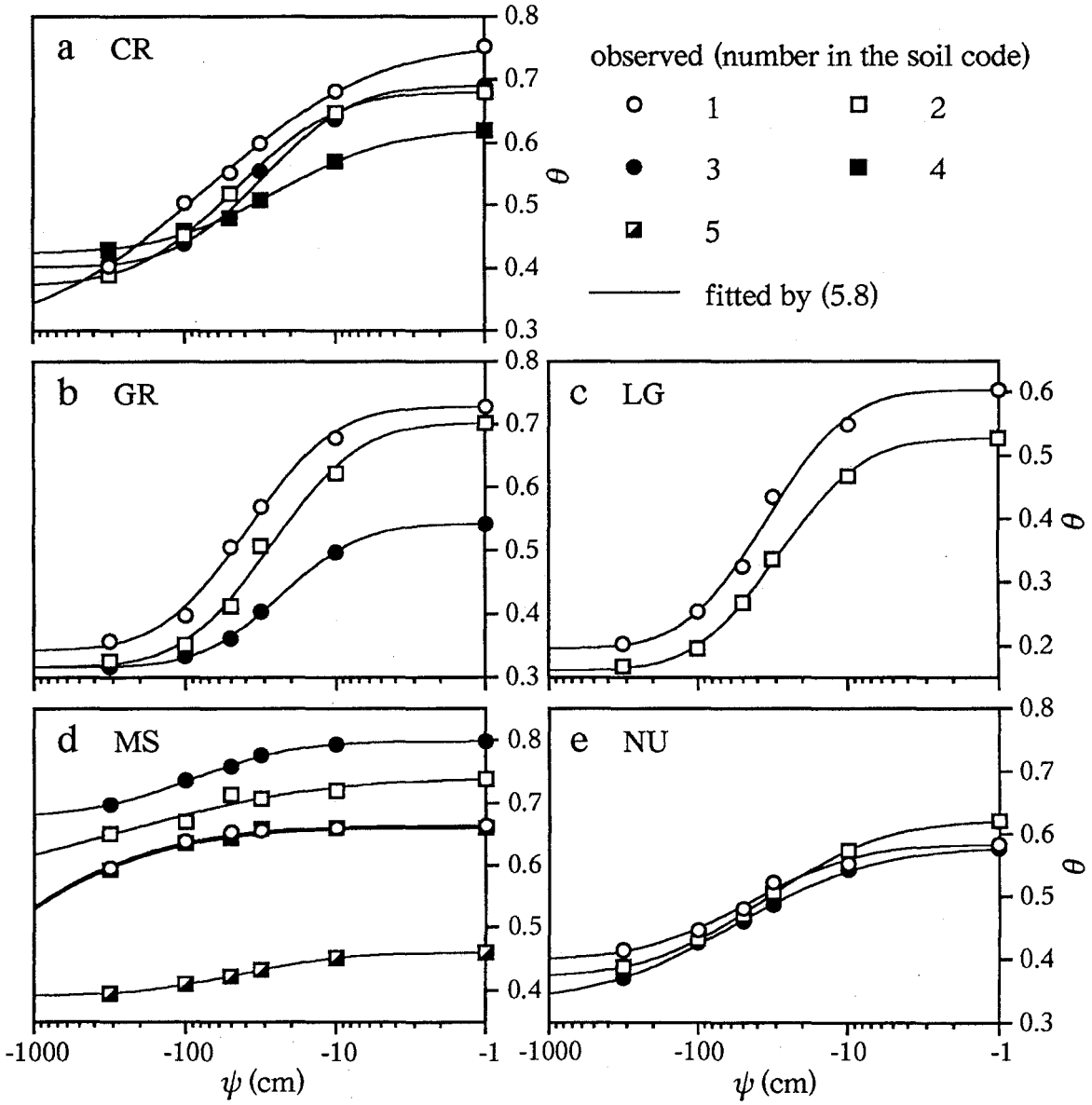

Figure 5.2 Observed and fitted θ-ψ curves for the forest soils with (a) crumb, (b) granular, (c) loose granular, (d) massive, and (e) nutty structures. Soil codes are summarized in Table 5.1.

Table 5.1 Fitted Values for Parameters of the LN2 Model and the Coefficient of Determination (R^2) of the Curve Fittings for the Retention Curves Plotted in Figure 5.2

Structure	Soil Code*1	R^2	θ_s*2	θ_r	ψ_m, cm	σ
Crumb	CR1	0.998	0.752	0.304	-71.2	1.98
	CR2	1.000	0.680	0.373	-45.8	1.21
	CR3	0.987	0.690	0.402	-29.8	1.08
	CR4	0.997	0.620	0.425	-24.2	1.38
Granular	GR1	0.993	0.728	0.344	-38.2	1.05
	GR2	0.986	0.702	0.317	-26.8	1.07
	GR3	0.999	0.542	0.317	-23.2	0.99
Loose granular	LG1	0.990	0.604	0.197	-34.3	0.99
	LG2	0.998	0.527	0.161	-28.6	1.02
Massive	MS1	0.987	0.664	0.000	-9.18×10^3	2.61
	MS2	0.889	0.739	0.568	-2.69×10^2	2.33
	MS3	0.998	0.798	0.679	-91.8	1.26
	MS4	0.972	0.660	0.000	-9.10×10^3	2.61
	MS5	0.999	0.460	0.391	-43.9	1.29
Nutty	NU1	0.981	0.584	0.400	-44.6	1.31
	NU2	0.999	0.622	0.372	-35.2	1.44
	NU3	0.998	0.578	0.335	-55.0	1.67

*1 Used in Figure 5.2.
*2 Taken from *Mashimo* [1960].

5.1 indicates that ψ_m values of the three soils (CR2, 3, and 4) were between -20 and -50 cm and estimated σ values of these soils were from 1.0 to 1.4. One soil (CR1) has the smaller ψ_m and greater σ values. The θ-ψ curves of three soils which have granular structure are shown in Figure 5.2b. These curves contrast with the θ-ψ curves shown in Figure 5.2a: changes in θ relatively concentrate around the inflection point. This is because of the smaller σ values estimated for these soils than those for the crumb-structure soils (see Table 5.1). Values of ψ_m for these soils were about the same as those for the three crumb-structure soils (CR2, 3, and 4). Figure 5.2c indicates that the θ-ψ

curves of the loose granular-structure soils are similar to those of the granular-structure soils shown in Figure 5.2b. Estimated ψ_m and σ for the loose granular-structure soils are about the same as those for the granular-structure soils. The water retention curves shown in Figure 5.2d are of soils whose structure was classified as massive. The observed θ-ψ curves have small decreases in θ as ψ decreases. Values of ψ_m estimated for these soils were smaller than those for the crumb and granular-structure soils. As a result, inflection points on these curves appear at small ψ value in comparison with the retention curves shown in Figures 5.2a and 5.2b. Two retention curves (MS3 and 5) have about the same σ values as those for the three crumb-structure soils (CR2, 3, and 4), and three curves (MS1, 2, and 4) have greater σ values. Two retention curves (MS1 and 4) have greater changes in θ in the range of $-300 < \psi < -100$ cm than in the range of $\psi > -100$ cm, and θ_r for these curves were estimated to be zero. Figure 5.2e shows the water retention curves of soils whose structure was classified as nutty. The θ-ψ curves have consistently gradual decreases in θ as ψ decreases. The rates of change of θ for these soils are smaller than those for the crumb-structure soils shown in Figure 5.2a. The nutty-structure soils have smaller ψ_m and greater σ values than many of the crumb, granular, and loose granular-structure soils. The ψ_m values of the nutty-structure soils are greater than those of the massive soils, and σ of the nutty-structure soils are smaller than those of the three massive soils (MS1, 2, and 4).

Figures 5.2a through 5.2e clearly show that the LN2 model is successfully used to derive the functional θ-ψ relationships of forest soils. The properties of the observed soil water retention curves are expressed by the estimated parameters of the model.

5.4.2 Effects of Soil Structure

Mashimo [1960] classified the soil structure of 60, 24, and 46 samples out of the 282 samples as crumb, granular, and massive, respectively. Figure 5.3 shows a scatterplot of the relationship between ψ_m and σ estimated for each retention data set of these 130 forest soils (indicated by circles). Value of r_m, which is related to ψ_m by (3.2) and equal to the median of $g(r)$, is also shown in the figure. The average and the standard deviation values of the estimated parameters (θ_r, ψ_m and σ) for each structure class are summarized in Table 5.2. This table includes the average values of observed θ_s taken from *Mashimo* [1960]. It should be noted that the geometric mean was used for ψ_m because the soil water retention curve is frequently plotted using a semi-logarithmic scale.

In Figure 5.3, most points representing the data sets of the crumb and granular-structure soils are in the range of $-80 < \psi_m < -10$ cm, and $1 < \sigma < 2$. Points for the crumb-structure soils are widely scattered in this range. More precisely, many of the points are located in the range of $\psi_m > -30$ cm. Values of σ estimated for several crumb-structure soils are greater than 2. The ψ_m and σ values for the many granular-structure soils are smaller than -30 cm and 1.5, respectively. As a result, the figure shows that many crumb-structure soils have greater ψ_m values (that is, median of $g(r)$ is greater) than

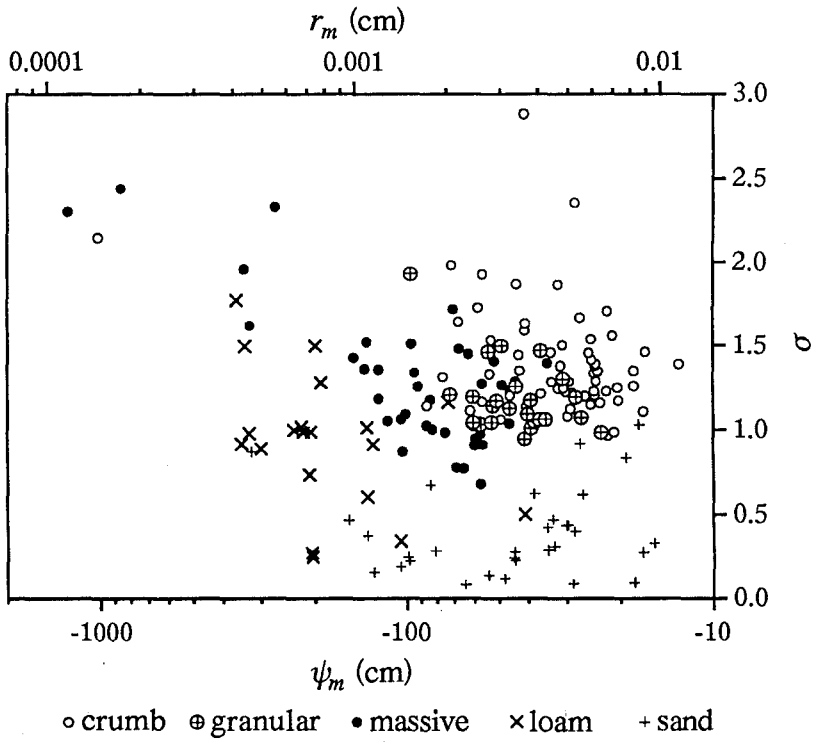

Figure 5.3 Relationship between ψ_m and σ of the LN2 model estimated for the undisturbed forest soils (circles), and for the disturbed loamy and sandy soils (crosses and pluses). Each plot symbol represents the soil structure for the forest soils. Value of r_m is related to ψ_m by (3.2).

the granular-structure soils, and σ values (which is equal to the width of $g(r)$) for many crumb-structure soils are greater than those for the granular-structure soils. As shown in Table 5.2, the crumb-structure soils have greater average ψ_m and σ values than the granular-structure soils. The standard deviations of both ψ_m and σ for the crumb-structure soils are larger than those for the granular-structure soils. The average θ_s value observed for the crumb-structure soils is about 0.02 smaller than that for the granular-structure soils, and the average θ_r values estimated for both the crumb and granular-structure soils resemble each other.

Figure 5.3 shows that most points representing the data sets of the massive soils are located in the region in which ψ_m is smaller than -50 cm, indicating that many massive soils have smaller median of $g(r)$ than the crumb and granular-structure soils. With respect to the σ axis, these points are widely scattered in the range of $\sigma > 0.7$. For some massive-structure soils, ψ_m values were estimated to be smaller than -200 cm and

Table 5.2 Average Values of the Estimated Parameters of the LN2 Model

Type of Soils	Structure	Number of Data Sets	θ_s*1	θ_r	ψ_m*2, cm	$\log(-\psi_m)$	σ
Forest soils	Crumb	60	0.621	0.399	-33.4	1.52	1.42
			(0.083)	(0.087)		(0.27)	(0.34)
	Granular	24	0.645	0.398	-43.9	1.64	1.19
			(0.059)	(0.056)		(0.14)	(0.22)
	Massive	46	0.668	0.459	-121.5	2.08	1.38
			(0.077)	(0.162)		(0.58)	(0.55)
Loamy soils	···	21	0.469	0.168	-222.7	2.35	1.00
			(0.049)	(0.100)		(0.43)	(0.51)
Sandy soils	···	31	0.342	0.067	-46.0	1.66	0.40
			(0.076)	(0.048)		(0.32)	(0.26)

Numbers in parentheses represent standard deviation of parameter.
*1 Obtained from the observed values.
*2 The geometric mean.

estimated σ values were greater than 1.5. Note that Figure 5.3 does not include three points representing massive soils for which ψ_m were about -10^4 cm and σ were greater than 2.5. The average ψ_m for the massive soils is much smaller than the average ψ_m for the crumb and granular-structure soils (see Table 5.2). Although the average σ for the massive soils is similar to that for the crumb-structure soils, the massive soils have the greatest standard deviation value of σ. The average θ_s and θ_r values for the massive soils are greater than those for the crumb and granular-structure soils.

Figure 5.3 also shows the relationship between ψ_m and σ estimated for the retention data sets of loamy and sandy soils taken from *Mualem*'s [1976] catalogue (indicated by crosses and pluses). Most of the data sets listed in this catalogue pertain to laboratory experiments involving disturbed soils [*van Genuchten and Nielsen*, 1985]. The θ-ψ curves of 12 loamy soils and 31 sandy soils, which have no distinct bubbling pressures, were analyzed by the LN2 model. Since the catalogue has less data sets for loamy soils than those for sandy soils, 9 sets of measured retention data of loamy soils (five sandy loams, two silty loams, and two loams), which were taken at a dune with poor vegetation [*Nakajima*, 1995], were analyzed additionally. The figure shows that many loamy soils have ψ_m values smaller than -100 cm, and σ values of many loamy soils are greater than 0.5. Note that the figure does not include a point which has ψ_m of about -10^4 cm and σ of 2.4. Many points representing the data sets of the sandy soils are in the range of $\psi_m > -100$ cm and $\sigma < 0.5$. As a result, it can be said that σ (that is, the width of $g(r)$) of the

loamy soils is greater than that of the sandy soils, and ψ_m, which is the median of $g(r)$, of the loamy soils is smaller than that of the sandy soils. Many of the undisturbed forest soils have greater median of $g(r)$ than the loamy soils and larger $g(r)$ width than the sandy soils. About one-third of the forest soils with massive structure have as small median of $g(r)$ (that is, ψ_m < -100 cm) as the loamy soils. Table 5.2 includes the average values of the parameters estimated for the loamy and sandy soils. The table indicates that the average ψ_m value of the loamy soils is smallest and the sandy soils have the smallest average σ value. The average θ_s and θ_r values for the loamy soils are smaller than those for the forest soils, and the sandy soils have the smallest average θ_s and θ_r values.

5.4.3 Effects of Soil Texture

Figure 5.4 again shows the relationship between ψ_m and σ estimated for the retention data sets of the forest soils analyzed in Figure 5.3. This time, each plot symbol represents not the soil structure but the soil texture class. The texture of 8 soils out of the 130 soils has not been measured, hence the points for these 8 soils are not included in the figure. It can be seen that the points are scattered regardless of the soil texture class. Figures 5.3 and 5.4 clearly show that the water retention characteristics of the undisturbed forest soils are related to the soil structure more closely than to the soil texture.

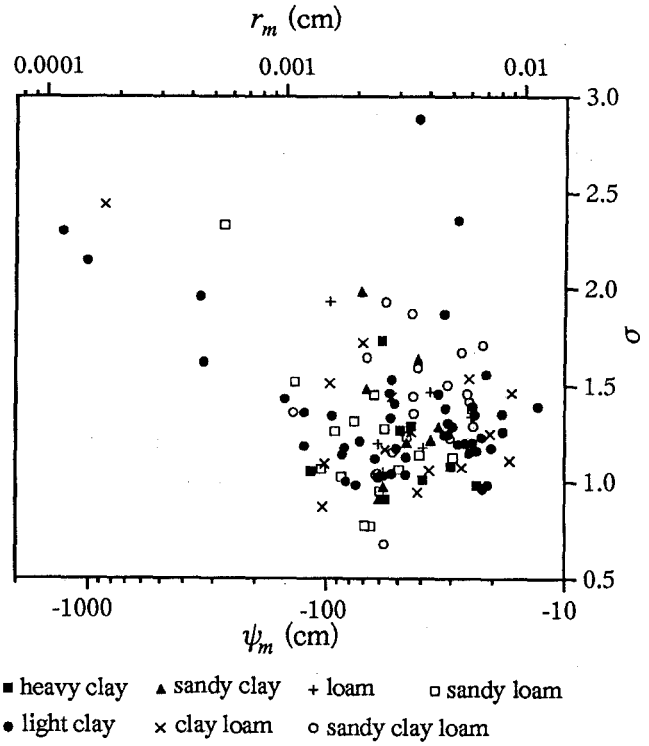

Figure 5.4 Relationship between ψ_m and σ for the undisturbed forest soils. Each plot symbol represents the soil texture.

Textures of the forest soils shown in Figure 5.4 range from heavy clay through sandy loam. Since the disturbed loamy soils have small ψ_m values as shown in Figure 5.3, it is reasonable to assume that the disturbed samples of these forest soils have smaller ψ_m values than the original undisturbed samples. In Figure 5.3, ψ_m values for the massive forest soils, which can be regarded as undeveloped field soils, are smaller than those for the crumb and granular-structure forest soils. As a result, the process of the change of the soil pore radius distribution affected by the forest ecosystem (forest plants and animals) can be regarded as the increasing process of the median of the distribution.

5.4.4 Effects of Soil Type and Horizon

Figures 5.5a and 5.5b show the relationships between ψ_m and σ estimated for the retention data sets of the brown forest soils and the black soils, respectively. Each plot symbol represents the horizon from which the soil samples were taken.

In Figure 5.5a, most of the points for the brown forest soils taken from A-horizon are distributed in the rage of $\psi_m > -100$ cm and $\sigma > 1.0$. Many of the soils taken from A-horizon have ψ_m values greater than -30 cm and some of the soils have σ values greater than 1.5. It should be noted that one point for the soil taken from A-horizon, which has ψ_m value of about -10^4 cm, is not shown in the figure. Many points representing the soils taken from B-horizon are located in the region where ψ_m is smaller than about -30 cm and σ is smaller than about 1.5. Values of σ for some of the soils are smaller than 1.0. In the range of $\psi_m < -70$ cm, points for the soils taken from the B-horizon are widely scattered with respect to the σ axis. Note that six points for the soils taken from B-horizon are distributed in the range of $-10^4 < \psi_m < -200$ cm and $1.5 < \sigma < 3.5$. As a result, it can be concluded that the brawn forest soils taken from A-horizon generally have the greater median of $g(r)$ than the brown forest soils taken from B-horizon. In the range of $\psi_m > -70$ cm, values of σ (that is, the width of $g(r)$) for the brown forest soils taken from A-horizon are generally greater than those for the brown forest soils taken from B-horizon.

In Figure 5.5b, most of the points for the black soils are located in the range of $0.5 < \sigma < 1.5$. That is, some of the brown forest soils have the greater width of $g(r)$ than the black soils. Some of the black soils taken from A-horizon have ψ_m values greater than about -30 cm, while the ψ_m values of the black soils taken from B-horizon are smaller than -30 cm.

The relationships between ψ_m and σ for the brown forest soils taken from A and B-horizons are shown in Figures 5.6a and 5.6b, respectively. In these figures, each plot symbol represents the soil type according to the classification system summarized by *Forest Soil Division* [1976]. Figure 5.6a indicates that many of the brown forest soils in dry condition (B_A, B_B, and B_C) have ψ_m values smaller than -30 cm. The points representing the moderately moist brown forest soils (B_D) are scattered widely with respect to the ψ_m axis, and most of the points representing the slightly wetted brown forest soils (B_E) are in the range of $\psi_m > -30$ cm. Consequently, it can be concluded that

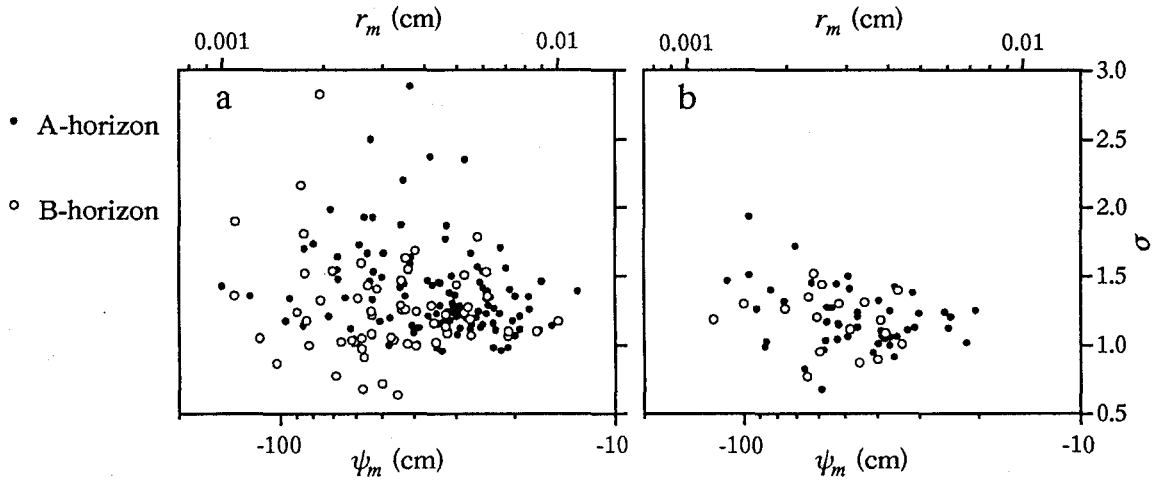

Figure 5.5 Relationships between ψ_m and σ for (a) the brown forest soils and (b) the black soils. Each plot symbol represents the horizon from which the soil samples were taken.

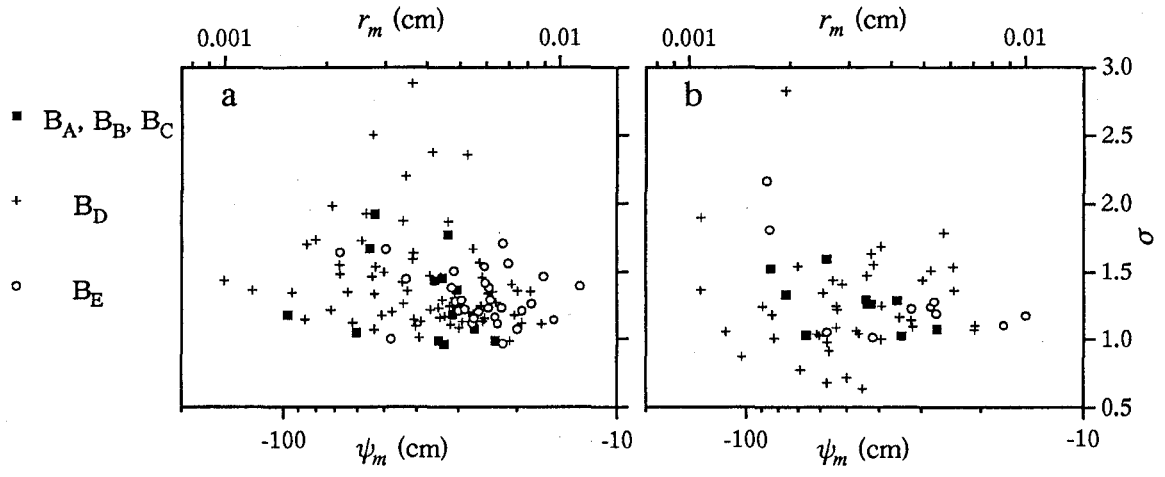

Figure 5.6 Relationships between ψ_m and σ for the brown forest soils taken from (a) A-horizon and (b) B-horizon. Each plot symbol represents the soil type according to *Forest Soil Division* [1976].

the median of $g(r)$ of brown forest soil taken from A-horizon generally becomes greater as the soil moisture condition becomes wet. Some of the B_D-soils taken from A-horizon have σ values greater than 2.0. Noted that one B_D-soil has ψ_m value of about -10^4 cm.

In Figure 5.6b, the trend is not clear for the brown forest soils taken from B-horizon. Points for six B_D-soils, which have ψ_m values smaller than -200 cm, are not shown in the figure.

5.5 SUMMARY AND CONCLUSIONS

In this chapter, the LN model for soil water retention proposed in Chapter 3 was modified to have a relatively simple functional form. The resulting water retention model (the LN2 model) contains two parameters ψ_m and σ both of which have physical significance on the θ-ψ curve and are related directly to the statistics of the soil pore radius distribution. Parameter ψ_m is the capillary pressure when the effective saturation is equal to 0.5 and is identical to the median and the geometric mean of the pore capillary pressure distribution $f(\psi)$. The pore radius r_m, which is related to ψ_m by the capillary pressure function, is the median of the pore radius distribution $g(r)$ and equal to the geometric mean of $g(r)$. Dimensionless parameter σ ($\sigma > 0$) determines the effective saturation at the inflection point on the θ-ψ curve and describes the slope of the curve. Value of σ is equal to the standard deviation of both the distribution of $\ln(-\psi)$ and the distribution of $\ln(r)$, and related to the width of $g(r)$.

The observed retention data sets of 282 undisturbed forest soils taken from *Mashimo* [1960] were analyzed using the LN2 model, and it was shown that the model performs fairly well for every retention data set. The average value of the coefficient of determination of the model for the 282 data sets was 0.993.

Using the estimated parameters ψ_m and σ, the effects of forest soil structure, texture, type, and horizon on the soil pore radius distribution and the soil moisture characteristic were analyzed. Results showed that many crumb-structure soils have greater median of $g(r)$ than the granular-structure soils, and the width of $g(r)$ for many crumb-structure soils are greater than those for the granular-structure soils. The massive soils have smaller median of $g(r)$ than the crumb and granular-structure soils. The disturbed loamy soils have smaller median of $g(r)$ than many of the forest soils and the disturbed sandy soils have smaller $g(r)$ width than the forest soils. It was concluded that the water retention characteristics of the undisturbed forest soils are related to the soil structure more closely than to the soil texture. The process of the change of $g(r)$ affected by the forest ecosystem (forest plants and animals) can be regarded as the increasing process of the median of the distribution. The brawn forest soils taken from A-horizon generally have the greater median of $g(r)$ than the brown forest soils taken from B-horizon. Some of the brown forest soils have the greater width of $g(r)$ than the black soils. The median of $g(r)$ of brown forest soil taken from A-horizon generally becomes greater as the soil moisture

condition becomes wet.

Since the LN2 model was developed by applying a distribution law available in general probability theory, the model and its parameters can be effectively used for theoretical studies on soil hydraulic properties. In the following chapters, the soil pore ratios derived from the widely used soil pore classification systems and the soil hydraulic conductivity will be analyzed in connection with the parameters of the LN2 model.

REFERENCES

Arimitsu, K., Analysis of soil pore radius distribution using a suction plate (in Japanese*), *Jpn. J. For. Environment, 12*(1), 31-35, 1970.

Brooks, R. H., and A. T. Corey, Hydraulic properties of porous media, *Hydrol. Pap. 3*, Civil Eng. Dept., Colo. State Univ., Fort Collins, 1964.

Forest Soil Division, Classification of forest soil in Japan (1975) (in Japanese with English Summary), *Bull. Gov. For. Exp. Sta., 280*, 1-28, 1976.

Kawada, H., *Introduction to Forest Soil Science* (in Japanese*), Hakuyu-sha, Tokyo, Japan, 1989.

Klute, A., and D. F. Heermann, Soil water profile development under a periodic boundary condition, *Soil Sci., 117*, 265-271, 1974.

Kobayashi, S., Changes in soil caused by forest clear-cutting (in Japanese), *Pedologist, 26*, 150-163, 1982.

Kubota, J., Y. Fukushima, and M. Suzuki, Observation and modeling of the runoff process on a hillslope (in Japanese with English Summary), *J. Jpn. For. Soc., 69*, 258-269, 1987.

Kumlung, A., and Y. Takeda, Changes of soil properties in relation to lapsed years of hillside works on a granite area, *J. Jpn. For. Soc., 73*, 327-338, 1991.

Marquardt, D. W., An algorithm for least-squares estimation on non-linear parameters, *J. Soc. Ind. Appl. Math., 11*, 431-441, 1963.

Mashimo, Y., Moisture condition (pF) of forest soil (in Japanese with English Summary), *Forest Soils Jpn., 8*, 43-66, 1957.

Mashimo, Y., Studies on the physical properties of forest soil and their relation to the growth of sugi (*Cryptomeria japonica*) and hinoki (*Chamaecyparis obtusa*) (in Japanese with English Summary), *Forest Soils Jpn., 11*, 1-182, 1960.

Mualem, Y., A catalogue of the hydraulic properties of unsaturated soils, *Proj. 442*, 100 pp., Technion-Israel Inst. of Technol., Haifa, Israel, 1976.

Nakajima, K., *Estimation of Evapotranspiration on Non-Irrigated Lands in the Arid District of Central Asia* (in Japanese*), A graduation thesis, Kyoto Univ., 1995.

Ogasiwa, K., T. Kondou, and Y. Mashimo, An analysis of factors affecting coarse pore volume of forest soil with the quantification-I method, I, Coarse pore volume of soil at various depth in sugi (*Cryptomeria japonica*) stands (in Japanese), *J. Jpn. For. Soc., 73*, 393-395, 1991.

Ohnuki, Y., R. Terazono, H. Ikuzawa, and I. Hirata, Distribution and physical properties of surficial soils in Minami-Meijiyama experimental watershed in Okinawa Island, Japan (in Japanese), *J. Jpn. For. Soc., 76*, 355-360, 1994.

Ohta, T., Y. Fukushima, and M. Suzuki, Research on runoff from hillsides by one-dimensional transient saturated-unsaturated flow (in Japanese with English Summary), *J. Jpn. For. Soc.,*

65, 125-134, 1983.

Ohta, T., Y. Tsukamoto, and M. Hiruma, The behavior of rainwater on a forested hillslope, I, The properties of vertical infiltration and the influence of bedrock on it (in Japanese with English Summary), *J. Jpn. For. Soc., 67*, 311-321, 1985.

Ohte, N., *Studies on Pore Structure and Hydraulic Properties of Forest Soils* (in Japanese*), A doctor thesis, Kyoto Univ., 1992.

Sammori, T., and Y. Tsuboyama, Study on method of slope stability considering infiltration phenomenon (in Japanese with English Summary), *J. Jpn. Soc. Erosion Control Eng., 43*(4), 14-21, 1990.

Soil Survey Staff, *Soil Survey Manual*, USDA Agric. Handbook, *18*, 1951.

Suzuki, M., The properties of a base-flow recession on small mountainous watersheds, I, Numerical analysis using the saturated-unsaturated flow model (in Japanese with English summary), *J. Jpn. For. Soc., 66*, 174-182, 1984.

Takeshita, K., Some considerations on the relation between forest soil and control function to river discharge (in Japanese), *Jpn. J. For. Environment, 27*(2), 19-26, 1985.

Tani, M., The properties of a water-table rise produced by a one-dimensional, vertical, unsaturated flow (in Japanese with English summary), *J. Jpn. For. Soc., 64*, 409-418, 1982.

Tani, M., Analysis of one-dimensional, vertical, unsaturated flow in consideration of runoff properties of a mountainous watershed (in Japanese with English summary), *J. Jpn. For. Soc., 67*, 449-460, 1985.

Tsuboyama, Y., and T. Sammori, Numerical simulation of seepage in a forested hillslope by finite element method (in Japanese with English Summary), *J. Jpn. Soc. Hydrol. Water Resour., 2*(2), 49-56, 1989.

Tsukamoto, Y., *Forest Hydrology* (in Japanese*), Buneido, Tokyo, Japan, 1992.

van Genuchten, M. Th., A closed-form equation for predicting the hydraulic conductivity of unsaturated soils, *Soil Sci. Soc. Am. J., 44*(5), 892-898, 1980.

van Genuchten, M. Th., and D. R. Nielsen, On describing and predicting the hydraulic properties of unsaturated soils, *Ann. Geophys., 3*(5), 615-628, 1985.

* The title is tentative translation from the original Japanese title by the author of this thesis.

CHAPTER 6

NEW DIAGRAM TO EVALUATE PORE RADIUS DISTRIBUTION OF FOREST SOIL

6.1 INTRODUCTION

The soil moisture characteristic, which is represented by the relationship between the volumetric water content θ and the soil capillary pressure ψ, is based on the soil pore radius (size) distribution. *Mashimo* [1960] proposed a soil pore classification system in which coarse and fine pores are divided by the pore capillary pressure value of -500 cm (that is, pF 2.7). Measurements of soil pore radius distribution using this classification system have been widely carried out by forest soil scientists. *Takeshita* [1985] suggested a soil pore classification system in which soil pores are classified into four kinds according to the pore capillary pressure values. This classification system was frequently used in measurements of pore radius distribution in order to estimate the water holding capacity of forest soils. However, knowledge accumulated by these measurements of soil pore radius distribution has not been effectively used in physical analyses of water flow in forest soils because of the lack of suitable functional models for soil water retention.

In the previous chapter, the LN model for soil water retention proposed in Chapter 3 was modified to have a relatively simple functional form. The parameters of the resulting water retention model (the LN2 model) have physical significance on the θ-ψ curve and are related directly to the statistics of the soil pore radius distribution. Analyzing the observed retention data sets of 282 soils, it was shown that the LN2 model is successfully used to derive functional θ-ψ relationships of forest soils. By combining the LN2 model with the widely used soil pore classification systems, knowledge accumulated by measurements of forest soil pore radius distribution will be effectively used for analyzing the hydrological phenomena on forestal watersheds. In this chapter, the parameters of the LN2 model are related to the soil pore ratios derived from the widely used soil pore classification systems. Simple means of estimating parameters of the LN2 model are also suggested.

6.2 RELATIONSHIPS BETWEEN PARAMETERS OF THE LN2 MODEL AND SOIL PORE RATIOS TO EVALUATE PORE RADIUS DISTRIBUTION

6.2.1 The LN2 Model for Soil Water Retention

In Chapter 5, the following expression for soil water retention (the LN2 model) was proposed:

$$S_e = Q\left(\ln(\psi/\psi_m)/\sigma\right) \tag{5.8}$$

where Q denotes the complementary normal distribution function defined as (5.2). A plot of (5.8) for ψ_m = -100 cm (that is, $\log(-\psi_m) = 2$) and $\sigma = 1.2$ is shown using a semi-logarithmic scale in Figure 6.1. It can be seen that ψ_m is identical to the capillary pressure at the inflection point on the S_e-$\log(-\psi)$ curve. Notice that the differences between $\log(-\psi_m)$ and the $\log(-\psi)$ value at S_e = 0.841, and between $\log(-\psi_m)$ and the $\log(-\psi)$ value at S_e =0.159 are equal to $\sigma\log(e)$ ($\approx 0.434\sigma$). Consequently, S_e-$\log(-\psi)$ curve becomes steeper near the inflection point as σ becomes smaller. With a large σ value the curve has consistently small decreases in S_e as $\log(-\psi)$ increases.

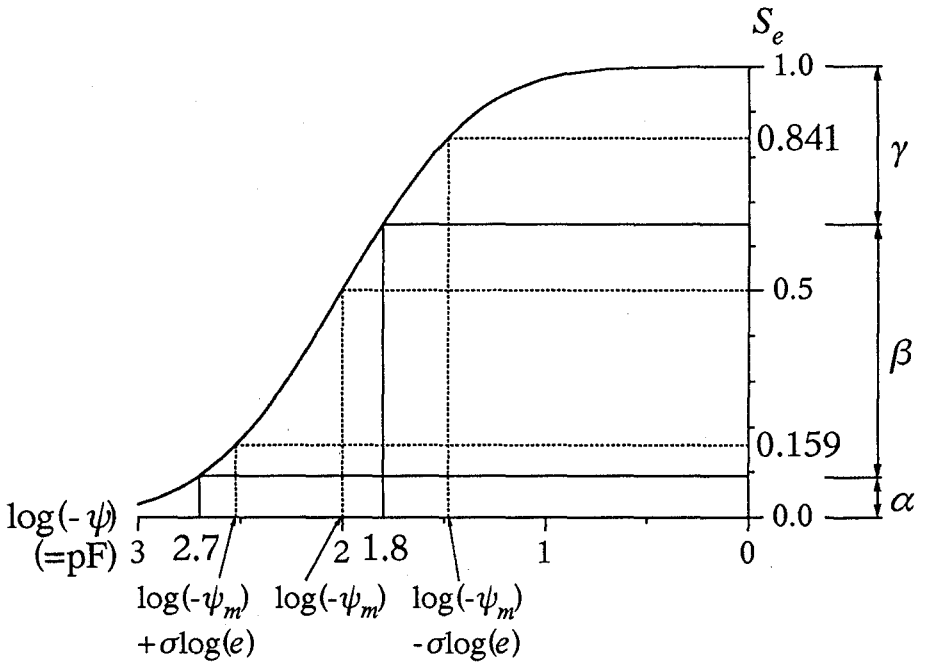

Figure 6.1 Curve for S_e-$\log(-\psi)$ based on the LN2 model, showing a plot of (5.8) for ψ_m = -100 cm ($\log(-\psi_m) = 2$) and $\sigma = 1.2$.

6.2.2 Soil Pore Ratios to Evaluate Pore Radius Distribution

The water contained in soil can be classified into several kinds. The gravitational water is held in soil at less than pF 1.8 (that is, $\psi > -63$ cm), and moves gravitationally in the non-capillary pores. The capillary water is held in soil at pF 1.8 ~ 4.2 in the capillary pores, and is equal to the total available water for plant growth. The point at pF 4.2 on the water retention curve is called the permanent wilting point. The water held in soil at more than pF 4.2 moves only in the vapor phase by evaporation, and is unavailable for plant growth [*Mashimo*, 1960; *Kawada*, 1989; *Tsukamoto*, 1992].

Mashimo [1960] proposed that soil pores can be classified as either coarse or fine. He defined coarse pores as those in which water is retained by capillary pressures greater than -500 cm (that is, pF 2.7). This classification system has been widely used in measurements of forest soil pore radius distribution [e.g., *Arimitsu*, 1970; *Kobayashi*, 1982; *Ogasiwa et al.*, 1991], since pF value of 2.7 is the boundary between the easily available water and the difficultly available water for the growth of sugi (*Cryptomeria japonica* D. DON) and Japanese cypress (*Chamaecyparis obtusa* (S. et Z.) ENDL.) [*Kawada and Kojima*, 1976].

Combining the above-mentioned two classification systems, effective soil pores for liquid water movement can be of three kinds: the non-capillary pores are pores in which water is retained by capillary pressures greater than -63 cm (that is, pF 1.8), the coarse capillary pores are those in which water is held at pF 1.8 ~ 2.7, and the fine capillary pores are those in which water is held at pF 2.7 ~ 4.2. *Kumlung and Takeda* [1991] and *Ohnuki et al.* [1994] have analyzed the physical properties of soil based on a similar classification system. Among these three kinds of pores, the coarse capillary pores have been said to be most effective for plant growth [*Kobashi et al.*, 1992]. The amount of the coarse capillary pores has been frequently used as the index of the water holding capacity of forest soils [e.g., *Takeshita*, 1985; *Arimitsu*, 1987].

Based on the assumption that the residual water content θ_r is the limit of the continuity of liquid water in soil and that water loses its capability to move responding to hydraulic gradients when θ is smaller than θ_r [*Brutsaert*, 1968; *Nishigaki*, 1983; *Luckner et al.*, 1989], the soil water content at the permanent wilting point can be equal to θ_r. Consequently, the fine capillary pore volume per unit volume of soil (that is, the fine capillary porosity) is equal to the difference between the water content at pF 2.7 and θ_r. Here, the author proposes ratios α, β, and γ to evaluate the soil pore radius distribution:

$$\alpha = \left(\theta_{\mathrm{pF2.7}} - \theta_r\right)/\left(\theta_s - \theta_r\right) \tag{6.1}$$

$$\beta = \left(\theta_{\mathrm{pF1.8}} - \theta_{\mathrm{pF2.7}}\right)/\left(\theta_s - \theta_r\right) \tag{6.2}$$

$$\gamma = \left(\theta_s - \theta_{\mathrm{pF1.8}}\right)/\left(\theta_s - \theta_r\right) \tag{6.3}$$

where $\theta_{\mathrm{pF1.8}}$ and $\theta_{\mathrm{pF2.7}}$ are the volumetric soil water contents at pF 1.8 and 2.7,

respectively. Parameter (θ_s - θ_r) is called the effective porosity. Ratios α, β, and γ are referred to as the fine capillary pore ratio, the coarse capillary pore ratio, and the non-capillary pore ratio, respectively. The relationship between the soil water retention curve and the ratios α, β, and γ is indicated in Figure 6.1. It is clear from the figure that $\alpha + \beta + \gamma = 1$.

6.2.3 Relationships between Parameters ψ_m and σ, and Ratios α, β, and γ

The pore ratios α, β, and γ, which are derived from the widely used soil pore classification systems, can be related to the parameters ψ_m and σ of the LN2 model by the following procedure. From Figure 6.1, it is clear that α is equal to the effective saturation S_e at pF 2.7 and the value of (α + β) is identical to S_e at pF 1.8. Consequently, the following relationships are derived from (5.8):

$$\sigma Q^{-1}(\alpha) = \ln\left(10^{2.7}\right) - \ln\left(-\psi_m\right) \tag{6.4}$$

$$\sigma Q^{-1}(\alpha+\beta) = \ln\left(10^{1.8}\right) - \ln\left(-\psi_m\right) \tag{6.5}$$

where Q^{-1} denotes the inverse function of Q defined as (5.2) and represents a percentage point of the normal distribution. Equations (6.4) and (6.5) yield the expressions of ψ_m and σ with respect to α and β:

$$\psi_m = -10^{\frac{1.8Q^{-1}(\alpha)-2.7Q^{-1}(\alpha+\beta)}{Q^{-1}(\alpha)-Q^{-1}(\alpha+\beta)}} \tag{6.6}$$

$$\sigma = \frac{0.9\ln(10)}{Q^{-1}(\alpha)-Q^{-1}(\alpha+\beta)} \tag{6.7}$$

Noted that (6.6) and (6.7) can be transformed to the expressions with respect to α and γ (or with respect to β and γ) by using the relationships of $Q^{-1}(\alpha + \beta) = -Q^{-1}(\gamma)$ and $Q^{-1}(\alpha) = -Q^{-1}(\beta + \gamma)$.

The relationship between ψ_m and the ratios α, β, and γ expressed as (6.6) is shown in Figure 6.2a using a triangle diagram. As shown in Chapter 5, ψ_m is related to the median r_m of the pore radius distribution $g(r)$ by the capillary pressure function, which is expressed as (3.2), and equal to the capillary pressure at S_e = 0.5 (see Figure 6.1). Consequently, ψ_m is equal to $-10^{2.7}$ cm when α = 0.5 regardless of β and γ values, and equal to $-10^{1.8}$ cm when γ = 0.5 regardless of α and β. Value of ψ_m is smaller than $-10^{2.7}$ cm for the soil which has α value greater than 0.5, and is greater than $-10^{1.8}$ cm for the soil with γ value greater than 0.5. For the soil having the same amount of the fine capillary pores as the non-capillary pores (that is, α = γ), ψ_m is equal to $-10^{2.25}$ cm regardless of the coarse capillary pore ratio β. Figure 6.2b is the triangle diagram which shows the constant σ lines derived from (6.7). Parameter σ is the standard deviation of the distribution of $\ln(-\psi)$ and is related to the width of the pore radius distribution. The

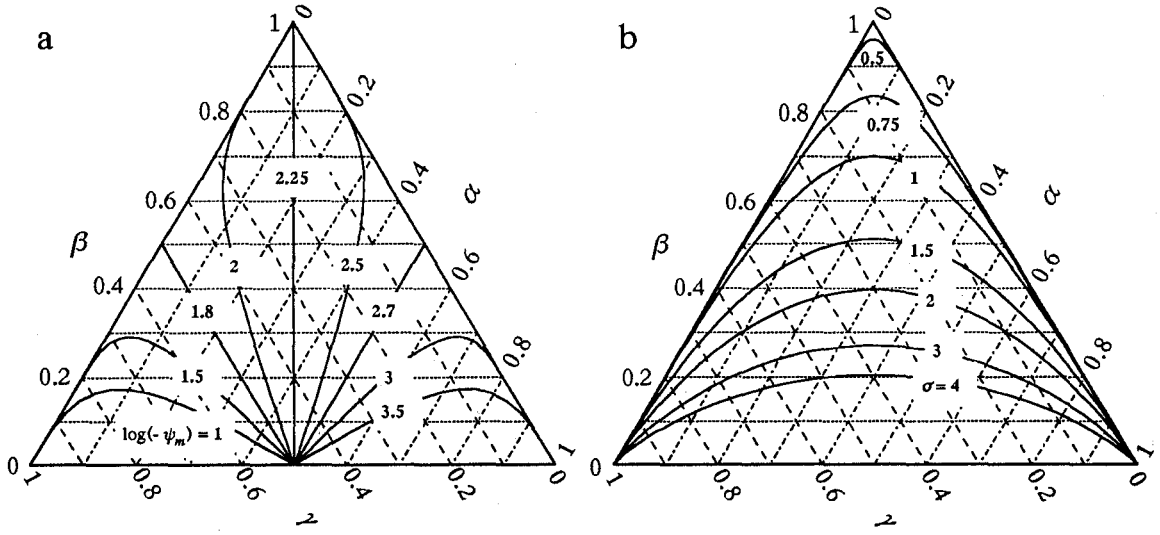

Figure 6.2 Relationships (a) between ψ_m and the soil pore ratios α, β, and γ, and (b) between σ and the ratios α, β, and γ. Constant ψ_m and σ lines were derived from (6.6) and (6.7), respectively.

figure shows that the constant σ lines are symmetrical. Value of σ becomes small as the coarse capillary pore ratio β increases. With a constant β value, σ is greatest when α is equal to γ.

6.3 DIAGRAMS TO EVALUATE SOIL PORE RADIUS DISTRIBUTION

6.3.1 Triangle Diagram to Evaluate Soil Pore Radius Distribution

Figure 6.3 is the triangle diagram which represents the ratios α, β, and γ determined for the retention data sets of the undisturbed forest soils taken from *Mashimo* [1960] (indicated by circles), and the disturbed loamy and sandy soils taken from *Mualem* [1976] and *Nakajima* [1995]. These data sets are the same data sets that are shown in Figure 5.3. The ratios α, β, and γ were computed from the θ-ψ curve utilizing the LN2 model which had been optimized for each retention data set by using a nonlinear least squares optimization procedure based on Marquardt's maximum neighborhood method [*Marquardt*, 1963].

The figure shows that most of the crumb and granular-structure forest soils have the

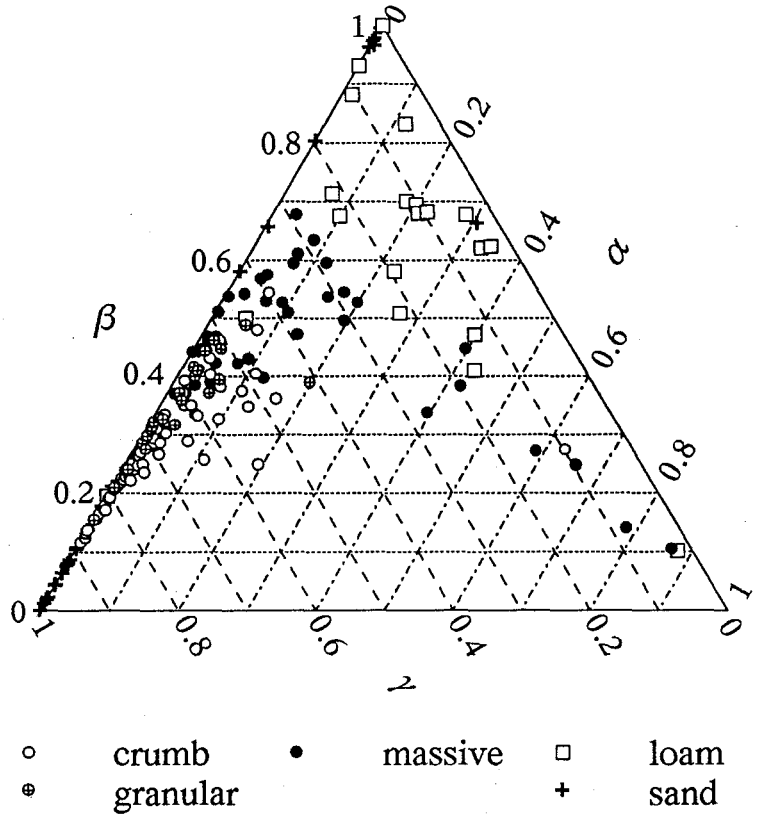

Figure 6.3 Triangle diagram representing the soil pore ratios α, β, and γ for the undisturbed forest soils (circles), and for the disturbed loamy and sandy soils (squares and pluses). Each plot symbol represents the soil structure for the forest soils.

non-capillary pore ratio (γ) greater than 0.4. More than half of the crumb-structure soils have γ values greater than 0.7. Values of the coarse capillary pore ratio (β) for the crumb and granular-structure soils are smaller than 0.5. Values of the fine capillary pore ratio (α) for most of the granular-structure soils are smaller than 0.08, while α for the crumb-structure soils were from 0 to 0.2. Points representing the massive forest soils are in the range of $\gamma < 0.6$ and widely scattered with respect to α values. Many Points for the massive soils are in the range of $\gamma > 0.25$ and $\beta > 0.4$, and α for these soils were estimated to be smaller than 0.2. Some of the massive soils have γ and β values smaller than 0.3 and 0.5, respectively, and α values greater than about 0.4. Values of γ estimated for most of the loamy soils are smaller than 0.25. Many points for the loamy soils are in the range of $\beta > 0.4$ and $\alpha < 0.4$. Values of α for the sandy soils were computed to be nearly equal to zero. Points for the sandy soils are widely scattered on the line of $\alpha = 0$. The figure shows that the triangle diagram is effectively used to evaluate the soil pore

radius distribution of various soils by representing the soil pore ratios α, β, and γ which are derived from the widely used soil pore classification systems.

6.3.2 New Diagram to Evaluate Soil Pore Radius Distribution

In Figure 6.4, the constant α, β, and γ lines generated by (6.6) and (6.7) are plotted on a coordinate system with ψ_m on the abscissa and σ on the ordinate. It can be seen that the constant α and γ lines are straight. When the ratios are equal to 0.5, the constant α and γ lines are parallel to the σ axis with ψ_m values of $-10^{2.7}$ and $-10^{1.8}$ cm, respectively. The constant β lines are symmetrical and have the largest σ at $\psi_m = -10^{2.25}$ cm. This figure also represents the relationship between ψ_m and σ estimated for the retention data sets of the forest soils, the loamy soils, and the sandy soils (the same data sets shown in Figure 6.3). Value of r_m, which is related to ψ_m by (3.2) and equal to the median of $g(r)$, is shown in the figure.

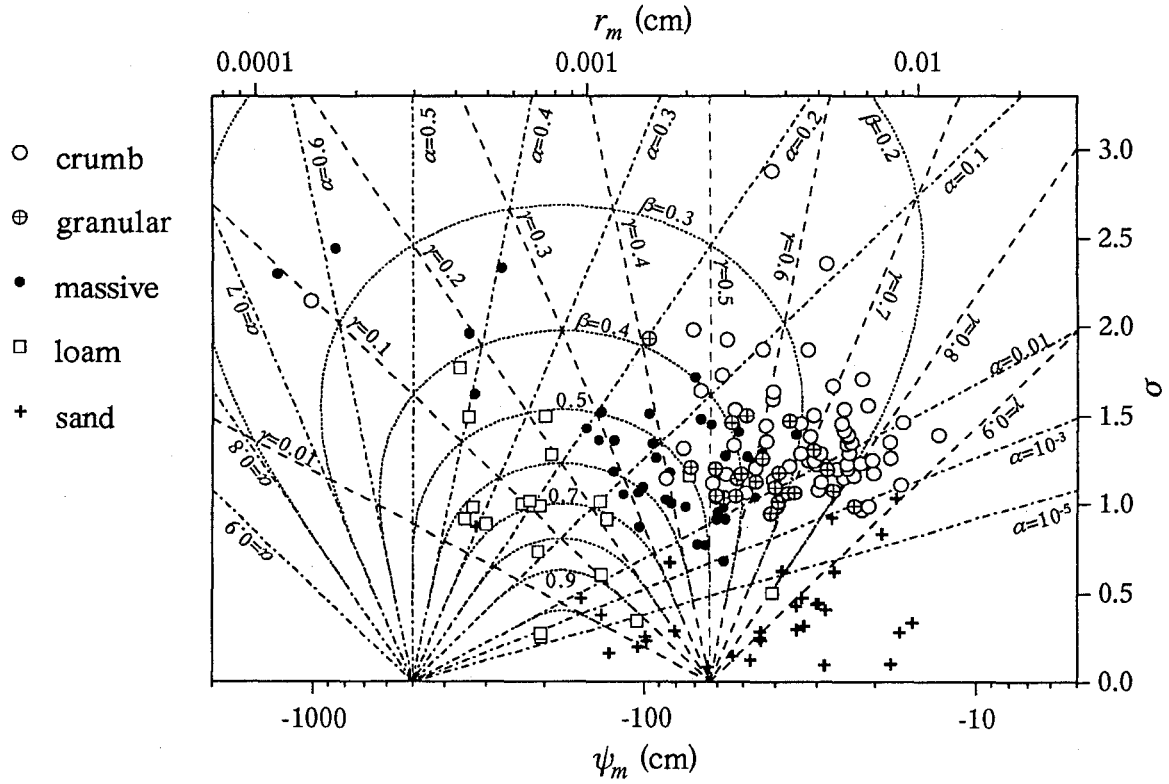

Figure 6.4 Coordinate system with ψ_m on the abscissa and σ on the ordinate, showing the constant α, β, and γ lines generated by (6.6) and (6.7). Figure also represents the relationship between ψ_m and σ estimated for the retention data sets of the forest soils, the loamy soils, and the sandy soils (the same data sets shown in Figure 6.3). Value of r_m is related to ψ_m by (3.2).

As shown in Figure 6.3, most of the crumb and granular-structure forest soils have the non-capillary pore ratio (γ) greater than 0.4. Figure 6.4 clearly indicates that ψ_m values for most of the crumb and granular-structure soils are greater than about -80 cm corresponding to these γ values. The large γ values ($\gamma > 0.7$) for more than half of the crumb-structure soils cause the large ψ_m values ($\psi_m >$ -30 cm) for these soils. Values of α for many of the crumb and granular-structure soils are from 0.001 to 0.08, hence the points representing these soils are approximately in the range of $1 < \sigma < 2$. Some of the crumb-structure soils have α greater than 0.08, which result in the high σ values for these soils. The small ψ_m values for the massive forest soils ($\psi_m <$ -50 cm) are attributable to the non-capillary pore ratio (γ) smaller than 0.6 estimated for the massive soils. Many points for the massive soils are in the range of $\gamma > 0.25$ and $\beta > 0.4$. Hence, ψ_m values of these soils are greater than -200 cm and σ values for these soils are smaller than 2. Some of the massive soils have γ and β values smaller than 0.3 and 0.5, respectively, and have the small ψ_m and the great σ values. Most of the loamy soils have the small non-capillary pore ratio ($\gamma < 0.25$). Consequently, ψ_m values for the loamy soils are smaller than about -100 cm. The values of fine capillary pore ratio (α) for many of the sandy soils are smaller than 10^{-5}, which resulted in the small σ values for the sandy soils.

In Figure 6.4, the pore ratios α, β, and γ, which are derived from the widely used soil pore classification systems, are related to the parameters ψ_m and σ of the LN2 model, which correspond to the statistics of the soil pore radius distribution and which have the physical significance on the water retention curve. This new diagram can be effectively used for evaluating the soil pore radius distribution in connection with the soil water retention characteristic.

6.4 SIMPLE MEANS OF ESTIMATING PARAMETERS OF THE LN2 MODEL

6.4.1 Estimation of ψ_m and σ by Using Ratios α, β, and γ

Using (6.6) and (6.7), the soil water retention curve based on the LN2 model can be estimated by measuring the soil pore ratios α, β, and γ. In Figure 6.5, the observed retention data set of the forest soil taken at Kiryu watershed (see Figure 4.1) is compared with the estimated curve (the solid line) generated by the following simple method using (6.6) and (6.7). Applying the simple method, the observed θ_s value of 0.5850 was used and θ_r was assumed to be identical to the smallest observed water content of 0.1695 at $\psi = -10^{3.2}$ cm. Measured soil water content at pF 1.8 ($\theta_{pF1.8}$) was 0.3371, and the water content at pF 2.7 ($\theta_{pF2.7}$) was computed to be 0.2199 as the average value of the measured water contents at pF 2.6 and 2.8. Using $\theta_s = 0.5850$ and $\theta_r = 0.1695$, the pore ratios α and ($\alpha + \beta$) were computed to be 0.121 and 0.403, respectively. From the obtained α and ($\alpha + \beta$) values, one can derive $Q^{-1}(\alpha) = 1.170$ and $Q^{-1}(\alpha + \beta) = 0.246$ by using the statistical table which shows percentage points of the normal distribution.

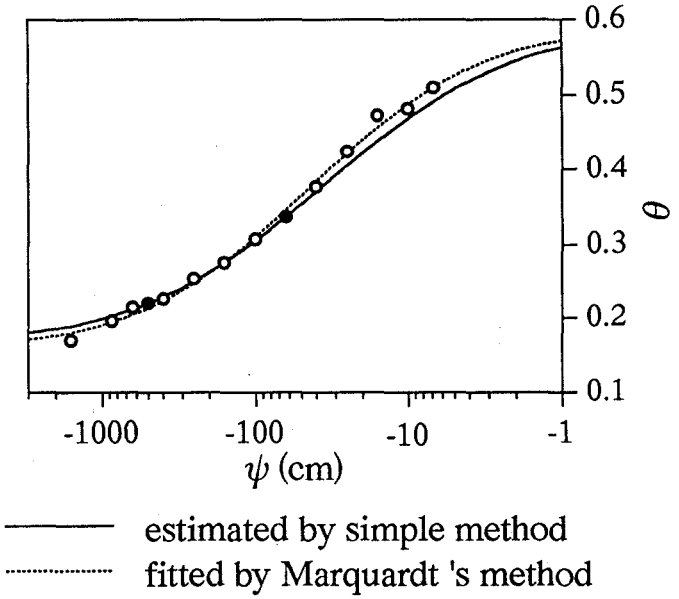

Figure 6.5 Observed, estimated, and fitted θ-ψ curves of forest soil taken at Kiryu watershed. Estimated curve was generated by the simple method using the observed soil pore ratios. Solid circles indicate two (θ, ψ) points used as inputs for the simple method. Fitted curve was generated by using the nonlinear least squares optimization procedure based on *Marquardt*'s [1963] method.

Substituting these $Q^{-1}(\alpha)$ and $Q^{-1}(\alpha + \beta)$ into (6.6) and (6.7) gives the predictions of ψ_m = -36.3 cm and σ = 2.24, respectively. It can be seen from Figure 6.5 that the simple parameter estimation procedure produced an acceptable estimate of the θ-ψ curve. The figure also shows the fitted θ-ψ curve based on the LN2 model (the dotted line) generated by using a nonlinear least squares optimization procedure based on Marquardt's maximum neighborhood method [*Marquardt*, 1963]. The estimated parameters by the simple method were about the same as the optimized θ_r (0.162), ψ_m (-45.3 cm), and σ (2.06) by using Marquardt's method. To be precise, the θ-ψ curve estimated by the simple method shows some discrepancies with the observed curve, especially near saturation. This is attributable to the small $\theta_{pF1.8}$ value of this forest soil used for the parameter estimation. Because values of the non-capillary pore ratio are large for many forest soils as shown in the previous section, θ value observed at less than pF 1.8 should be used instead of $\theta_{pF1.8}$ for more accurate parameter estimations.

6.4.2 Simple Means of Estimating ψ_m, σ, and θ_r

The parameters of the LN2 model can be estimated by measuring a small number of (θ, ψ) points on the soil water retention curve. Equation (5.8) has four parameters (θ_s, θ_r, ψ_m and σ) to be estimated. In these four parameters, θ_s is easy to measure experimentally.

For some retention data sets, it can be assumed that θ_r is equal to a measured water content at a low capillary pressure [*van Genuchten*, 1980]. When θ_s and θ_r have been determined with sufficient accuracy, measurements of water contents θ_1 and θ_2 at two different capillary pressures ψ_1 and ψ_2, respectively, can produce the estimates of ψ_m and σ by the following procedure. Values of effective saturation S_{e1} and S_{e2} are derived by substituting θ_1 and θ_2 in (2.2) using θ_s and θ_r values known apriori. When the soil water retention curve is described by the LN2 model, the relationships between S_{e1} and ψ_1, and S_{e2} and ψ_2 are derived from (5.8):

$$\sigma Q^{-1}(S_{e1}) = \ln(-\psi_1) - \ln(-\psi_m) \tag{6.8}$$

$$\sigma Q^{-1}(S_{e2}) = \ln(-\psi_2) - \ln(-\psi_m) \tag{6.9}$$

Equations (6.8) and (6.9) yields the expressions of ψ_m and σ with respect to S_{e1}, S_{e2}, ψ_1, and ψ_2:

$$\psi_m = -\exp\left\{\frac{Q^{-1}(S_{e1})\ln(-\psi_2) - Q^{-1}(S_{e2})\ln(-\psi_1)}{Q^{-1}(S_{e1}) - Q^{-1}(S_{e2})}\right\} \tag{6.10}$$

$$\sigma = \frac{\ln(-\psi_1) - \ln(-\psi_2)}{Q^{-1}(S_{e1}) - Q^{-1}(S_{e2})} \tag{6.11}$$

In Figure 6.6, the observed retention data set of the Gravelly sand G. E. 9 [*Reisenauer*, 1963] taken from *Mualem*'s [1976] catalogue (Mualem's soil index 4135) is compared with the estimated curves generated by using both the above-mentioned simple method and the nonlinear least squares optimization procedure based on Marquardt's method. Applying the simple method, the value of θ_s (= 0.326) was taken from Mualem's catalogue and θ_r was assumed to be identical to the smallest water content of 0.080 measured at ψ = -10^3 cm. Measured (θ, ψ) points of (0.270, -53.5 cm) and (0.120, -175 cm) were used as (θ_1, ψ_1) and (θ_2, ψ_2), respectively, for the parameter estimation procedure. Using θ_s = 0.326 and θ_r = 0.080, effective saturations S_{e1} and S_{e2} were computed to be 0.772 and 0.163, respectively. From the obtained S_{e1} and S_{e2} values, one can derive $Q^{-1}(S_{e1})$ = -0.745 and $Q^{-1}(S_{e2})$ = 0.982 by using the statistical table which shows percentage points of the normal distribution. Substituting $Q^{-1}(S_{e1})$, $Q^{-1}(S_{e2})$, ψ_1 and ψ_2 into (6.10) and (6.11) gives the predictions of ψ_m = -89.2 cm and σ = 0.686, respectively. The estimated parameters were about the same as the optimized θ_r (0.083),

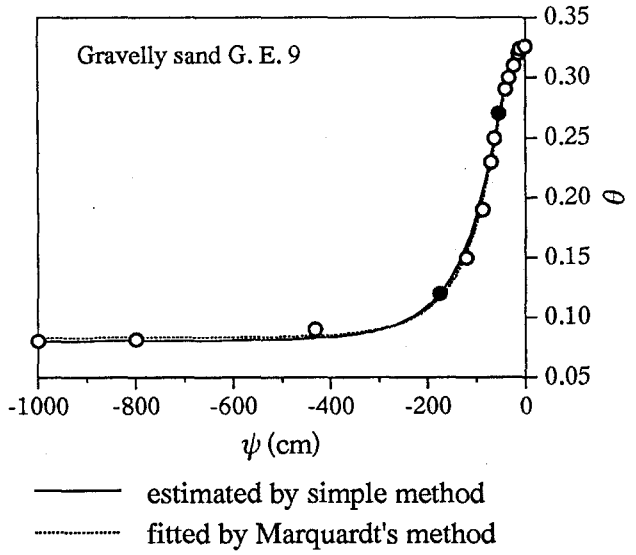

Figure 6.6 Observed, estimated, and fitted θ-ψ curves of Gravelly sand G. E. 9. Estimated curve was generated by using the simple method. Solid circles indicate two observed (θ, ψ) points used as inputs ((θ_1, ψ_1) and (θ_2, ψ_2)) for the simple method. Fitted curve was generated by using the nonlinear least squares optimization procedure based on *Marquardt*'s [1963] method.

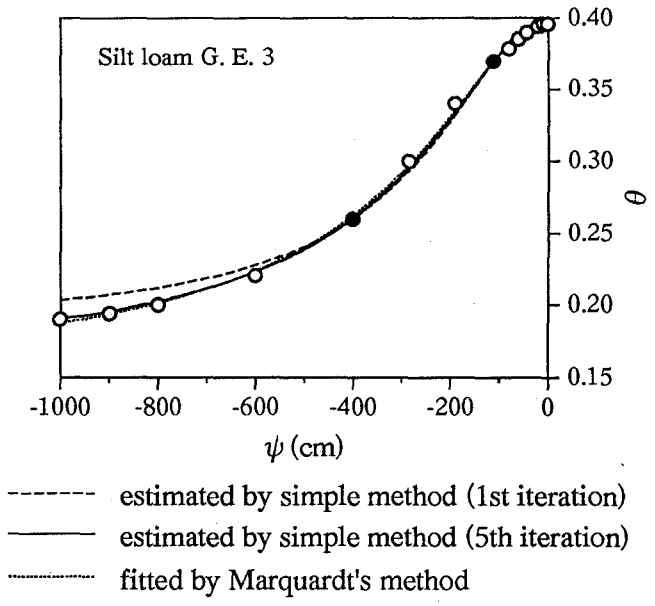

Figure 6.7 Observed, estimated, and fitted θ-ψ curves of Silt loam G. E. 3. Estimated curve was generated by using the simple method. Fitted curve was generated by using the nonlinear least squares optimization procedure based on *Marquardt*'s [1963] method. Solid circles are as defined in Figure 6.6.

ψ_m (-83.5 cm), and σ (0.675) by using Marquardt's method. It can be seen from Figure 6.6 that the simple parameter estimation procedure produced an acceptable estimate of the θ-ψ curve.

When observed soil water retention data are not available sufficiently in a dry region, the assumption of θ_r being equal to the smallest measured water content causes significant errors in the parameter estimation. In this case, θ_r can be estimated from a measurement of water content θ_3 at a low capillary pressure ψ_3. Assuming for the moment that $\theta_r = \theta_3$, parameter ψ_m and σ are computed by the above-mentioned procedure from two observed (θ, ψ) points. Using these first estimates of ψ_m and σ, one can compute θ_r' values by

$$\theta_r' = \frac{\theta_3 - \theta_s Q\left(\ln(\psi_3/\psi_m)/\sigma\right)}{1 - Q\left(\ln(\psi_3/\psi_m)/\sigma\right)} \tag{6.12}$$

Equation (6.12) was derived from (5.8) since the observed (θ_3, ψ_3) point should be located on the estimated θ-ψ curve. When θ_r' is not similar to the assumed θ_r, θ_r' is used as a new guess of θ_r to compute ψ_m and σ. This procedure is repeated until the agreement between θ_r and θ_r' is satisfactory.

Figure 6.7 shows the updating processes of the θ-ψ curve for the observed retention data set of Silt loam G. E. 3 [*Reisenauer*, 1963] taken from *Mualem*'s [1976] catalogue (Mualem's soil index 3310). In this example, the observed θ-ψ curve contrasts with the observed θ-ψ curve shown in Figure 6.6: the large changes in θ continue at $\psi = -10^3$ cm. The parameter estimation procedure was applied using measured (θ, ψ) points of (0.370, -111 cm) and (0.260, -400 cm) as (θ_1, ψ_1) and (θ_2, ψ_2), respectively. Measured (θ, ψ) point of (0.190, -1000 cm) was used as (θ_3, ψ_3) for estimating θ_r. Assuming that θ_r was equal to θ_3, the first estimates of ψ_m = -285 cm and σ = 0.823 were derived by (6.10) and (6.11), respectively. As shown in Figure 6.7, the estimated θ-ψ curve had larger θ values than the observed retention curve in the range of ψ < -600 cm. Values of θ_r' computed by (6.12) using the first estimates of ψ_m and σ was 0.176, which is smaller than θ_3. The second iteration using the θ_r value of 0.176 produced the estimates of ψ_m = -309 cm and σ = 0.863, and the computed θ_r' value by (6.12) was 0.170. After the 5th iteration, the agreement between θ_r and θ_r' was satisfactory and the estimated θ-ψ curve was fairly similar to the observed curve. Final values of θ_r, ψ_m and σ were 0.167, -324 cm and 0.887, respectively, which were about the same as the optimized θ_r (0.158), ψ_m (-347 cm), and σ (0.916) by using Marquardt's method.

As shown in this subsection, the concept of residual water content θ_r is an essential but problematic element in the LN2 model. The same is true of other existing water retention models such as those proposed by *Brooks and Corey* [1964] (the BC model) and *van Genuchten* [1980] (the VG model). The nature of θ_r is still controversial: *Luckner et al.* [1989] suggested a physically based definition of θ_r which was not widely accepted because it is not supported by observation [*Nimmo*, 1991]. Since the water content theoretically goes to zero as ψ being infinitely small, use of water retention

models which contain θ_r as a parameter might be restricted in the high-suction range. Several kinds of method to modify the BC and VG models to be successful in the high-suction range, have been proposed recently [e.g., *Campbell and Shiozawa*, 1992; *Rossi and Nimmo*, 1994; *Fayer and Simmons*, 1995; *Nakaegawa et al.*, 1995]. Such methods may be applicable also to the LN and LN2 models.

6.5 SUMMARY AND CONCLUSIONS

This chapter proposed soil pore ratios α, β, and γ based on the soil pore classification systems which are widely used in the measurements of forest soil pore radius distribution. Here, α, β, and γ represent ratios of the fine capillary porosity, coarse capillary porosity, and non-capillary porosity to the effective porosity, respectively. Then, the parameters ψ_m and σ of the soil water retention model developed in Chapter 5 (the LN2 model) were correlated with the pore ratios α, β, and γ. Parameter ψ_m is related to the median of the pore radius distribution by the capillary pressure function, and σ represents the width of the pore radius distribution.

By analyzing the observed retention data sets of the undisturbed forest soils taken from *Mashimo* [1960] and the disturbed loamy and sandy soils taken from *Mualem* [1976] and *Nakajima* [1995], it was shown that most of the crumb and granular-structure forest soils have the non-capillary pore ratio γ greater than 0.4 and the coarse capillary pore ratio β smaller than 0.5. Values of γ estimated for the massive forest soils are smaller than 0.6, and those for the loamy soils are smaller than 0.25. Values of fine capillary pore ratio α estimated for the sandy soils were nearly equal to zero. As a result, it was concluded that the triangle diagram representing the soil pore ratios α, β, and γ is effectively used to evaluate the soil pore radius distribution. A coordinate system with ψ_m on the abscissa and σ on the ordinate, which represents the constant α, β, and γ lines, was proposed as the new diagram to evaluate the soil pore radius distribution in connection with the soil water retention characteristic.

The method was suggested to estimate ψ_m and σ from measured soil pore ratios by using the statistical table which shows percentage points of the normal distribution. The simple means to estimate the parameters of the LN2 model from a small number of measured (θ, ψ) points were also proposed.

REFERENCES

Arimitsu, K., Analysis of soil pore radius distribution using a suction plate (in Japanese*), *Jpn. J. For. Environment, 12*(1), 31-35, 1970.

Arimitsu, K., *Water Holding Mechanism of Forest Soils* (in Japanese*), Sobun, Tokyo, Japan, 1987.

Brooks, R. H., and A. T. Corey, Hydraulic properties of porous media, *Hydrol. Pap. 3*, Civil Eng. Dept., Colo. State Univ., Fort Collins, 1964.

Brutsaert, W., The permeability of a porous medium determined from certain probability laws for pore size distribution, *Water Resour. Res.*, *4*(2), 425-434, 1968.

Campbell, G. S., and S. Shiozawa, Prediction of hydraulic properties of soils using particle-size distribution and bulk density data, in *International Workshop on Indirect Methods for Estimating the Hydraulic Properties of Unsaturated Soils*, edited by M. Th. van Genuchten, R. J. Leij, and L. J. Lund, 317-328, University of California, Riverside, 1992.

Fayer, M. J., and C. S. Simmons, Modified soil water retention functions for all matric suctions, *Water Resour. Res.*, *31*(5), 1233-1238, 1995.

Kawada, H., *Introduction to Forest Soil Science* (in Japanese*), Hakuyu-sha, Tokyo, Japan, 1989.

Kawada, H., and T. Kojima, *Means of Environmental Research, IV, Forest Soils* (in Japanese*), Kyoritsu, Tokyo, Japan, 1976.

Kobashi, S., H. Murai, and A. Kameyama, *Environmental Revegetation Technology* (in Japanese*), Asakura, Tokyo, Japan, 1992.

Kobayashi, S., Changes in soil caused by forest clear-cutting (in Japanese), *Pedologist, 26*, 150-163, 1982.

Kumlung, A., and Y. Takeda, Changes of soil properties in relation to lapsed years of hillside works on a granite area, *J. Jpn. For. Soc.*, *73*, 327-338, 1991.

Luckner, L., M. Th. van Genuchten, and D. R. Nielsen, A consistent set of parametric models for the two-phase flow of immiscible fluids in the subsurface, *Water Resour. Res.*, *25*(10), 2187-2193, 1989.

Marquardt, D. W., An algorithm for least-squares estimation on non-linear parameters, *J. Soc. Ind. Appl. Math.*, *11*, 431-441, 1963.

Mashimo, Y., Studies on the physical properties of forest soil and their relation to the growth of sugi (*Cryptomeria japonica*) and hinoki (*Chamaecyparis obtusa*) (in Japanese with English Summary), *Forest Soils Jpn.*, *11*, 1-182, 1960.

Mualem, Y., A catalogue of the hydraulic properties of unsaturated soils, *Proj. 442*, 100 pp., Technion-Israel Inst. of Technol., Haifa, Israel, 1976.

Nakaegawa, T., S. Hironaka, T. Oki, and K. Mushiake, Physical extrapolation of water retention curve in high suction range (in Japanese with English summary), *J. Jpn. Soc. Hydrol. Water Resour.*, *8*(5), 453-461, 1995.

Nakajima, K., *Estimation of Evapotranspiration on Non-Irrigated Lands in the Arid District of Central Asia* (in Japanese*), A graduation thesis, Kyoto Univ., 1995.

Nimmo, J. R., Comment on the treatment of residual water content in "A consistent set of parametric models for the two-phase flow of immiscible fluids in the subsurface" by L. Luckner et al., *Water Resour. Res.*, *27*(4), 661-662, 1991.

Nishigaki, M., Some aspects on hydraulic parameters of saturated-unsaturated regional ground-water flow (in Japanese), *Soils and Foundations*, *23*(3), 165-177, 1983.

Ogasiwa, K., T. Kondou, and Y. Mashimo, An analysis of factors affecting coarse pore volume of forest soil with the quantification-I method, I, Coarse pore volume of soil at various depth in sugi (*Cryptomeria japonica*) stands (in Japanese), *J. Jpn. For. Soc.*, *73*, 393-395, 1991.

Ohnuki, Y., R. Terazono, H. Ikuzawa, and I. Hirata, Distribution and physical properties of surficial soils in Minami-Meijiyama experimental watershed in Okinawa Island, Japan (in Japanese), *J. Jpn. For. Soc.*, *76*, 355-360, 1994.

Reisenauer, A. E., Methods for solving problems of multi-dimensional partially saturated

steady flow in soils, *J. Geophys. Res.*, *68*, 5725-5733, 1963.

Rossi, C., and J. R. Nimmo, Modeling of soil water retention from saturation to oven dryness, *Water Resour. Res.*, *30*(3), 701-708, 1994.

Takeshita, K., Some considerations on the relation between forest soil and control function to river discharge (in Japanese), *Jpn. J. For. Environment*, *27*(2), 19-26, 1985.

Tsukamoto, Y., *Forest Hydrology* (in Japanese*), Buneido, Tokyo, Japan, 1992.

van Genuchten, M. Th., A closed-form equation for predicting the hydraulic conductivity of unsaturated soils, *Soil Sci. Soc. Am. J.*, *44*(5), 892-898, 1980.

* The title is tentative translation from the original Japanese title by the author of this thesis.

CHAPTER 7

TWO-PARAMETER LOGNORMAL DISTRIBUTION MODEL FOR SOIL HYDRAULIC PROPERTIES

7.1 INTRODUCTION

Modeling water flow in soil requires knowledge of the hydraulic properties of the soil. The hydraulic properties of unsaturated soil are represented by the relationship between the volumetric water content θ and the soil capillary pressure ψ and the relationship between the unsaturated hydraulic conductivity K and ψ.

Some models for water retention [e.g., *Brooks and Corey*, 1964; *van Genuchten*, 1980; *Russo*, 1988] have been developed to be compatible with models by *Burdine* [1953] and *Mualem* [1976a] for the purpose of deriving analytical expressions that can be used to predict the relative hydraulic conductivity of soil. The sets of the water retention model and the derived model for relative hydraulic conductivity are referred to as the combined water-retention-hydraulic-conductivity models, and have been widely used for modeling purposes [e.g., *Russo et al.*, 1994; *Letha and Elango*, 1994].

In recent years, these combined water-retention-hydraulic-conductivity models have been widely used for theoretical studies on soil hydraulic properties. Some models have been used for expressing the hysteretic phenomena found in the θ-ψ and K-ψ relationships [e.g., *Luckner et al.*, 1989; *Stauffer et al.*, 1992]. Works on statistical analysis of spatial variability in parameters of these models have been published by *Wierenga et al.* [1991] and *Russo and Bouton* [1992], and scaling methods of soil water retention and hydraulic conductivity, based on these combined models, have been proposed by *Hopmans* [1987], *Ahuja and Williams* [1991] and *Clausnitzer et al.* [1992]. Parameters of these models have been related to the soil texture and other soil properties such as bulk density and percentage of organic matter by *Clapp and Hornberger* [1978], *McCuen et al.* [1981], *Carsel and Parrish* [1988] and *Wösten and van Genuchten* [1988]. Despite their usefulness, these combined models use empirical curve-fitting equations for the soil water retention curve. They do not emphasize the physical significance of their empirical parameters.

Several attempts have been made to derive models for the pore radius distribution for the purpose of analyzing the soil hydraulic properties on the basis of soil pore structure.

Brutsaert [1966] applied several distribution laws such as the incomplete gamma distribution, the lognormal distribution, and his own original distribution form, to the model for the pore radius distribution, and derived expressions for the soil water retention. By combining some of these water retention models with the model for predicting the hydraulic conductivity suggested by *Childs and Collis-George* [1950], *Brutsaert* [1968] obtained some models for the saturated and unsaturated hydraulic conductivities. However, rather complicated forms of the derived conductivity models limited their usefulness for modeling purposes. Although *Laliberte* [1969] suggested his own distribution form for the soil pore radius distribution and derived a water retention model, the corresponding model for relative hydraulic conductivity was not developed. This chapter proposes a model for hydraulic conductivity, which was developed by applying a distribution law available in general probability theory, and which has a relatively simple functional form, hence, can be effectively used both for theoretical studies on soil hydraulic properties and for numerical models for processes in soils.

In Chapter 5, the LN model for soil water retention, which was developed by applying a three-parameter lognormal distribution law to the soil pore radius distribution function, was modified to have a relatively simple functional form. The parameters of the resulting water retention model (the LN2 model) have physical significance on the θ-ψ curve and are related directly to the statistics of the soil pore radius distribution. In this chapter, the LN2 model is combined with *Mualem*'s [1976a] model in order to derive an analytical expression for the relative hydraulic conductivity. The accuracy of the resulting combined water-retention-hydraulic-conductivity model (C-LN2 model) is verified for observed data sets for some soils having widely varying hydraulic properties.

The saturated hydraulic conductivity K_s is also important for modeling water movement in soil. It has been indicated that the value of K_s is closely related to the soil pore radius distribution [*Kutílek and Nielsen*, 1994]. Several attempts have been made to derive relationships between K_s and the parameters of some combined water-retention-hydraulic-conductivity models [e.g., *Mishra and Parker*, 1990; *Wise et al.*, 1994]. The relationship between K_s of forest soils and the parameters of the C-LN2 model is also discussed in this chapter.

7.2 COMBINED WATER-RETENTION-HYDRAULIC-CONDUCTIVITY MODEL

In Chapter 5, the following expression for $f(\psi)$ and the corresponding model for soil water retention (the LN2 model) were proposed:

$$f(\psi) = \frac{\theta_s - \theta_r}{\sqrt{2\pi}\sigma(-\psi)} \exp\left[-\frac{\{\ln(\psi/\psi_m)\}^2}{2\sigma^2} \right] \tag{5.7}$$

$$S_e = Q\left(\ln(\psi/\psi_m)/\sigma\right) \tag{5.8}$$

where Q denotes the complementary normal distribution function defined as (5.2). The pore radius distribution function $g(r)$ corresponding to (5.8) is

$$g(r) = \frac{\theta_s - \theta_r}{\sqrt{2\pi}\sigma r}\exp\left[-\frac{\{\ln(r/r_m)\}^2}{2\sigma^2}\right] \tag{5.9}$$

where r_m is the pore radius which is related to ψ_m by the capillary pressure function expressed as (3.2) (that is, $r_m = A/\psi_m$). Equation (5.9) represents a lognormal distribution since the distribution of $\ln(r)$ conforms to $N(\ln(r_m), \sigma^2)$. Parameter r_m is equal to the median and the geometric mean of $g(r)$. Parameter σ is related to the width of $g(r)$ since it is the standard deviation of the distribution of $\ln(r)$.

On the other hand, *Mualem*'s [1976a] model for predicting the relative hydraulic conductivity K_r from soil water retention curve is written in the form

$$K_r = K/K_s = S_e^{1/2}\left\{\int_0^{S_e}\frac{dS_e}{|\psi|}\Big/\int_0^1\frac{dS_e}{|\psi|}\right\}^2 \tag{7.1}$$

Notice that (7.1) is identical to (2.10) with the constant value of $l = 1/2$ [*Mualem*, 1976a]. Combining (5.8) with (7.1) gives the functional relationships between K_r and S_e, and K_r and ψ. The integral in (7.1) is transformed as follows:

$$\int_0^{S_e}\frac{dS_e}{|\psi|} = \frac{1}{\theta_s-\theta_r}\int_{\theta_r}^{\theta}\frac{d\theta}{|\psi|} = \frac{1}{\theta_s-\theta_r}\int_{-\infty}^{\psi}\frac{1}{|\psi|}f(\psi)d\psi = \frac{1}{|A|(\theta_s-\theta_r)}\int_0^r rg(r)dr \tag{7.2}$$

When $g(r)$ is expressed as (5.9), the integration can be carried out without difficulties (see Appendix A):

$$\int_0^{S_e}\frac{dS_e}{|\psi|} = \frac{1}{|\psi_m|}\exp(\sigma^2/2)Q\left(\ln(\psi/\psi_m)/\sigma+\sigma\right) \tag{7.3}$$

Substituting $S_e = 1$ (that is, $\psi = 0$) into (7.3) yields

$$\int_0^1\frac{dS_e}{|\psi|} = \frac{1}{|\psi_m|}\exp(\sigma^2/2) \tag{7.4}$$

Hence (7.1) becomes

$$K_r = S_e^{1/2}Q^2\left(\ln(\psi/\psi_m)/\sigma+\sigma\right) \tag{7.5}$$

By substituting (5.8) into (7.5), K_r can be expressed in the term of S_e or ψ:

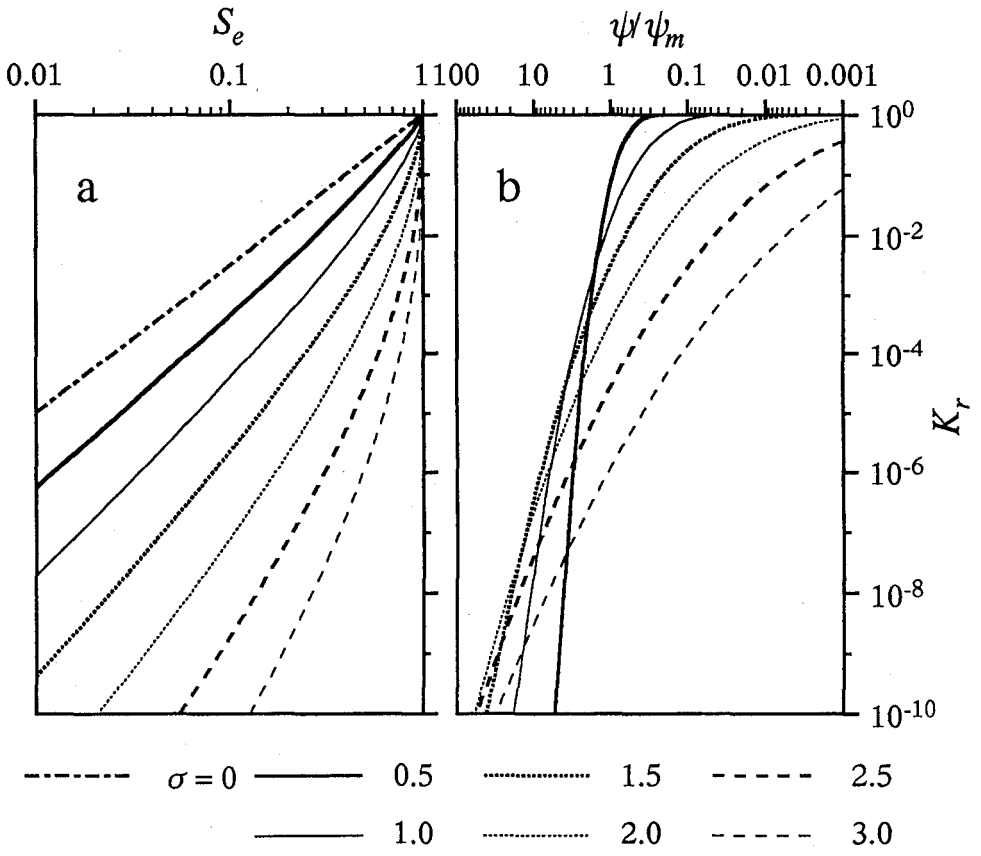

Figure 7.1 Curves for (a) K_r-S_e and (b) K_r-ψ/ψ_m based on the C-LN2 model, showing plots of (7.6) and (7.7) for different σ values.

$$K_r(S_e) = S_e^{1/2} Q^2\left(Q^{-1}(S_e) + \sigma\right) \tag{7.6}$$

$$K_r(\psi) = Q^{1/2}\left(\ln(\psi/\psi_m)/\sigma\right) Q^2\left(\ln(\psi/\psi_m)/\sigma + \sigma\right) \tag{7.7}$$

where Q^{-1} denotes the inverse function of Q defined as (5.2) and represents a percentage point of the normal distribution. The combination of the water retention model expressed as (5.8) and the hydraulic conductivity model expressed as (7.6) or (7.7) is referred to as the C-LN2 model. Noted that another expression for K_r can be derived by combining (5.8) with *Burdine*'s [1953] model for predicting the relative hydraulic conductivity (see Appendix B).

Plots of (7.6) for different σ values are shown using a logarithmic scale in Figure 7.1a. When $\sigma \to 0$, the medium has a uniform pore radius. It is clear from Figure 7.1a and also from (7.6) that for this case K_r is expressed as a power function of S_e (that is, K_r

$= S_e^{2.5}$) which is identical to the K_r model derived by application of the Kozeny model for saturated hydraulic conductivity [*Leibenzon*, 1947]. As σ becomes large, the ratio of change of K_r near saturation becomes great. Figure 7.1b shows the relationships between K_r and the reduced capillary pressure (ψ/ψ_m) obtained by (7.7) for different σ values. Actual ψ values are obtained by shifting the logarithmic scale by $\log(-\psi_m)$. With a small σ value, K_r remains near 1 for the small ψ/ψ_m value, and then there is an immediate sharp decline. With a large σ value, the curve has consistently small decreases in K_r as ψ decreases.

7.3 COMPARISON WITH EXPERIMENTAL DATA

To verify the accuracy of the C-LN2 model, observed water retention curves and hydraulic conductivities for five soils were analyzed. Data sets for four soils have been already analyzed by *van Genuchten* [1980] using the combined water-retention-hydraulic-conductivity model suggested by himself. This model has been reported to perform relatively well in comparison with other models such as the Brooks and Corey model [*Brooks and Corey*, 1964] and has been used extensively in numerical modeling [*van Genuchten and Nielsen*, 1985; *Jury et al.*, 1991].

Van Genuchten's water retention model (the VG model) is already reviewed in Chapter 2:

$$S_e = 1/\left\{1+\left(\alpha_V|\psi|\right)^n\right\}^m \tag{2.3}$$

where α_V and n ($n > 1$) are parameters and m is related to n by $m = 1 - 1/n$ ($0 < m < 1$). *Van Genuchten* [1980] substituted (2.3) into (7.1) and integrated to yield

$$K_r(S_e) = S_e^{1/2}\left\{1-\left(1-S_e^{1/m}\right)^m\right\}^2 \tag{7.8}$$

$$K_r(\psi) = \frac{\left[1-\left(\alpha_V|\psi|\right)^{n-1}\left\{1+\left(\alpha_V|\psi|\right)^n\right\}^{-m}\right]^2}{\left\{1+\left(\alpha_V|\psi|\right)^n\right\}^{m/2}} \tag{7.9}$$

where $m = 1 - 1/n$. Noted that (7.8) and (7.9) are equal to (2.13) and (2.14) with the constant value of $l = 1/2$, respectively. The combination of the water retention model expressed as (2.3) and the hydraulic conductivity model expressed as (7.8) or (7.9) is referred to as the C-VG model.

In Figures 7.2 through 7.5, the observed θ-ψ and K_r-ψ curves for 4 soils taken from Mualem's catalogue [*Mualem*, 1976b] are compared with the fitted θ-ψ and the predicted K_r-ψ curves obtained by the C-LN2 model. Parameters ψ_m, σ, and θ_r in (5.8) were optimized to fit the functional θ-ψ curves to the observed retention data sets using a

Table 7.1 Fitted Values for Parameters of the C-LN2 Model for the Retention Curves Plotted in Figures 7.2 through 7.6

Soil Name	K_s[*1], cm/sec	θ_s [*1]	θ_r	ψ_0, cm	ψ_m, cm	σ
Hygiene sandstone	1.25×10^{-3}	0.250	0.154	-124.5	-127.8	0.161
Touchet silt loam G. E. 3	3.51×10^{-3}	0.469	0.191	-191.8	-204.5	0.253
Silt loam G. E. 3	5.74×10^{-5}	0.396	0.158	-150.0	-347.2	0.916
Gravelly sand G. E. 9	2.78×10^{-4}	0.326	0.083	-52.9	-83.5	0.675
Guelph loam (drying)	3.66×10^{-4}	0.520	0.237	-52.3	-132.7	0.966
Guelph loam (wetting)	-	0.434	0.237	-35.8	-54.6	0.649

[*1] Taken from Mualem's catalogue [*Mualem*, 1976b].

nonlinear least squares optimization procedure based on Marquardt's maximum neighborhood method [*Marquardt*, 1963]. Applying Marquardt's method, the θ_s values were taken from Mualem's catalogue. The K_r-ψ curves were predicted by substituting the estimated ψ_m and σ in (7.7). The estimated parameters for each soil are summarized in Table 7.1 with the θ_s and K_s values taken from the catalogue. The table includes value of ψ_0 for each soil computed by (5.6) using the estimated ψ_m and σ. Parameter ψ_0 corresponds to the capillary pressure at the inflection point on the θ-ψ curve. The fitted θ-ψ and the predicted K_r-ψ curves obtained by the C-VG model ((2.3) and (7.9)) are also shown in Figures 7.2 through 7.5. These curves were plotted using the estimated parameter values summarized in Table 1 of *van Genuchten* [1980], with the exception of the soil shown in Figure 7.5.

Figure 7.2 shows results obtained for Hygiene sandstone [*Brooks and Corey*, 1964] (Mualem's soil index 4130). It can be seen that the fitted θ-ψ curve generated by the C-LN2 model matches the observed θ-ψ curve as well as the fitted curve by the C-VG model. *Van Genuchten* [1980] pointed out that a rather narrow pore radius distribution of this soil caused the water retention curve to become very steep at around ψ = -125 cm. This is clearly described by the estimated parameters of the C-LN2 model; σ was estimated to be rather small (σ = 0.16) and the estimated ψ_0 value was about -125 cm as shown in Table 7.1. Figure 7.2b shows both the C-LN2 and the C-VG models match the observed K_r-ψ curve equally well.

Results for Touchet silt loam G. E. 3 [*Brooks and Corey*, 1964] (Mualem's soil index 3307) are given in Figure 7.3. Again the C-LN2 model performed quite well for the observed θ-ψ and K_r-ψ curves. The small σ value for this soil indicates the narrow pore radius distribution of this soil. The estimated ψ_m value for this soil is smaller than that for Hygiene sandstone. That is, Touchet silt loam G. E. 3 has a smaller median of the pore radius distribution than the Hygiene sandstone.

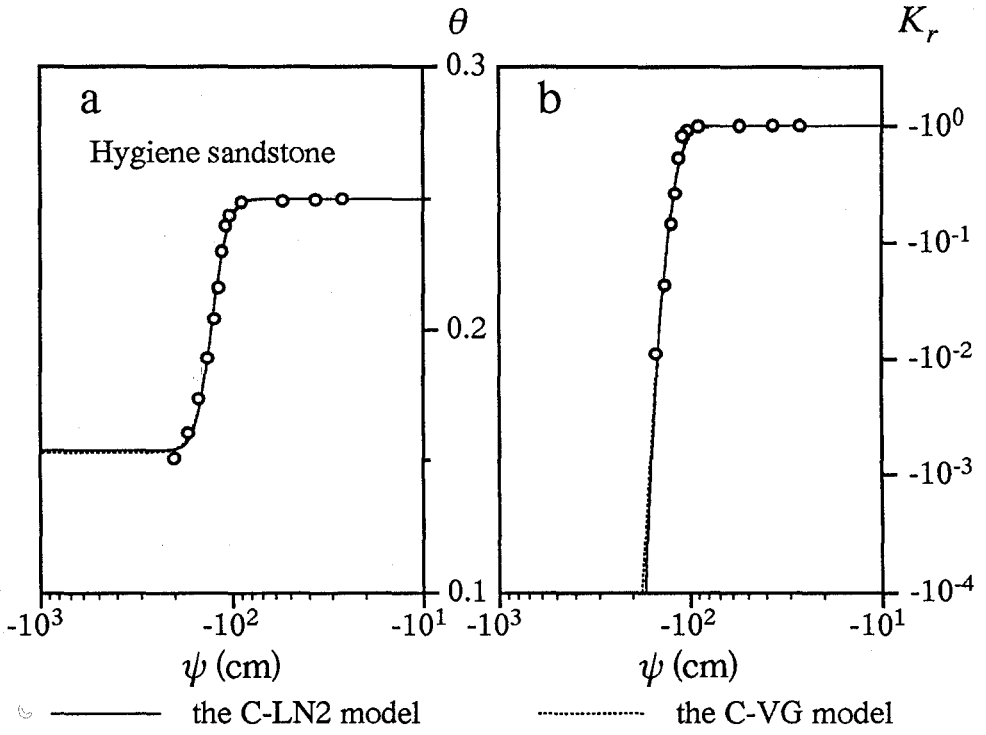

Figure 7.2 (a) Observed and fitted θ-ψ curves, and (b) observed and predicted K_r-ψ curves for Hygiene sandstone.

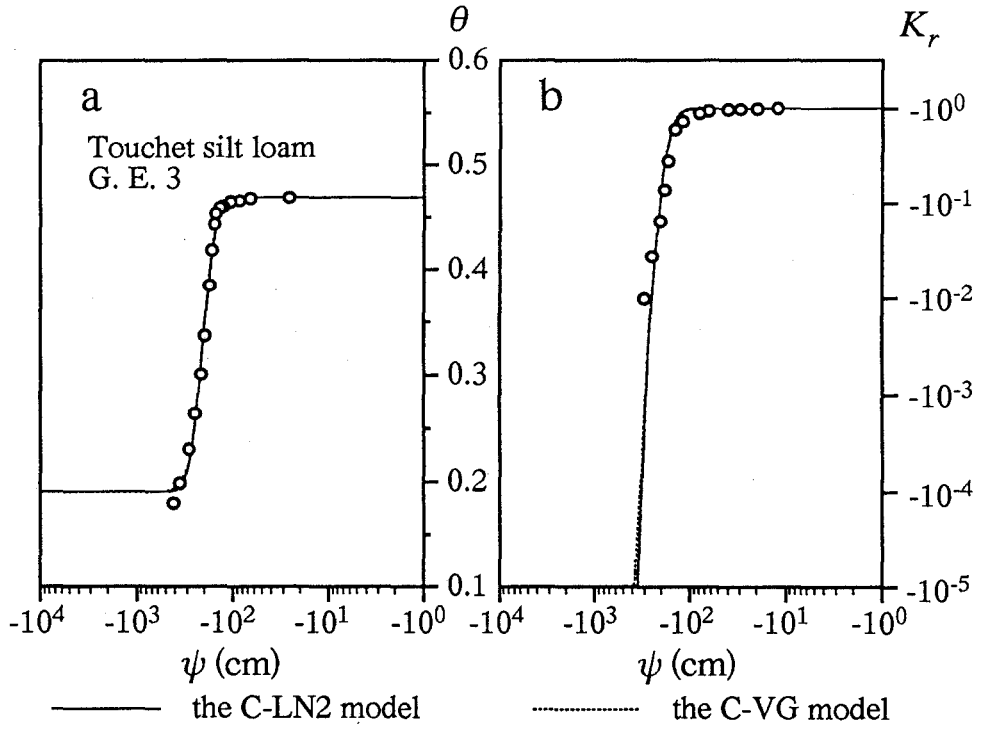

Figure 7.3 (a) Observed and fitted θ-ψ curves, and (b) observed and predicted K_r-ψ curves for Touchet silt loam G. E. 3.

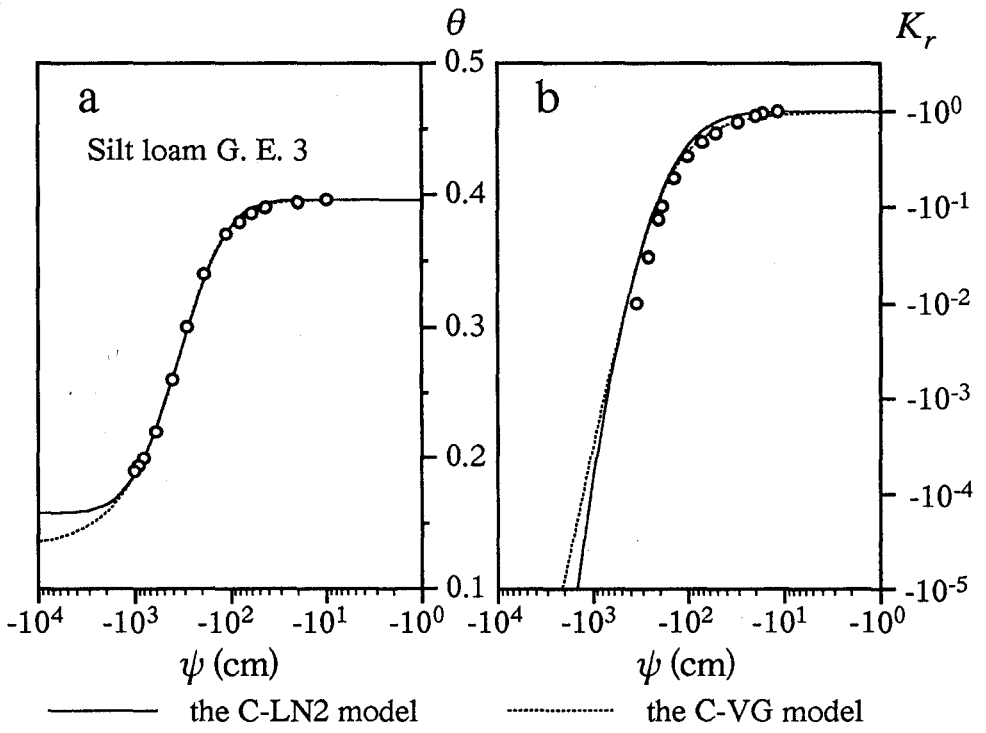

Figure 7.4 (a) Observed and fitted θ-ψ curves, and (b) observed and predicted K_r-ψ curves for Silt loam G. E. 3.

In Figure 7.4, observed θ-ψ and K_r-ψ curves for Silt loam G. E. 3 [*Reisenauer*, 1963] (Mualem's soil index 3310) are compared with the fitted θ-ψ curves and the predicted K_r-ψ curves generated by the C-LN2 and the C-VG models. As *van Genuchten* [1980] pointed out, only a limited portion of the water retention curve was observed for this soil. This caused a difference between the θ_r value estimated by the C-LN2 model (0.158) and that estimated by the C-VG model (0.131): the former was about 0.03 greater than the latter. Figure 7.4a shows that the fitted curve obtained by the C-LN2 model was quite similar to that obtained by the C-VG model in the region where the observed retention data exist. Each model produced an acceptable fit. Estimated σ value for this soil is greater than those for the former two soils, which make the retention curve have more gradual changes in θ. It can be seen from Figure 7.4b that the predicted K_r-ψ curves by both models match the observed K_r-ψ curve of this soil. To be precise, the C-VG model performed slightly better than the C-LN2 model especially for the higher conductivity values.

The observed θ-ψ and K_r-ψ curves of the Gravelly sand G. E. 9 [*Reisenauer*, 1963] (Mualem's soil index 4135) shown in Figure 7.5, have not been analyzed by *van Genuchten* [1980]. Hence Marquardt's method was used to fit (2.3) to the observed retention data set. Estimated values of θ_r, α_V, and n were 0.079, 0.0150 cm^{-1}, and 2.84,

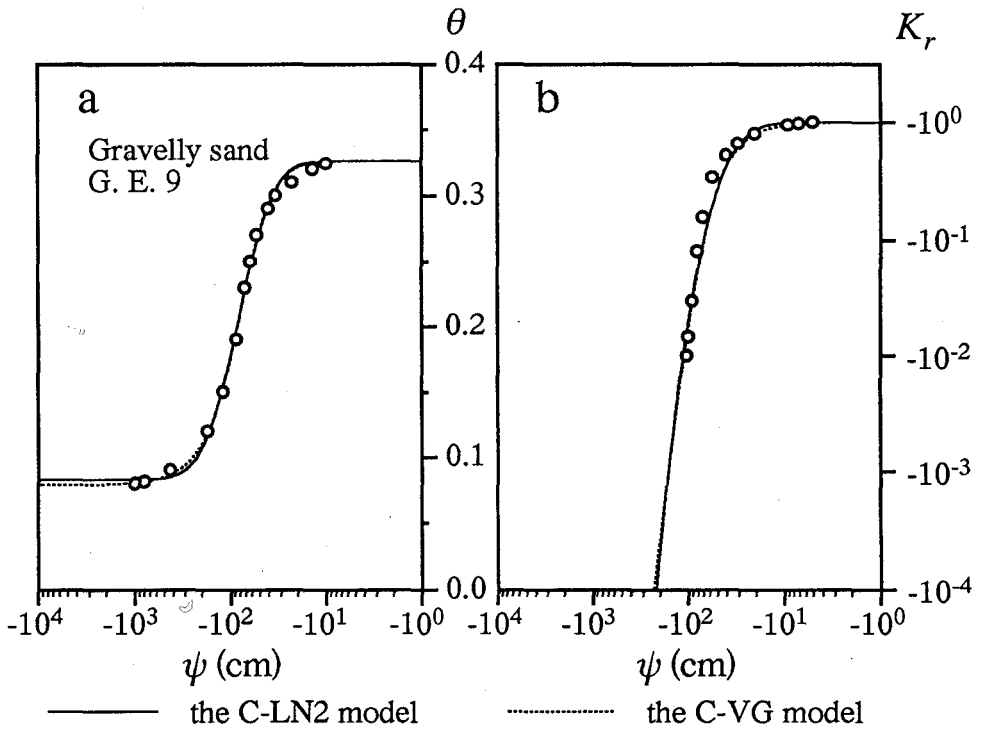

Figure 7.5 (a) Observed and fitted θ-ψ curves, and (b) observed and predicted K_r-ψ curves for Gravelly sand G. E. 9.

respectively. Again each model produced an acceptable match with the observed θ-ψ curve. Estimated ψ_m value for this soil is the largest in the four soils shown in Figures 7.2 through 7.5, indicating that this soil has a large median of the pore radius distribution. Figure 7.5b shows that the C-LN2 model predicted the observed K_r-ψ curve as well as the C-VG model.

For illustration of a typical retention data set in which a hysteretic phenomenon is found, the observed data set for Guelph loam [*Elrick and Bowman*, 1964] is compared with the fitted θ-ψ curve and the predicted K_r-θ curve generated by the C-LN2 model in Figure 7.6. The fitted θ-ψ curve and the predicted K_r-θ curve generated by the C-VG model (Figure 9 of *van Genuchten* [1980]) are also shown in the figure. Marquardt's method was applied to optimize parameters in (5.8) for the observed retention data set using the same assumptions as *van Genuchten* [1980] did; θ_s for the wetting branch was assumed to be the highest measured value (θ_s = 0.434) and θ_r for the wetting branch was assumed to be the same as θ_r estimated from the drying branch of the θ-ψ curve. Estimated parameters are summarized in Table 7.1. Estimated σ for the wetting branch of the retention curve was smaller than that for the drying branch, and estimated ψ_m and ψ_0 for the wetting branch were greater than those for the drying branch. Value of θ_r estimated by the C-LN2 model (0.237) was slightly higher than that estimated by the C-

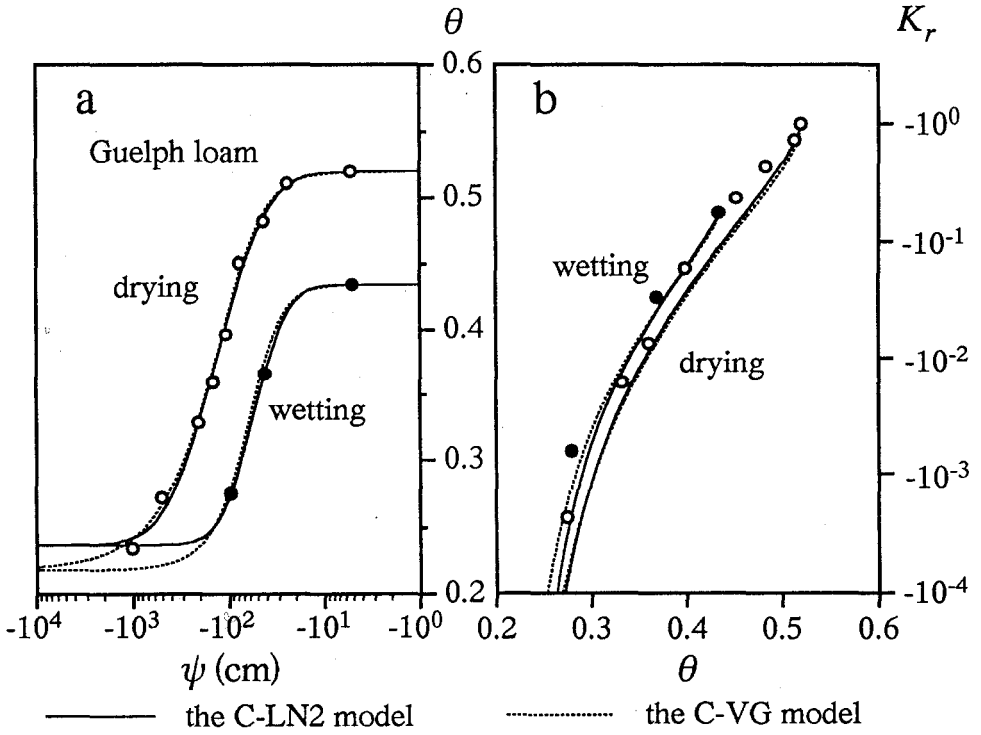

Figure 7.6 (a) Observed and fitted θ-ψ curves, and (b) observed and predicted K_r-θ curves for Guelph loam.

VG model (0.218). Figure 7.6a tells that both models succeeded to reproduce both drying and wetting branches of the retention curve. In Figure 7.6b, the K_r-θ curves predicted for the wetting branch by both the C-LN2 and the C-VG models ((7.6) and (7.8), respectively) were matched to the highest K_r value observed during the wetting process. It can be seen that the C-LN2 model performed as well as the C-VG model for both the drying and wetting branches of the K_r-θ curve. Note that the relative hydraulic conductivity $K_r(S_e)$ expressed as (7.6) does not depend on the value of ψ_m (or ψ_0). The same is true of (7.8), in which parameter α_v does not exist.

Figures 7.2 through 7.6 clearly show that the C-LN2 model produces acceptable matches with observed soil water retention curves and adequate predictions of relative hydraulic conductivities. The θ-ψ and K_r-ψ (or K_r-θ) curves generated by this model are similar to those generated by the C-VG model.

7.4 EFFECTS OF SOIL PORE RADIUS DISTRIBUTION ON SATURATED HYDRAULIC CONDUCTIVITY

The saturated hydraulic conductivity K_s is one of the fundamental parameters in the

physical analysis of water flow in soil. In this section, K_s values observed for 257 forest soil samples are correlated with the soil pore radius distributions using both the coordinate system with ψ_m on the abscissa and σ on the ordinate, and the triangle diagram showing the soil pore ratios α, β, and γ which were suggested in the previous chapter.

Figure 7.7 shows a scatterplot of the relationship between ψ_m and σ estimated for the retention data sets of the undisturbed forest soils taken from *Mashimo* [1960]. Value of r_m, which is related to ψ_m by (3.2), is also shown in the figure. The plot for each soil was classified by the K_s value of the soil. For K_s measurements, 400 ml cylindrical samples were used [*Mashimo*, 1960]. Maximal and minimal observed K_s values for the 257 soils were 1.6×10^{-1} and 5.3×10^{-5} cm/sec, respectively. The figure indicates that K_s becomes higher as ψ_m (or r_m) becomes greater. That is, the saturated hydraulic conductivity is higher for the soil with a greater median of the pore radius distribution $g(r)$. With respect to the σ axis, the trend is that the soil with a greater σ value (that is, the soil with a greater width of $g(r)$) has the higher K_s value under the same ψ_m value condition. Note that Figure 7.7 does not include two points representing soils which have ψ_m, σ, and K_s values of ($-10^{3.8}$ cm, 3.2, $10^{-3.0}$ cm/sec) and ($-10^{4.0}$ cm, 2.6, $10^{-3.9}$ cm/sec).

The functional relationship between K_s and the parameters of the pore radius distribution based on the C-LN2 model (ψ_m or r_m, and σ) is obtained by the following procedure. *Mualem* [1976a] developed the model for predicting soil hydraulic conductivity from soil water retention curve, which is expressed as (7.1), by characterizing the macroscopic flux in a soil using the microscopic soil pore radius distribution [*Kutílek and Nielsen*, 1994]. Mualem's model is similar to the model proposed by *Childs and Collis-George* [1950] which computes the probability of the connection of pairs of pores, but uses a modified assumption concerning the hydraulic conductivity of the pore sequence. He assumed an empirical power function with respect to $(\theta-\theta_r)$ (suggested by *Burdine* [1953]) for the pore tortuosity factor. Derived model for the unsaturated hydraulic conductivity K can be written as

$$K \propto (\theta - \theta_r)^l \left\{ \int_0^r r g(r) dr \right\}^2 \tag{7.10}$$

The exponent l in the tortuosity factor ($(\theta-\theta_r)^l$) was suggested to be 1/2 by *Mualem* [1976a] as an average for some 45 soils. The factor of $\int_0^r r g(r) dr$ is computed using the microscopic pore radius distribution $g(r)$ derived from the soil water retention curve. For the saturated hydraulic conductivity K_s, (7.10) is transformed as

$$K_s \propto (\theta_s - \theta_r)^l \left\{ \int_0^\infty r g(r) dr \right\}^2 \tag{7.11}$$

Assuming that l and $(\theta_s-\theta_r)$ values do not vary considerably from soil to soil, (7.11) is transformed as follows:

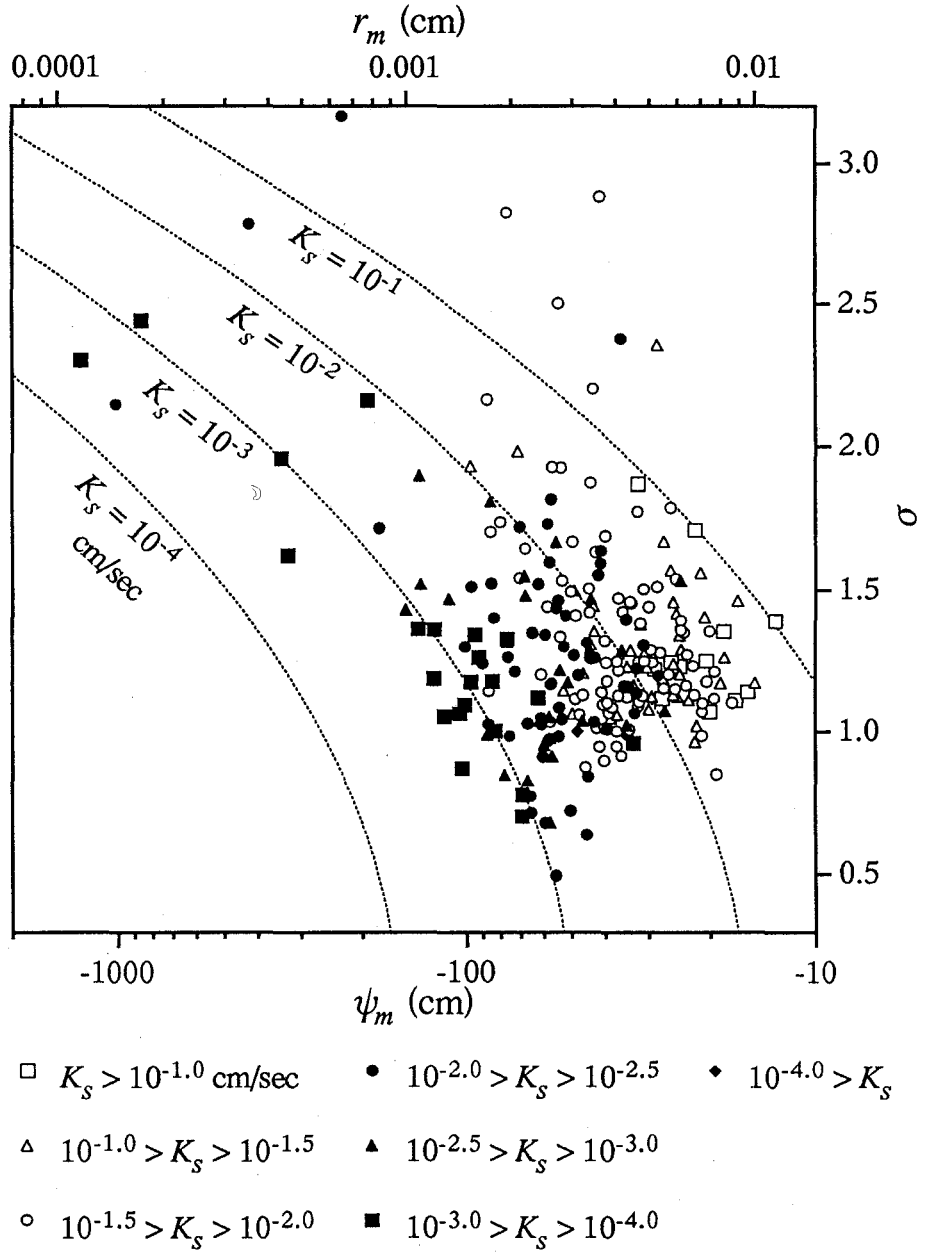

Figure 7.7 Relationship between ψ_m and σ estimated for the undisturbed forest soils. The plot for each soil was classified by the K_s value of the soil. Dotted lines indicate the analytical relationship between K_s and the parameters ψ_m and σ expressed as (7.14) with $B = 10^{0.4}$ cm^3/sec, and $K_s = 10^{-1}$, 10^{-2}, 10^{-3}, and 10^{-4} cm/sec. Value of r_m is related to ψ_m by (3.2).

$$K_s \propto \left\{\int_0^\infty rg(r)dr\right\}^2 \propto r_a^2 \tag{7.12}$$

where r_a is the arithmetic mean of the pore radius distribution $g(r)$. Equation (7.12) indicates that K_s is in proportion to the square of the mean pore radius. The arithmetic mean of the pore radius distribution $g(r)$ based on the C-LN2 model (that is, (5.9)) is expressed by the following function with respect to r_m and σ, or ψ_m and σ (see Appendix A):

$$r_a = r_m \exp(\sigma^2/2) = (A/\psi_m)\exp(\sigma^2/2) \tag{7.13}$$

By substituting (7.13) into (7.12), K_s is correlated with r_m (or ψ_m) and σ:

$$K_s = B' r_m^2 \exp(\sigma^2) = B\frac{\exp(\sigma^2)}{(-\psi_m)^2} \tag{7.14}$$

where B' is a constant and B is related to B' by $B = B'(-A)^2$. Equation (7.14) indicates that K_s becomes higher as r_m (or ψ_m) becomes greater and as σ becomes greater. The dotted lines in Figure 7.7 show plots of (7.14) for K_s = 10^{-1}, 10^{-2}, 10^{-3}, and 10^{-4} cm/sec assuming the constant B value of $10^{0.4}$ cm^3/sec (the corresponding B' value is 114 cm^{-1}sec^{-1}). In general, the analytical curves succeeded to reproduce the relationship between K_s and the parameters of the pore radius distribution (r_m and σ) obtained for the data sets of the 257 forest soils. As a result, (7.14) can be used for evaluating the effects of parameters r_m (or ψ_m) and σ on K_s. To be precise, differences can be found between the plots for the measured data sets and the analytical curves generated by (7.14). This is partly because of the assumption that l and $(\theta_s$-$\theta_r)$ values do not vary from soil to soil.

Figure 7.8 is the triangle diagram showing the relationship between K_s and the soil pore ratios α, β, and γ obtained for the 257 forest soils. Here, α, β, and γ represent ratios of the fine capillary porosity, coarse capillary porosity, and non-capillary porosity to the effective porosity, respectively (see (6.1) through (6.3)). It has been reported that the soil with the larger amount of non-capillary pores has the higher saturated hydraulic conductivity [*Mashimo*, 1960; *Kobashi et al.*, 1992]. The figure indicates that K_s increases as the non-capillary pore ratio γ becomes greater and as the coarse capillary pore ratio β becomes smaller. In the range of $\beta < 0.4$ and $\alpha < 0.2$, increases in the fine capillary pore ratio α result in increases in K_s. This is because σ (that is the width of the pore radius distribution) becomes greater as α increases in this range as already shown in Figure 6.2b. The functional relationship between K_s and the ratios α, β, and γ is yielded as follows by substituting (6.6) and (6.7) into (7.14):

$$K_s = B\exp\left[\left\{\frac{0.9\ln(10)}{Q^{-1}(\alpha)-Q^{-1}(\alpha+\beta)}\right\}^2 - 2\ln(10)\frac{1.8Q^{-1}(\alpha)-2.7Q^{-1}(\alpha+\beta)}{Q^{-1}(\alpha)-Q^{-1}(\alpha+\beta)}\right] \tag{7.15}$$

The constant K_s lines derived from (7.15) with the constant B value of $10^{0.4}$ cm^3/sec are

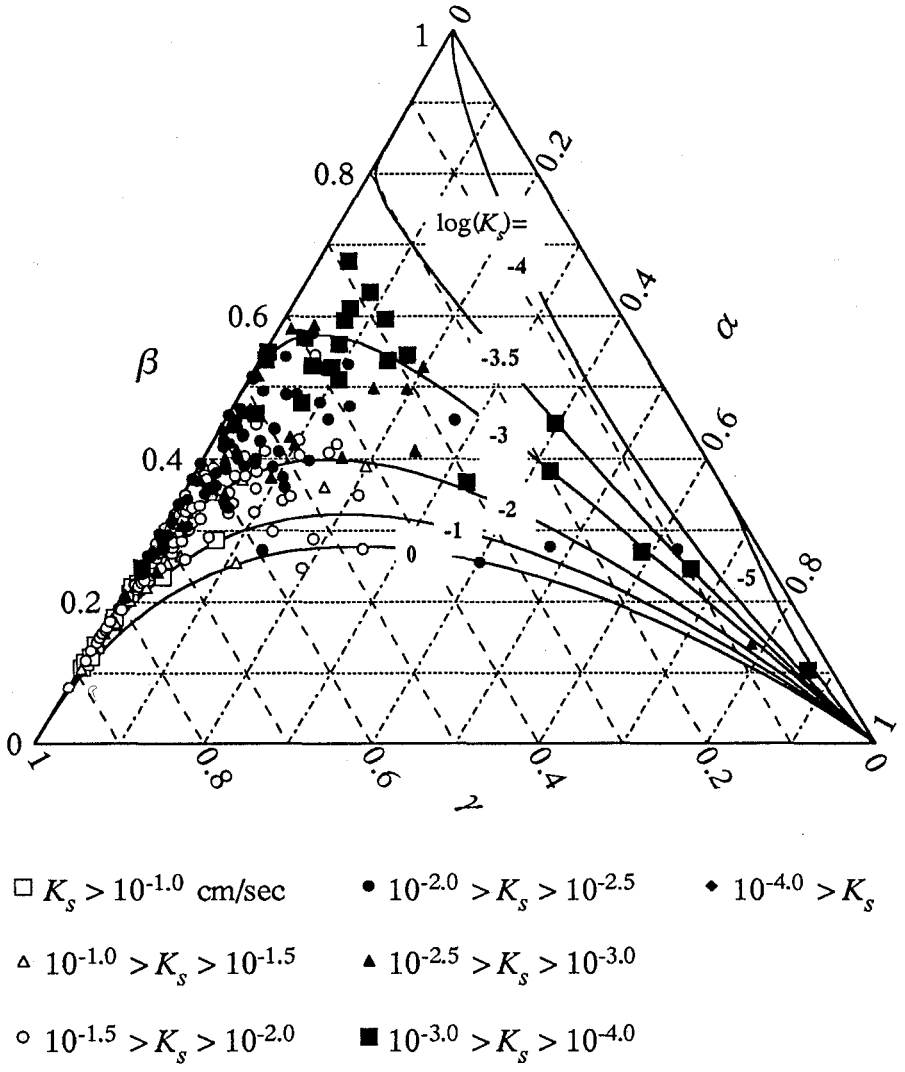

Figure 7.8 Triangle diagram representing the soil pore ratios α, β, and γ for the undisturbed forest soils. The plot for each soil was classified by the K_s value of the soil. Solid lines indicate the analytical relationship between K_s and the ratios α, β, and γ expressed as (7.15) with $B = 10^{0.4}$ cm^3/sec, and $K_s = 10^0$, 10^{-1}, 10^{-2}, 10^{-3}, $10^{-3.5}$, 10^{-4}, and 10^{-5} cm/sec.

shown in Figure 7.8. It can be seen that the analytical curves succeeded to reproduce the effects of the soil pore ratios on K_s.

7.5 MODEL FOR HYDRAULIC CONDUCTIVITY

By substituting the relationship between K_s and the parameters ψ_m and σ expressed as (7.14) into (7.6) and (7.7), the following expressions of K with respect to S_e and with respect to ψ are derived:

$$K(S_e) = B\frac{\exp(\sigma^2)}{(-\psi_m)^2} S_e^{1/2} Q^2\left(Q^{-1}(S_e) + \sigma\right) \tag{7.16}$$

$$K(\psi) = B\frac{\exp(\sigma^2)}{(-\psi_m)^2} Q^{1/2}\left(\frac{1}{\sigma}\ln\left(\frac{\psi}{\psi_m}\right)\right) Q^2\left(\frac{1}{\sigma}\ln\left(\frac{\psi}{\psi_m}\right) + \sigma\right) \tag{7.17}$$

The value of B was suggested to be $10^{0.4}$ cm^3/sec in the previous section. Consequently, the soil hydraulic conductivity as well as the soil water retention curve is characterized by the two parameters ψ_m and σ by application of the C-LN2 model. Both ψ_m and σ are related directly to the statistics of the soil pore radius distribution $g(r)$: ψ_m is related to the median of $g(r)$ by the capillary pressure function and σ represents the width of $g(r)$.

In Figure 7.9, the observed θ-ψ and K-ψ curves for two undisturbed forest soils are compared with the fitted θ-ψ and the predicted K-ψ curves obtained by the C-LN2 model. The soil samples were taken at a forestal hillslope consisting of weathered granite in the southern part of Hyogo Prefecture in Japan. One sample was taken from A-horizon (5 ~ 10 cm deep from the soil surface), and the other sample was taken from B-horizon (30 ~ 40 cm deep from the surface). Parameters θ_s, θ_r, ψ_m, and σ in (5.8) were optimized to reproduce the observed θ-ψ curves by using Marquardt's method, then the K-ψ curves were predicted by substituting the estimated ψ_m and σ into (7.17). The figure clearly shows that the C-LN2 model produces acceptable matches with the observed θ-ψ curves and adequate predictions of the K-ψ curves. Table 7.2 summarizes the optimized values of θ_s, θ_r, ψ_m, and σ, and the observed and predicted K_s values. The table indicates that the soil taken from A-horizon has the greater median and the greater width of $g(r)$ than the

Table 7.2 Fitted Values for Parameters of the C-LN2 Model for the Retention Curves Plotted in Figure 7.9 and Observed and Predicted Values of Saturated Hydraulic Conductivity

Horizon	θ_s	θ_r	ψ_m, cm	σ	K_s*1, cm/sec (predicted)	K_s, cm/sec (observed)
A	0.788	0.412	-11.6	1.105	6.37×10^{-2}	5.12×10^{-2}
B	0.703	0.396	-25.9	0.9252	8.80×10^{-3}	1.97×10^{-2}

*1 Derived by (7.14) with $B = 10^{0.4}$ cm^3/sec using fitted ψ_m and σ values.

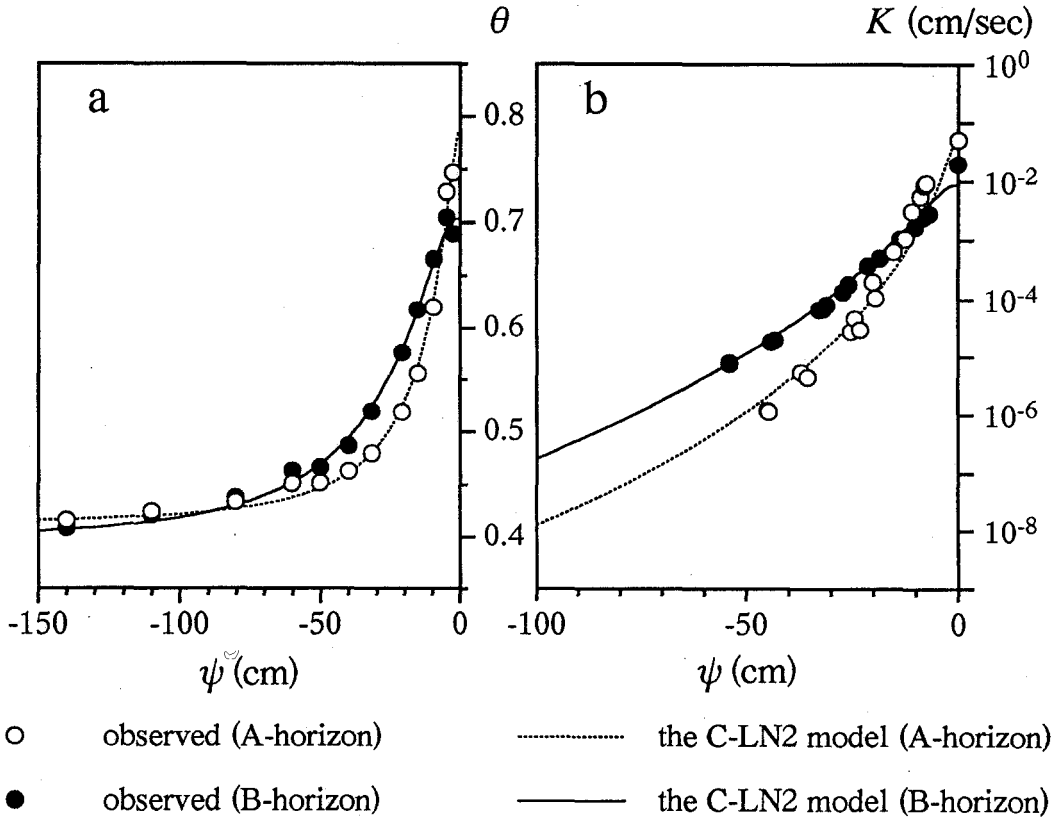

Figure 7.9 (a) Observed and fitted θ-ψ curves, and (b) observed and predicted K-ψ curves for undisturbed forest soils. The fitted θ-ψ curves and the predicted K-ψ curves were generated with the C-LN2 model.

soil taken from B-horizon. The predicted K_s values are about the same as the observed K_s values.

7.6 SUMMARY AND CONCLUSIONS

In this chapter, the soil water retention model proposed in Chapter 5 (the LN2 model) was combined with *Mualem*'s [1976a] model for the purpose of deriving an analytical expression for the relative hydraulic conductivity K_r. The accuracy of the resulting combined water-retention-hydraulic-conductivity model (the C-LN2 model) was verified for observed data sets for five soils. Results showed that the C-LN2 model produces acceptable matches with observed soil water retention curves and adequate predictions of relative hydraulic conductivities. The θ-ψ and K_r-ψ (or K_r-θ) curves generated by this model are similar to those generated by *van Genuchten*'s [1980] combined water-

retention-hydraulic-conductivity model, which has been used extensively in numerical modeling.

The parameters of the C-LN2 model are related directly to the statistics of the soil pore radius distribution $g(r)$: ψ_m is related to the median of $g(r)$ by the capillary pressure function and σ represents the width of $g(r)$. Observed values of the saturated hydraulic conductivity K_s of the forest soils were correlated with the soil pore radius distributions using both the coordinate system with ψ_m on the abscissa and σ on the ordinate, and the triangle diagram showing the soil pore ratios α, β, and γ which were suggested in Chapter 6. Results showed that K_s is higher for the soil with a greater median of the pore radius distribution. There was the trend that the soil with a greater width of the pore radius distribution has a higher K_s value under the same median condition. Value of K_s increases as the non-capillary pore ratio γ becomes greater and as the coarse capillary pore ratio β becomes smaller. Analytical curves derived from *Mualem*'s [1976a] model generally succeeded to reproduce the relationship between K_s and the parameters of the C-LN2 model, and the relationship between K_s and the ratios α, β, and γ.

By substituting the functional relationship between K_s and the parameters ψ_m and σ into the model for the relative hydraulic conductivity, expressions of the soil hydraulic conductivity K with respect to S_e and with respect to ψ were developed. The derived expression of the K-ψ curve succeeded to reproduce observed K-ψ curves for undisturbed forest soils. As a result, the soil hydraulic conductivity as well as the soil water retention curve was characterized by the two parameters ψ_m and σ by application of the C-LN2 model.

The C-LN2 model was developed by applying a distribution law available in general probability theory. The parameters of the model are related directly to the statistics of the soil pore radius distribution. Through Chapters 5 to 7, it was shown that the C-LN2 model can be successfully used to derive functional θ-ψ and K-ψ relationships of various soils. This retention model and its parameters are discussed in Chapter 8 connected to physical analyses of water flow in forest soils.

APPENDIX A: PROCEDURE FOR DERIVING (7.3) AND (7.13)

In order to derive analytical expressions for K_r based on *Mualem*'s [1976a] model, the following integral should be solved:

$$G = \frac{1}{\theta_s - \theta_r} \int_0^r r g(r) dr \tag{A7.1}$$

When $g(r)$ is expressed as (5.9), (A7.1) becomes

$$G = \frac{1}{\sqrt{2\pi}\sigma} \int_0^r \exp\left[-\frac{\{\ln(r/r_m)\}^2}{2\sigma^2} \right] dr \tag{A7.2}$$

Substituting $y = \ln(r/r_m)$ into (A7.2) leads to

$$G = \frac{r_m}{\sqrt{2\pi}\sigma}\int_{-\infty}^{\ln(r/r_m)} \exp\left(y - y^2/2\sigma^2\right)dy \tag{A7.3}$$

Substitution of $Y = (\sigma^2 - y)/(2^{1/2}\sigma)$ into (A7.3) gives

$$G = \frac{r_m \exp\left(\sigma^2/2\right)}{-\sqrt{\pi}}\int_{\infty}^{\{\sigma^2 - \ln(r/r_m)\}/\sqrt{2}\sigma} \exp\left(-Y^2\right)dY \tag{A7.4}$$

The error function (erf) is defined as

$$\mathrm{erf}(x) = \frac{2}{\sqrt{\pi}}\int_0^x \exp\left(-x^2\right)dx \tag{A7.5}$$

Because $\mathrm{erf}(\infty) = 1$, combining (A7.5) with (A7.4) yields

$$G = \frac{r_m \exp\left(\sigma^2/2\right)}{2}\left\{1 - \mathrm{erf}\left(\left\{\sigma^2 - \ln\left(r/r_m\right)\right\}/\sqrt{2}\sigma\right)\right\} \tag{A7.6}$$

Since the complementary normal distribution function (Q) is related to the error function by $\mathrm{erf}(x) = 1 - 2Q(2^{1/2}x)$, (A7.6) is transformed as

$$G = r_m \exp\left(\sigma^2/2\right)Q\left(\ln\left(r_m/r\right)/\sigma + \sigma\right) \tag{A7.7}$$

Substituting $r = A/\psi$ and $r_m = A/\psi_m$ into (A7.7) yields

$$G = \frac{A}{\psi_m}\exp\left(\sigma^2/2\right)Q\left(\ln\left(\psi/\psi_m\right)/\sigma + \sigma\right) \tag{A7.8}$$

Dividing (A7.8) by $|A|$ gives (7.3).

The arithmetic mean r_a of the pore radius distribution is defined as

$$r_a = \frac{1}{\theta_s - \theta_r}\int_0^{\infty} rg(r)dr \tag{A7.9}$$

Consequently, substitution of $r = \infty$ into (A7.7) or substitution of $\psi = 0$ into (A7.8) yields the expression for r_a (that is, (7.13)).

APPENDIX B: EQUATION FOR K_r BASED ON BURDINE'S MODEL

Burdine's [1953] model for predicting K_r is written in the form

$$K_r = K/K_s = S_e^2\int_0^{S_e}\frac{dS_e}{|\psi|^2}\Big/\int_0^1\frac{dS_e}{|\psi|^2} \tag{A7.10}$$

The integral in (A7.10) is transformed as follows:

$$\int_0^{S_e} \frac{dS_e}{|\psi|^2} = \frac{1}{|A|^2(\theta_s - \theta_r)} \int_0^r r^2 g(r) dr \qquad \text{(A7.11)}$$

When $g(r)$ is expressed as (5.9), (A7.11) can readily be integrated with the similar procedure as mentioned in Appendix A:

$$\int_0^{S_e} \frac{dS_e}{|\psi|^2} = \frac{1}{|\psi_m|^2} \exp(2\sigma^2) Q\left(\ln(\psi/\psi_m)/\sigma + 2\sigma\right) \qquad \text{(A7.12)}$$

Consequently, K_r based on Burdine's model is expressed as

$$K_r = S_e^2 Q\left(\ln(\psi/\psi_m)/\sigma + 2\sigma\right) \qquad \text{(A7.13)}$$

REFERENCES

Ahuja, L. R., and R. D. Williams, Scaling water characteristic and hydraulic conductivity based on Gregson-Hector-McGowan approach, *Soil Sci. Soc. Am. J., 55*(2), 308-319, 1991.

Brooks, R. H., and A. T. Corey, Hydraulic properties of porous media, *Hydrol. Pap. 3*, Civil Eng. Dept., Colo. State Univ., Fort Collins, 1964.

Brutsaert, W., Probability laws for pore-size distributions, *Soil Sci., 101*, 85-92, 1966.

Brutsaert, W., The permeability of a porous medium determined from certain probability laws for pore size distribution, *Water Resour. Res., 4*(2), 425-434, 1968.

Burdine, N. T., Relative permeability calculation from size distribution data, *Trans. Am. Inst. Min. Metall. Pet. Eng., 198*, 71-78, 1953.

Carsel, R. F., and R. S. Parrish, Developing joint probability distribution of soil water retention characteristics, *Water Resour. Res., 24*(5), 755-769, 1988.

Childs, E. C., and N. Collis-George, The permeability of porous materials, *Proc. Roy. Soc., Ser. A, 201*, 392-405, 1950.

Clapp, R. B., and G. M. Hornberger, Empirical equations for some soil hydraulic properties, *Water Resour. Res., 14*(4), 601-604, 1978.

Clausnitzer, V., J. W. Hopmans, and D. R. Nielsen, Simultaneous scaling of soil water retention and hydraulic conductivity curves, *Water Resour. Res., 28*(1), 19-31, 1992.

Elrick, D. E., and D. H. Bowman, Note on an improved apparatus for soil moisture flow measurements, *Soil Sci. Soc. Am. Proc., 28*, 450-453, 1964.

Hopmans, J. W., A comparison of various methods to scale soil hydraulic properties, *J. Hydrol., 93*, 241-256, 1987.

Jury, W. A., W. R. Gardner, and W. H. Gardner, *Soil Physics*, Wiley, New York, 1991.

Kobashi, S., H. Murai, and A. Kameyama, *Environmental Revegetation Technology* (in Japanese*), Asakura, Tokyo, Japan, 1992.

Kutílek, M., and D. R. Nielsen, *Soil Hydrology*, Catena Verlag, Cremlingen, Germany, 1994.

Laliberte, G. E., A mathematical function for describing capillary pressure-desaturation data, *Bull. Int. Ass. Sci. Hydrol., 14*(2), 131-149, 1969.

Leibenzon, L. S., *Flow of Natural Liquids and Gases in Porous Medium* (in Russian), Gostekhizdat, Moscow, 1947.

Letha, J., and K. Elango, Simulation of mildly unsaturated flow, *J. Hydrol., 154*, 1-17, 1994.

Luckner, L., M. Th. van Genuchten, and D. R. Nielsen, A consistent set of parametric models for the two-phase flow of immiscible fluids in the subsurface, *Water Resour. Res.*, *25*(10), 2187-2193, 1989.

Marquardt, D. W., An algorithm for least-squares estimation on non-linear parameters, *J. Soc. Ind. Appl. Math.*, *11*, 431-441, 1963.

Mashimo, Y., Studies on the physical properties of forest soil and their relation to the growth of sugi (*Cryptomeria japonica*) and hinoki (*Chamaecyparis obtusa*) (in Japanese with English Summary), *Forest Soils Jpn.*, *11*, 1-182, 1960.

McCuen, R. H., W.J. Rawls, and D. L. Brakensiek, Statistical analysis of the Brooks-Corey and the Green-Ampt parameters across soil textures, *Water Resour. Res.*, *17*(4), 1005-1013, 1981.

Mishra, S., and J. C. Parker, On the relation between saturated conductivity and capillary retention characteristics, *Ground Water*, *28*(5), 775-777, 1990.

Mualem, Y., A new model for predicting the hydraulic conductivity of unsaturated porous media, *Water Resour. Res.*, *12*(3), 513-522, 1976a.

Mualem, Y., A catalogue of the hydraulic properties of unsaturated soils, *Proj. 442*, 100 pp., Technion-Israel Inst. of Technol., Haifa, Israel, 1976b.

Reisenauer, A. E., Methods for solving problems of multi-dimensional partially saturated steady flow in soils, *J. Geophys. Res.*, *68*, 5725-5733, 1963.

Russo, D., Determining soil hydraulic properties by parameter estimation: On the selection of a model for the hydraulic properties, *Water Resour. Res.*, *24*(3), 453-459, 1988.

Russo, D., J. Zaidel, and A. Laufer, Stochastic analysis of solute transport in partially saturated heterogeneous soil, I, Numerical experiments, *Water Resour. Res.*, *30*(3), 769-779, 1994.

Russo, D., and M. Bouton, Statistical analysis of spatial variability in unsaturated flow parameters, *Water Resour. Res.*, *28*(7), 1911-1925, 1992.

Stauffer, F., H. J. Franke, and T. Dracos, Hysteretic storativity concept for aquifer simulation, *Water Resour. Res.*, *28*(9), 2307-2314, 1992.

van Genuchten, M. Th., A closed-form equation for predicting the hydraulic conductivity of unsaturated soils, *Soil Sci. Soc. Am. J.*, *44*(5), 892-898, 1980.

van Genuchten, M. Th., and D. R. Nielsen, On describing and predicting the hydraulic properties of unsaturated soils, *Ann. Geophys.*, *3*(5), 615-628, 1985.

Wierenga, P. J., R. G. Hills, and D. B. Hudson, The Las Cruces trench site: Characterization, experimental results, and one-dimensional flow predictions, *Water Resour. Res.*, *27*(10), 2695-2705, 1991.

Wise, W. R., T. P. Clement, and F. J. Molz, Variably saturated modeling of transient drainage: Sensitivity to soil properties, *J. Hydrol.*, *161*, 91-108, 1994.

Wösten, J. H. M., and M. Th. van Genuchten, Using texture and other soil properties to predict the unsaturated soil hydraulic functions, *Soil Sci. Soc. Am. J.*, *52*, 1762-1770, 1988.

*The title is tentative translation from the original Japanese title by the author of this thesis.

CHAPTER 8

EFFECT OF SOIL PORE RADIUS DISTRIBUTION ON VERTICAL DRAINAGE PROCESS IN SURFACE SOIL

8.1 INTRODUCTION

Modeling the storm runoff process in forestal watershed is important for the management of water resources, as well as for predicting slope failure caused by heavy rainfall. Because forestal hillslope is usually covered with forest soils which have peculiar pore radius distribution and hydraulic properties, many studies have been done to evaluate the effect of forest soil on the water movement in forestal watersheds. It has been frequently pointed out that the existence of large size pores increases the permeability of forest soil. This reduces the surface flow on forestal hillslope and increases the amount of water which infiltrates into the soil profile [e.g., *Kirkby*, 1978; *Tsukamoto*, 1992]. However, the effect of the pore radius distribution of forest soil on the movement of water infiltrated into the soil profile has not been clarified. Forest soil scientists have published some works on the relationship between the amount of forest soil pores, which are effective for water holding, and the water discharge from forestal watersheds [e.g., *Takeshita*, 1985; *Arimitsu et al.*, 1995; *Kato and Hotta*, 1995]. Although these studies provided some estimates of water holding capacities of forestal watersheds, the physical process of soil water movement has not been considered.

On the other hand, many hydrologists have done physical analyses of soil water flow on forestal hillslope by using the models for water retention and hydraulic conductivity. *Kubota et al.* [1987] analyzed the relationship between the volumetric water content θ and the soil capillary pressure ψ of forest soil by using the soil water retention model proposed by *Klute and Heermann* [1974]. They combined the Klute and Heermann model with the relative hydraulic conductivity model proposed by *Leibenzon* [1947] for analyzing the downslope flow on forestal hillslope. The set of the Klute and Heermann model and the Leibenzon model was adopted by *Ohta et al.* [1983] for modeling vertical unsaturated flow in a forest soil profile. *Ohte* [1992] determined the θ-ψ curves of undisturbed forest soils taken with large-size samplers, and analyzed vertical soil water flow using the combined water-retention-hydraulic-conductivity model developed by

Brooks and Corey [1964]. Moreover, *Tani*'s [1982] retention model was combined with the Leibenzon model and used for analyzing the properties of one-dimensional unsaturated flow in a soil column [*Tani*, 1985]. The set of the Tani model and the Leibenzon model has been used to analyze water flow on forestal hillslope [*Suzuki*, 1984; *Tsuboyama and Sammori*, 1989]. *Sammori and Tsuboyama* [1990] adopted the combined water-retention-hydraulic-conductivity model developed by *van Genuchten* [1980] to analyze slope stability taking the phenomena of infiltration into consideration.

Despite their usefulness, these combined models use empirical curve-fitting equations for the soil water retention curve. They are not derived based on soil pore radius distribution, nor do they emphasize the physical significance of their empirical parameters. Moreover, these combined models employ equations for the relative hydraulic conductivity. That is, the saturated hydraulic conductivity, which is closely related to the soil pore radius distribution [*Kutílek and Nielsen*, 1994], is regarded as one of the independent parameters in these combined models. Hence, these combined models cannot be effectively used for analyzing the effect of the soil pore radius distribution on the soil water movement phenomena.

Applying the combined water-retention-hydraulic-conductivity model developed in Chapter 7 (the C-LN2 model), soil hydraulic properties are characterized by two parameters, both of which are related directly to the statistics of the soil pore radius distribution. In this chapter, the C-LN2 model is adopted for physical analyses of soil water flow in order to evaluate the effect of the pore radius distribution of forest soil on the water movement phenomena on forestal hillslope.

8.2 THEORY

8.2.1 One-Dimensional Vertical Flow Equation for Soil Water

According to the Darcy-Backingham equation, vertical water flux q in unsaturated soil is expressed as follows:

$$q = -K(\psi)(\partial\psi / \partial z + 1) \tag{8.1}$$

where $K(\psi)$ is the hydraulic conductivity at a certain capillary pressure ψ and z is the vertical distance taken positive upward. The continuity equation for water is

$$\partial\theta / \partial t = -\partial q / \partial z \tag{8.2}$$

where t is time. Substituting (8.1) into (8.2) yields the one-dimensional, vertical flow equation for soil water (the Richards' equation):

$$C(\psi)\frac{\partial\psi}{\partial t} = \frac{\partial}{\partial z}\left\{K(\psi)\frac{\partial\psi}{\partial z}\right\} + \frac{\partial}{\partial z}K(\psi) \tag{8.3}$$

where $C(\psi) = d\theta/d\psi$ is the water capacity function defined as the slope of the soil water retention curve. In this study, $C(\psi)$ is regarded as the pore capillary pressure distribution

function $f(\psi)$ (see (3.4)). Solving (8.3) requires the models for soil water retention and hydraulic conductivity.

8.2.2 Model for Soil Hydraulic Properties

The combined water-retention-hydraulic-conductivity model developed in Chapter 7 (the C-LN2 model), was used to solve (8.3). Based on the C-LN2 model, the effective saturation $S_e(\psi)$ and $C(\psi)$ are expressed as follows:

$$S_e(\psi) = Q\left(\ln(\psi/\psi_m)/\sigma\right) \tag{5.8}$$

$$C(\psi) = f(\psi) = \frac{\theta_s - \theta_r}{\sqrt{2\pi}\sigma(-\psi)} \exp\left[-\frac{\{\ln(\psi/\psi_m)\}^2}{2\sigma^2}\right] \tag{5.7}$$

The expressions of K with respect to S_e and with respect to ψ are

$$K(S_e) = B\frac{\exp(\sigma^2)}{(-\psi_m)^2} S_e^{1/2} Q^2\left(Q^{-1}(S_e) + \sigma\right) \tag{7.16}$$

$$K(\psi) = B\frac{\exp(\sigma^2)}{(-\psi_m)^2} Q^{1/2}\left(\frac{1}{\sigma}\ln\left(\frac{\psi}{\psi_m}\right)\right) Q^2\left(\frac{1}{\sigma}\ln\left(\frac{\psi}{\psi_m}\right) + \sigma\right) \tag{7.17}$$

where $B = 10^{0.4}$ cm^3/sec. The saturated hydraulic conductivity K_s is given by substituting $S_e = 1$ into (7.16) or by substituting $\psi = 0$ into (7.17):

$$K_s = B\frac{\exp(\sigma^2)}{(-\psi_m)^2} \tag{7.14}$$

Applying the C-LN2 model, soil hydraulic properties are characterized by two parameters both of which are related directly to the statistics of the soil pore radius distribution $g(r)$: ψ_m is related to the median of $g(r)$ by the capillary pressure function and σ represents the width of $g(r)$. The effective porosity (θ_s - θ_r), which affects $C(\psi)$ value, is treated as a constant in this chapter.

8.2.3 Dimensionless Form of Vertical Flow Equation

All the aforementioned equations were made dimensionless by using the following dimensionless variables:

$$\begin{aligned} z_* &= z/L \qquad t_* = tK_s/L(\theta_s - \theta_r) \\ q_* &= q/K_s \qquad \psi_* = -\psi/\psi_m \end{aligned} \tag{8.4}$$

where L is the vertical soil length. The resulting dimensionless forms of (8.1), (8.2), and

(8.3) are

$$q_* = -K_r\{\xi(\partial\psi_*/\partial z_*)+1\} \tag{8.5}$$

$$\partial S_e/\partial t_* = -\partial q_*/\partial z_* \tag{8.6}$$

$$C_*\frac{\partial\psi_*}{\partial t_*} = \frac{\partial}{\partial z_*}\left\{K_r\left(\xi\frac{\partial\psi_*}{\partial z_*}\right)\right\}+\frac{\partial}{\partial z_*}K_r \tag{8.7}$$

where

$$\xi = -\psi_m/L \tag{8.8}$$

Dimensionless forms of the models for soil water retention and hydraulic conductivity are

$$S_e = Q(\ln(-\psi_*)/\sigma) \tag{8.9}$$

$$C_* = \frac{dS_e}{d\psi_*} = \frac{1}{\sqrt{2\pi}\sigma(-\psi_*)}\exp\left[-\frac{\{\ln(-\psi_*)\}^2}{2\sigma^2}\right] \tag{8.10}$$

$$K_r = K/K_s = S_e^{1/2}Q^2(Q^{-1}(S_e)+\sigma) \tag{8.11}$$

$$K_r = K/K_s = Q^{1/2}(\ln(-\psi_*)/\sigma)Q^2(\ln(-\psi_*)/\sigma+\sigma) \tag{8.12}$$

As a result, dimensionless vertical soil water flow is characterized by the two dimensionless parameters ξ and σ.

8.3 DIMENSIONLESS HYDROGRAPHS UNDER CONSTANT WATER TABLE CONDITION

Drainage process from a totally saturated soil profile to the ground water table was simulated. Equation (8.7) was solved using the dimensionless capillary pressure ψ_* as a dependent variable and a Crank-Nicholson finite difference scheme with equally spaced nodes (element length was 0.05) and a variable time step. The initial condition was the water saturation with a constant flux of q_* = -1, that is

$$\psi_* = 0 \qquad (0 \le z_* \le 1) \tag{8.13}$$

A zero-flux condition (q_* = 0) at the soil surface (z_* = 1) and a constant water table condition (ψ_* = 0) at the bottom of soil profile (z_* = 0) were imposed to compute the water discharge q_{out*}. Cumulative errors in the mass balance at the end of calculations were negligible.

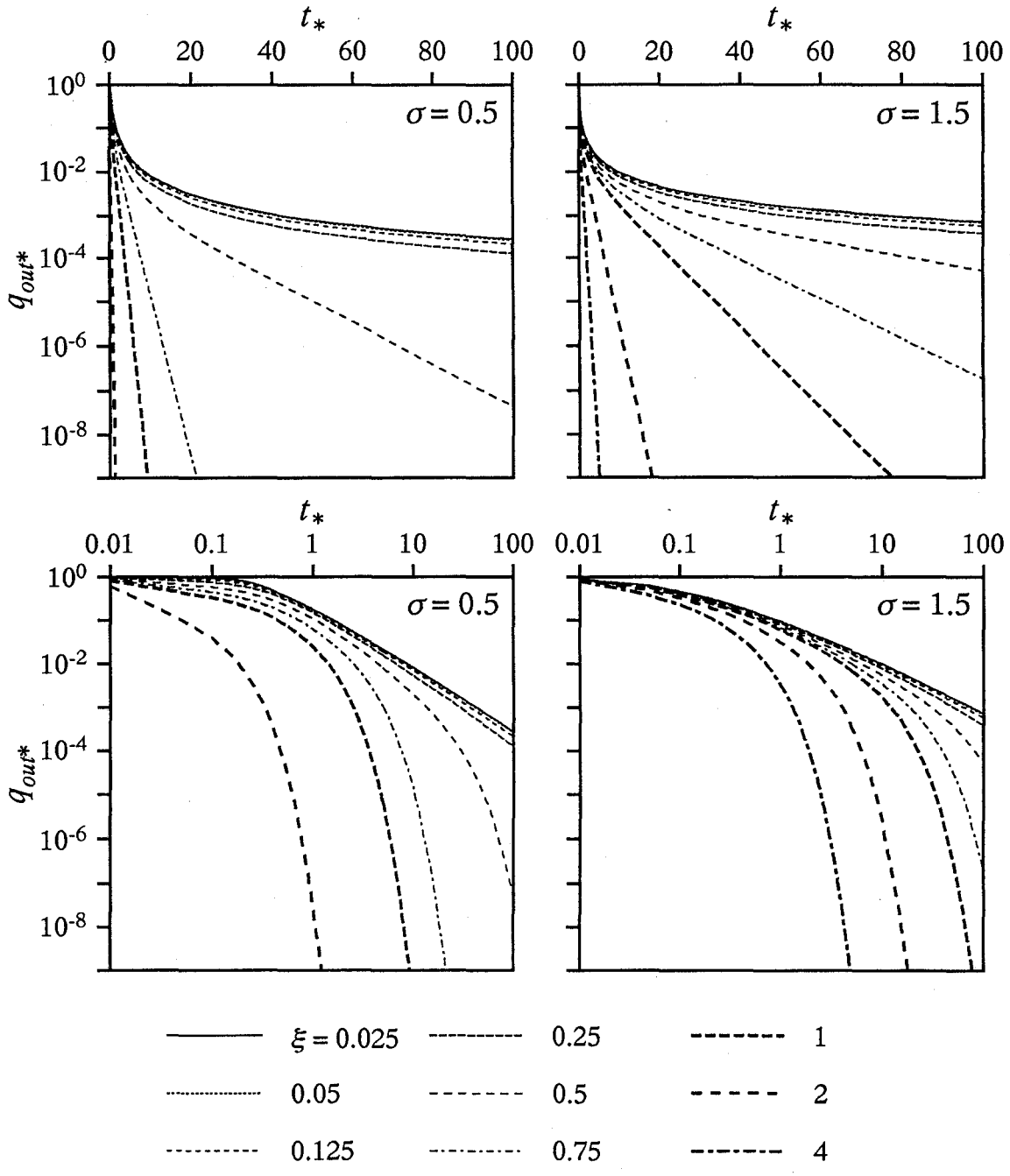

Figure 8.1 Simulated dimensionless hydrographs under the constant water table condition.

Figure 8.1 shows the relationships between q_{out*} and t_* computed by using 17 different parameter sets (ξ, σ). Value of σ was either 0.5 or 1.5, and values of ξ were from 0.025 to 4. The computed dimensionless hydrographs are plotted using both a semi-logarithmic scale and a logarithmic scale. The figure indicates that decreases in q_{out*} become smaller (the hydrograph becomes more gradual) as ξ becomes smaller. Change of the slope of the hydrograph as ξ changes is greater in the case of $\sigma = 0.5$ than in the case of $\sigma = 1.5$. When $\xi \leq 0.125$, the hydrographs with the same σ value resemble each other. Decreases in q_{out*} of these hydrographs are greater in the case of $\sigma = 0.5$ than in the case of $\sigma = 1.5$. The figure also indicates that the hydrographs with large ξ values are straight when plotted using a semi-logarithmic scale, and that the hydrographs with small ξ values are straight when plotted using a logarithmic scale. Consequently, q_{out*} is expressed as an exponential function with respect to t_* when ξ is large, and is expressed as a power function with respect to t_* when ξ is small.

The phenomena of water discharge from forestal hillslope can be regarded as the combination of two different processes as shown in Figure 8.2 [*Kirkby*, 1978; *Ohta et al.*, 1983; *Hino et al.*, 1989]. The two processes are the vertical drainage process in surface soil and the downslope drainage process in subsurface soil. In the vertical drainage process, water supplied by rainfall to the soil surface infiltrates into the soil

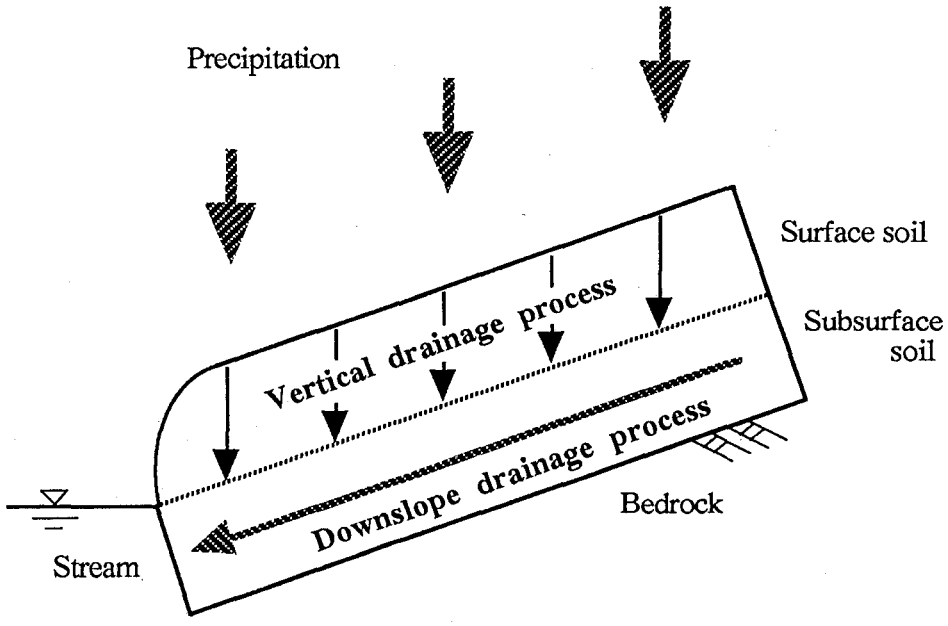

Figure 8.2 Schematic of the phenomena of water discharge from forestal hillslope.

profile unless the rainfall intensity is greater than the soil water permeability. The water moves vertically in the surface soil and discharges at the bottom of the soil profile. The hydrograph in the vertical drainage process in surface soil is regarded as an input for the downslope drainage process in subsurface soil. Hence, the vertical drainage process in surface soil, as well as the downslope drainage process in subsurface soil, is closely related to the hydrograph from forestal hillslope. In both processes, the dominant phenomenon is the one-dimensional flow of soil water [*Suzuki*, 1984; *Kubota et al.*, 1987].

As shown in Figure 5.3, ψ_m values of many soils are in the range of -20 to -400 cm. When the thickness of surface soil (L) is assumed to be 100 cm, the corresponding ξ values derived by (8.8) are from 0.2 to 4. Consequently, the dimensionless hydrographs with relatively large ξ values ($\xi \geq 0.25$) shown in Figure 8.1 are hydrographs in the vertical drainage process in surface soil. In this process, the q_{out*}-t_* relationship changes significantly as ξ changes and is straight when plotted using a semi-logarithmic scale. Value of ξ for the downslope drainage process in subsurface soil is much smaller than that for the vertical drainage process in surface soil, because the length of forestal hillslope is generally greater than several tens of meters. In the downslope drainage process, the dimensionless hydrographs with the same σ value resemble each other regardless of ξ values and are straight when plotted using a logarithmic scale.

Changes of soil pore radius distribution and hydraulic properties affected by forest ecosystem (forest plants and animals) are more significant in the surface soil than in the subsurface soil. Hence, the effect of the pore radius distribution of forest soil on the vertical drainage process in surface soil is discussed in the following section.

8.4 VERTICAL DRAINAGE PROCESS IN SURFACE SOIL

8.4.1 Hydrographs under Natural Rainfall

The vertical drainage process in surface soil was simulated by using observed rainfall data as inputs for the water flux at the soil surface. The rainfall data set was observed at Toinotani watershed of the Kyoto University Forest in Ashu in September 1992. This forest is situated in the northeastern part of Kyoto Prefecture in Japan (see Figure 4.1). Equation (8.3) was solved using a Crank-Nicholson finite difference scheme with 11 equally spaced nodes and a variable time step. The initial condition was hydraulic equilibrium under a zero-flux condition, that is

$$\psi = -z \qquad (0 \leq z \leq L) \tag{8.14}$$

A constant water table condition (ψ = 0) at the bottom of a soil profile (z = 0) was imposed to compute the water discharge q_{out}. Value of σ was either 0.5 or 1.5, and ψ_m were from -25 to -200 cm. The constant value of 0.3 was used as the effective porosity (θ_s - θ_r).

Figure 8.3 shows the hydrographs computed with the vertical soil length L of 100 cm.

The q_{out}-t relationships are plotted using a semi-logarithmic scale. The figure shows that the peak of the flood hydrograph becomes small and the slope of the recession hydrograph becomes gradual as ψ_m becomes great in both cases of $\sigma = 0.5$ and $\sigma = 1.5$. One can see the recession hydrographs are almost straight. The recession hydrograph with the parameter set (ψ_m, σ) of (-25, 0.5) has greater q_{out} and smaller decreases in q_{out} than that with the parameter set of (-25, 1.5). The recession hydrograph with the parameter set of (-50, 0.5) is about the same as that with the parameter set of (-25, 1.5). To be precise, the former has a little greater q_{out} than the latter. The recession hydrograph with the parameter set of (-100, 0.5) has smaller q_{out} and greater decreases in q_{out} than any recession hydrograph with σ value of 1.5. That is, the change of the recession hydrograph as ξ changes is greater in the case of $\sigma = 0.5$ than in the case of $\sigma = 1.5$.

The computed q_{out}-t relationships with the L value of 50 cm, are shown in Figure 8.4. The hydrographs have greater peak flow and greater changes in q_{out} than the hydrographs with L = 100 cm shown in Figure 8.3. The recession hydrograph becomes more gradual as ψ_m becomes greater in both cases of $\sigma = 0.5$ and $\sigma = 1.5$. The recession hydrograph with the parameter set of (-25, 0.5) has the smallest decreases in q_{out}, and the recession hydrograph with the parameter set of (-100, 0.5) has the greatest decreases in q_{out}. The decreases in q_{out} of the recession hydrograph with the parameter set of (-50, 0.5) are about the same as those of the recession hydrographs with the parameter sets of (-100, 1.5) and (-200, 1.5).

Figure 8.5 shows the computed q_{out}-t relationships when L is 150 cm. The peaks of the flood hydrographs are small and the recession hydrographs are gradual in comparison with the hydrographs shown in Figures 8.3 and 8.4. The recession hydrograph with the parameter set of (-50, 0.5) has greater q_{out} values and smaller decreases in q_{out} than that with the parameter set of (-50, 1.5), and the recession hydrograph with the parameter set of (-200, 0.5) has smaller q_{out} and greater decreases in q_{out} than that with the parameter set of (-200, 1.5). It should be noted that, with the parameter set of (-200, 0.5), all of the water supplied by the heavy rainfall on September 25 and 29 did not infiltrate into the soil profile because of the low permeability of the soil (K_s value derived by (7.14) is 8.06 $\times 10^{-5}$ cm/sec). Hence, the accurate q_{out} values could not be computed during the heavy rainfall. Values of q_{out} of the recession hydrograph with the parameter set of (-100, 0.5) are about the same as those of the recession hydrograph with the parameter set of (-100, 1.5). To be precise, the former are a little greater than the latter.

Figures 8.3 through 8.5 clearly show that the increase in the vertical soil length L makes the slope of the recession hydrograph gradual. Under the same L and σ condition, the recession hydrograph with greater ψ_m value has greater q_{out} and smaller decreases in q_{out}. With a large ψ_m value, the slope of the recession hydrograph becomes steeper as σ increases. When ψ_m is small, the slope of the recession hydrograph becomes gradual as σ increases. This critical ψ_m value increases as L decreases.

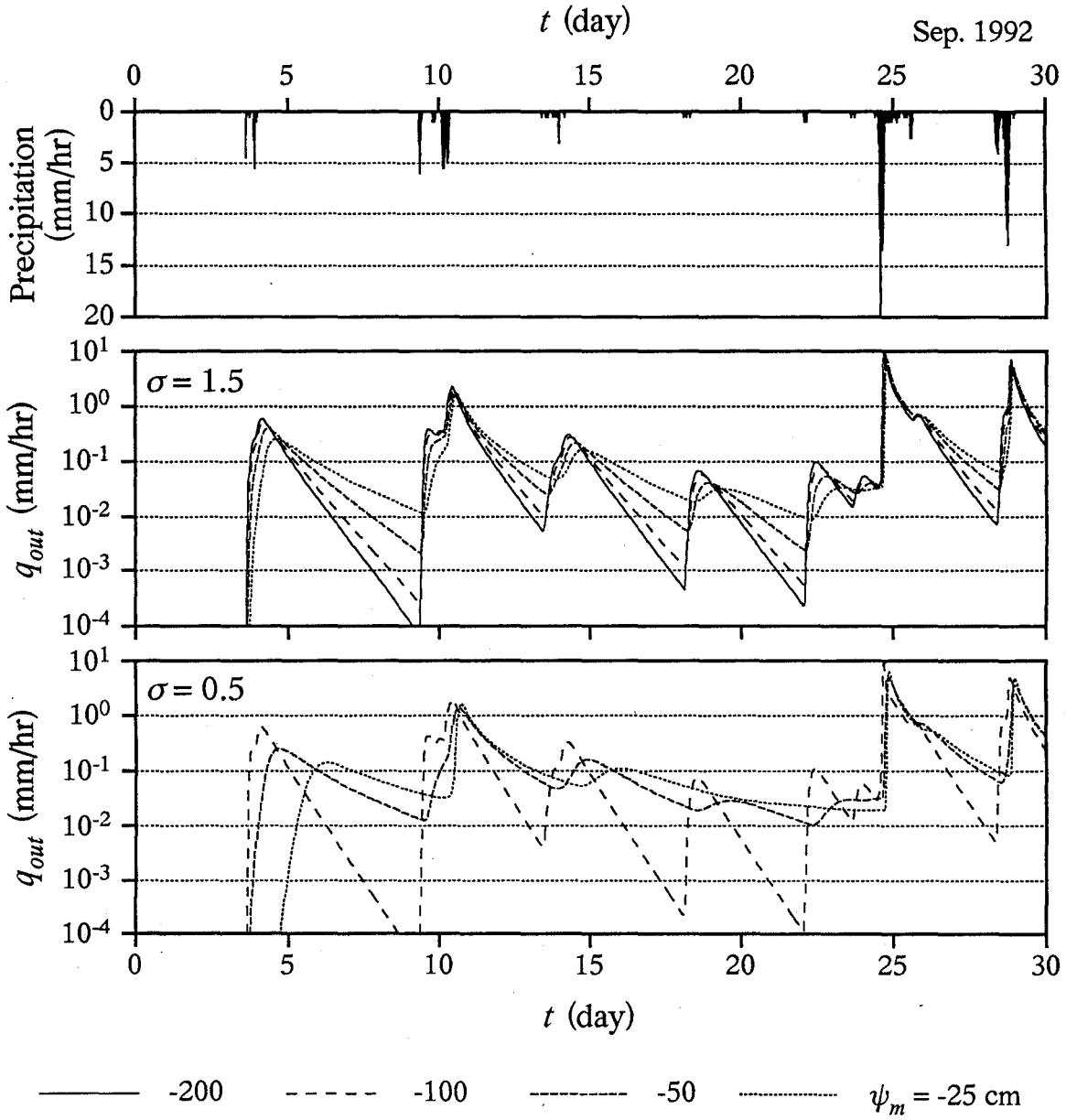

Figure 8.3 Simulated hydrographs in the vertical drainage process in the surface soil with the length of 100 cm. The rainfall data observed at Toinotani watershed of the Kyoto University Forest in Ashu in September 1992, were used as inputs for the water flux at the soil surface.

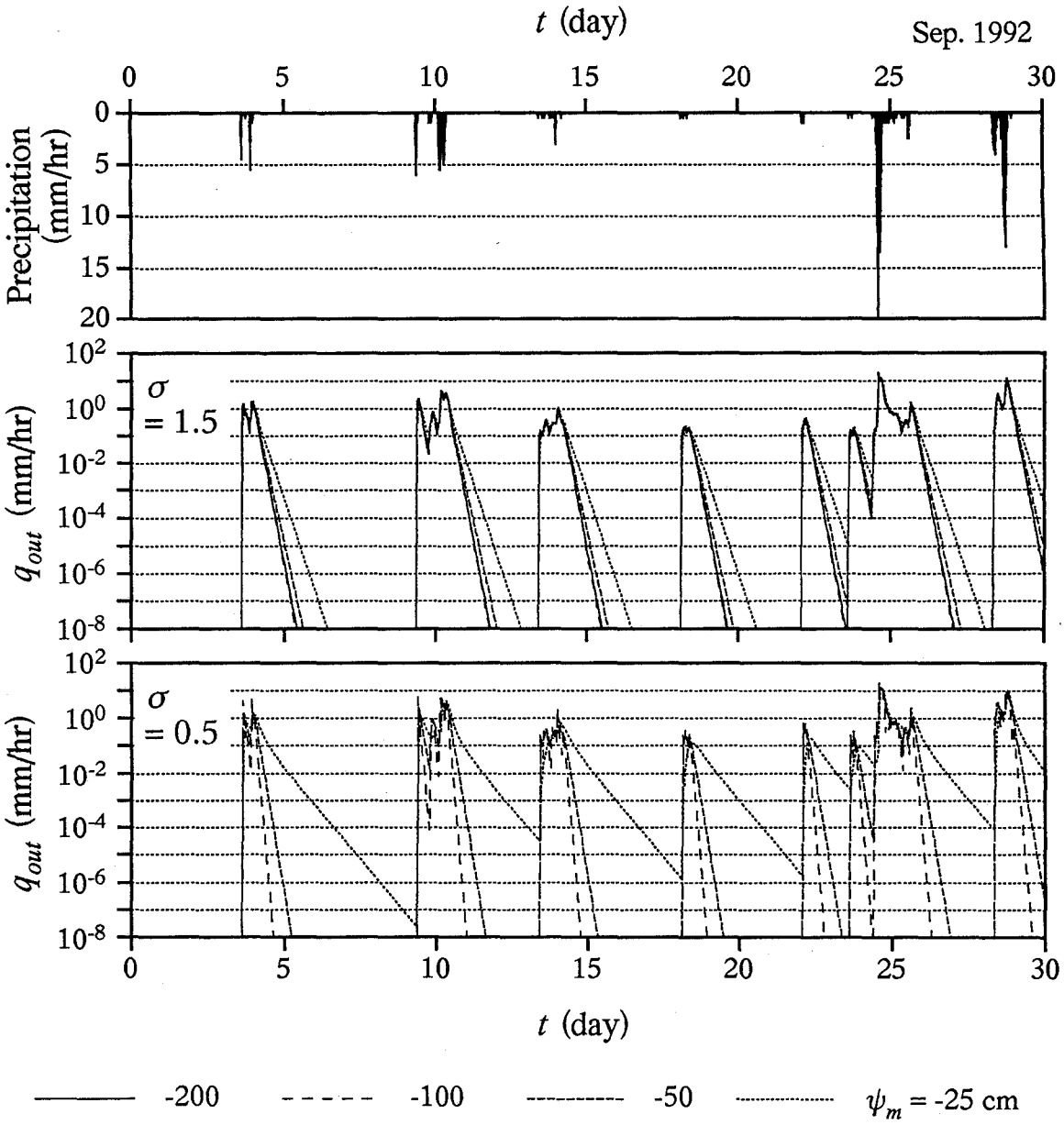

Figure 8.4 Simulated hydrographs in the vertical drainage process in the surface soil with the length of 50 cm. The rainfall data observed at Toinotani watershed of the Kyoto University Forest in Ashu in September 1992, were used as inputs for the water flux at the soil surface.

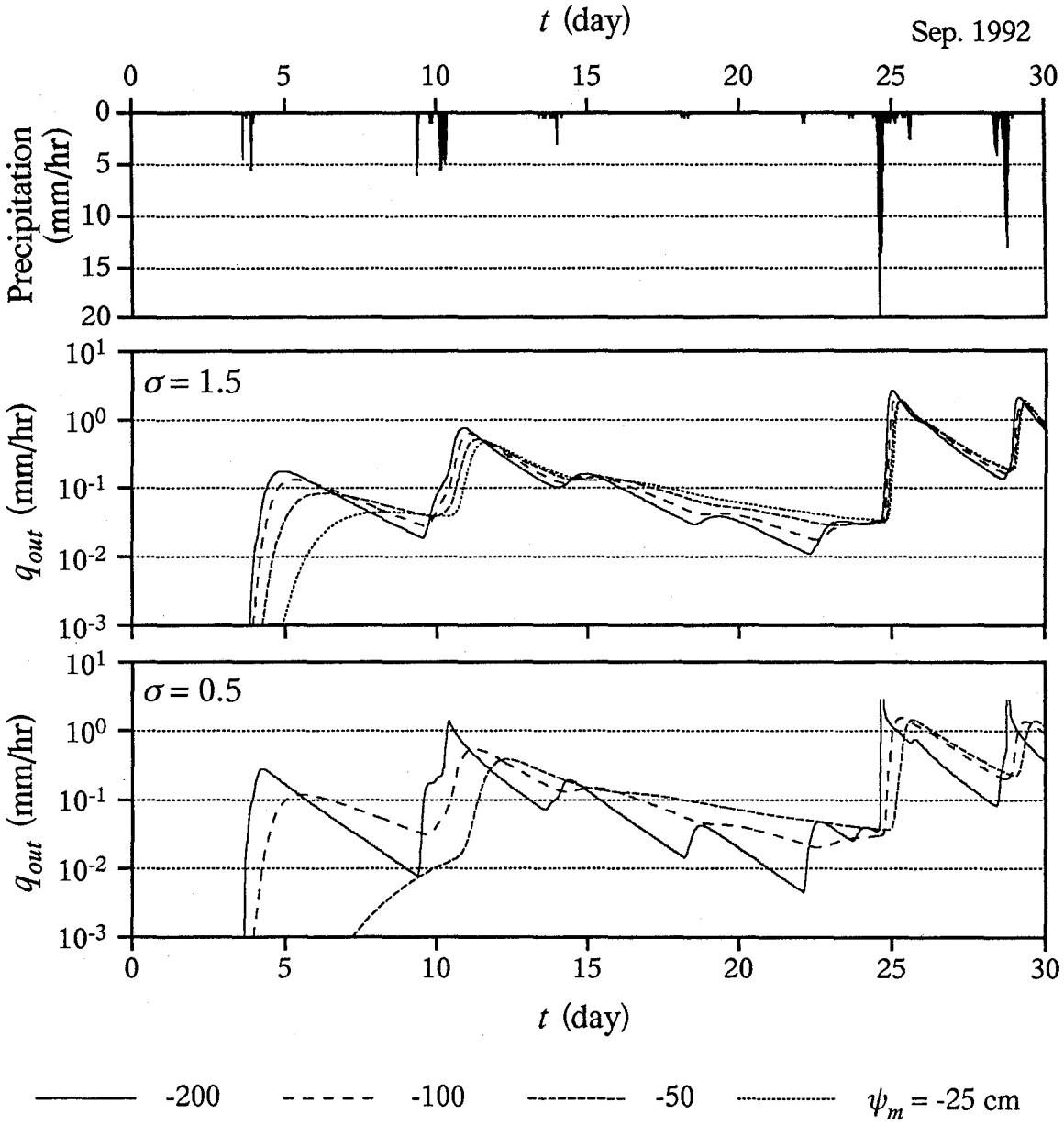

Figure 8.5 Simulated hydrographs in the vertical drainage process in the surface soil with the length of 150 cm. The rainfall data observed at Toinotani watershed of the Kyoto University Forest in Ashu in September 1992, were used as inputs for the water flux at the soil surface.

As shown in Figure 7.7, the saturated soil hydraulic conductivity K_s becomes larger as the median of the soil pore radius distribution becomes greater (that is, ψ_m becomes greater), and the width of the pore radius distribution (σ) becomes greater. However, Figures 8.3 through 8.5 indicate that the increase in K_s does not necessarily make the recession hydrograph steep. The relationship between the soil pore radius distribution and the slope of the recession hydrograph is analyzed in the following subsections by using the soil water diffusivity, which is defined as the ratio of the hydraulic conductivity K to the soil water capacity C.

8.4.2 Analytical Solution of the One-Dimensional Vertical Flow Equation

When the vertical soil length is not so large, the second term of the right-hand side of (8.3) is negligible in comparison with the first term for analyzing the recession hydrograph [*Shiozawa and Nakano*, 1981; *Seguchi et al.*, 1982]. By neglecting the second term of (8.3) and assuming that the soil water diffusivity D (= K/C) in a constant D_a [*Gardner*, 1962; *Fujioka and Kitamura*, 1964; *Seguchi et al.*, 1982], (8.3) is transformed as follows:

$$\frac{\partial \theta}{\partial t} = D_a \frac{\partial^2 \theta}{\partial z^2} \tag{8.15}$$

The constant D_a is referred to as the mean diffusivity. Equation (8.15) can be solved analytically under the following initial and boundary conditions [*Swartzendruber*, 1969]:

$$\begin{aligned} &\theta = \theta_s && (0 \le z \le L,\ t = 0) \\ &\theta = \theta_s && (z = 0,\ t > 0) \\ &\partial\theta / \partial z = -b && (z = L,\ t > 0) \end{aligned} \tag{8.16}$$

where b is a positive constant. The analytical solution of (8.15) is

$$\theta = \theta_s - bz - \frac{8bL}{\pi^2} \sum_{i=1}^{\infty} \frac{(-1)^i}{(2i-1)^2} \sin\left(\frac{2i-1}{2}\frac{\pi}{L} z\right) \exp\left\{-\left(\frac{2i-1}{2}\right)^2 \frac{\pi^2 D_a}{L^2} t\right\} \tag{8.17}$$

The water discharge at the bottom of soil profile q_{out} is expressed as

$$q_{out} = \frac{\partial}{\partial t} \int_0^L (\theta_s - \theta) dz \tag{8.18}$$

Neglecting all but the first term of the series of (8.17) and substituting into (8.18) yields

$$q_{out} = \frac{4bD_a}{\pi} \exp\left(-\frac{\pi^2 D_a}{4L^2} t\right) \tag{8.19}$$

Equation (8.19) indicates that q_{out} is expressed as an exponential function with respect to t. This coincides with the result derived by numerical simulation of the drainage process in surface soil: the recession hydrographs plotted using a semi-logarithmic scale are almost

straight as shown in Figures 8.3 through 8.5. According to (8.19), the absolute value of the slope of the recession hydrograph plotted using a semi-logarithmic scale (a) is expressed as follows:

$$a = \frac{\pi^2}{4}\frac{D_a}{L^2} \tag{8.20}$$

Value of a increase as L decreases. This also coincides with the result shown in Figures 8.3 through 8.5: the decrease in L makes the simulated recession hydrographs steep. As a result, (8.19) can be successfully used to analyze the vertical drainage process in surface soil.

Equation (8.20) indicates that a is in proportion to the mean diffusivity D_a. On the other hand, the soil water diffusivity D based on the C-LN2 model is expressed as the following function with respect to ψ:

$$D(\psi) = B\frac{\exp(\sigma^2)}{(-\psi_m)^2}\frac{Q^{1/2}\left(\ln(\psi/\psi_m)/\sigma\right)Q^2\left(\ln(\psi/\psi_m)/\sigma+\sigma\right)}{(\theta_s-\theta_r)\exp\left[-\left\{\ln(\psi/\psi_m)\right\}^2/2\sigma^2\right]/\sqrt{2\pi}\sigma(-\psi)} \tag{8.21}$$

where B = $10^{0.4}$ cm^3/sec. Plots of (8.21) with 8 different parameter sets (ψ_m, σ) are shown in Figure 8.6. The parameter sets are the same as those used for computing the hydrographs shown in Figures 8.3 through 8.5. One can see the D-ψ curves with σ value of 0.5 have greater decreases in D as ψ decreases than the D-ψ curves with σ value of 1.5. Under the same σ value condition, D at a certain ψ value decreases as ψ_m increases. The change of D-ψ curve as ψ_m changes is greater in the case of σ = 0.5 than in the case of σ = 1.5.

When the vertical length of surface soil is L, ψ value in the soil profile changes in the range of 0 to -L during the vertical drainage process with the constant water table at the bottom of the soil profile. Here, it is assumed that D_a has a positive correlation with D at a certain ψ value in the range of 0 to -L, which can be written as $D(-\eta L)$ using a constant η ($0 < \eta < 1$). Assuming for the moment that η is equal to 0.75, the simulated recession hydrographs shown in Figures 8.3 through 8.5 are correlated with $D(-\eta L)$ values shown in Figure 8.6.

With the η value of 0.75, $-\eta L$ is equal to -75 cm for the soil profile with the length of 100 cm. Figure 8.6 shows that D(-75) decreases as ψ_m increases, under the same σ value condition. Values of D(-75) for the parameter sets (ψ_m, σ) of (-25, 0.5) and (-50, 0.5) are smaller than that for the parameter set of (-25, 1.5). Value of D(-75) for the parameter set of (-100, 0.5) is greater than any D(-75) value for the parameter set with σ value of 1.5. Comparing these D(-75) values with the hydrographs shown in Figure 8.3, it is clear that the slopes of the recession hydrographs are closely related to the D(-75) values: the absolute value of the slope of the recession hydrograph becomes smaller as D(-75) becomes smaller.

With the assumption of η = 0.75, $-\eta L$ value is equal to -37.5 cm for the soil profile

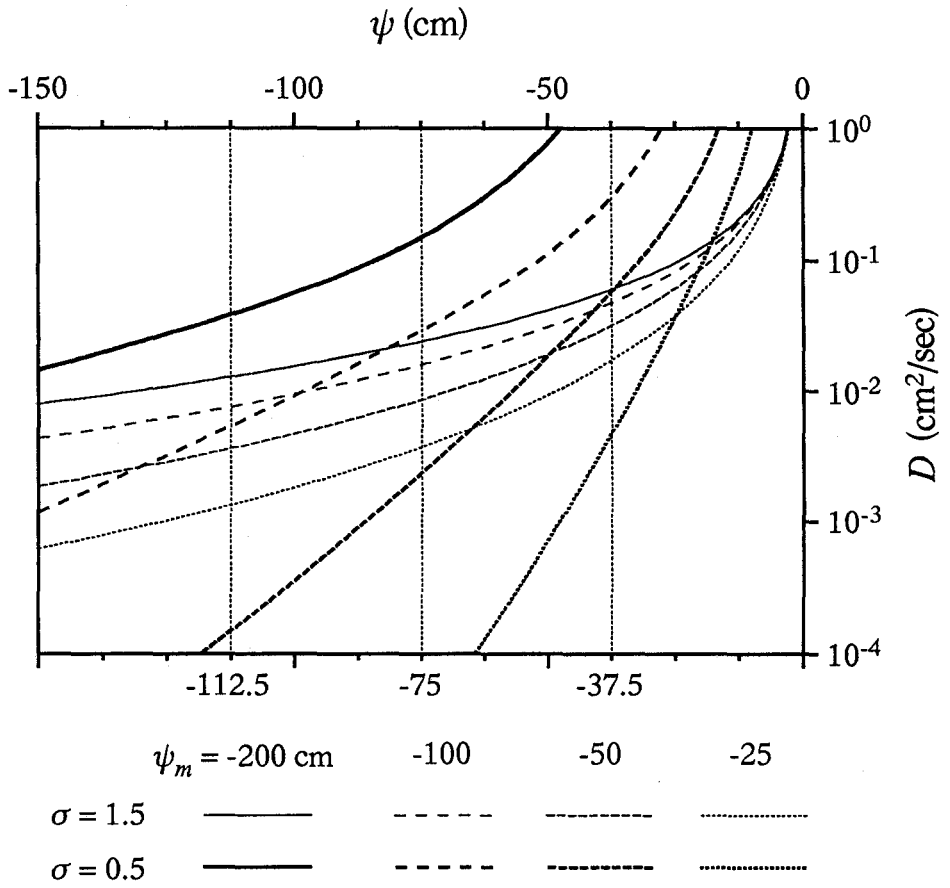

Figure 8.6 Curves for D-ψ based on the C-LN2 model, showing plots of (8.21) with 8 different parameter sets (ψ_m, σ). The parameter sets were the same as those used for computing the hydrographs shown in Figures 8.3 through 8.5.

with the length of 50 cm. Value of D(-37.5) for the parameter set of (-25, 0.5) is smallest in Figure 8.6, and the recession hydrograph with the same parameter set has the smallest decreases in q_{out} as shown in Figure 8.4. Value of D(-37.5) for the parameter set of (-100, 0.5) is great, which results in the steep recession hydrograph with this parameter set. Value of D(-37.5) for the parameter set of (-50, 0.5) is about the same as those for the parameter sets of (-100, 1.5) and (-200, 1.5). Hence, the recession hydrographs with these parameter sets resemble each other. As a result, it can be said that D(-37.5) values are closely related to the slopes of the recession hydrographs shown in Figure 8.4.

For the soil profile with the length of 150 cm, $-\eta L$ value is -112.5 cm when η is assumed to be 0.75. Value of D(-112.5) for the parameter set of (-50, 0.5) is smaller than that for the parameter set of (-50, 1.5), and D(-112.5) for the parameter set of (-200, 0.5)

is greater than that for the parameter set of (-200, 1.5). Values of $D(-112.5)$ for the parameter sets of (-100, 0.5) and (-100, 1.5) resemble each other. Precisely, the former is a little smaller than the latter. From Figure 8.5, it is clear that there is a positive correlation between the $D(-112.5)$ values and the absolute values of the slopes of the recession hydrographs.

From Figures 8.3 through 8.6, it seems reasonable to regard $D(-0.75L)$ as an index of the mean diffusivity D_a, which describes the slope of the recession hydrograph. For the soil profile with the length of L, the absolute value of the slope of the recession hydrograph becomes smaller as $D(-0.75L)$ value for the soil becomes smaller.

8.4.3 Relationship between the Slope of the Recession Hydrograph and the Soil Water Diffusivity

In the previous subsection, the one-dimensional vertical flow equation was solved analytically by assuming the mean diffusivity D_a. The dimensionless form of the flow equation (that is, (8.7)) is transformed as follows by neglecting the second term of the right-hand side of (8.7) and assuming that the dimensionless soil water diffusivity D_* (= K_r/C_*) in a constant D_{a*}:

$$\frac{\partial S_e}{\partial t_*} = \xi D_{a*} \frac{\partial^2 S_e}{\partial z_*^2} \tag{8.22}$$

The relationship between the dimensionless mean diffusivity D_{a*} and D_a is

$$D_a = \frac{(-\psi_m)K_s}{\theta_s - \theta_r} D_{a*} = \frac{B}{L(\theta_s - \theta_r)} \frac{\exp(\sigma^2)}{\xi} D_{a*} \tag{8.23}$$

where $B = 10^{0.4}$ cm^3/sec. Equation (8.22) can be solved analytically under the following initial and boundary conditions by the same procedure used to solve (8.15):

$$\begin{aligned} &S_e = 1 && (0 \le z_* \le 1,\ t_* = 0) \\ &S_e = 1 && (z_* = 0,\ t_* > 0) \\ &\partial S_e / \partial z_* = -b_* / \xi && (z_* = 1,\ t_* > 0) \end{aligned} \tag{8.24}$$

where b_* is a positive constant. Resulting q_{out*}-t_* relationship is expressed as

$$q_{out*} = \frac{4 b_* D_{a*}}{\pi} \exp\left(-\frac{\pi^2 \xi D_{a*}}{4} t_* \right) \tag{8.25}$$

Hence, the absolute value of the slope of the dimensionless recession hydrograph plotted using a semi-logarithmic scale (a_*) is expressed as follows:

$$a_* = \frac{\pi^2}{4} \xi D_{a*} \tag{8.26}$$

On the other hand, the expression of the dimensionless soil water diffusivity D_* with respect to ψ_* is

$$D_*(\psi_*) = \frac{Q^{1/2}\left(\ln(-\psi_*)/\sigma\right)Q^2\left(\ln(-\psi_*)/\sigma+\sigma\right)}{\exp\left[-\left\{\ln(-\psi_*)\right\}^2/2\sigma^2\right]/\sqrt{2\pi}\sigma(-\psi_*)} \tag{8.27}$$

The relationship between D_* and D is

$$D(\psi) = \frac{(-\psi_m)K_s}{\theta_s-\theta_r}D_*(\psi_*) = \frac{B}{L(\theta_s-\theta_r)}\frac{\exp(\sigma^2)}{\xi}D_*(\psi_*) \tag{8.28}$$

where $B = 10^{0.4}$ cm^3/sec.

In the dimensionless vertical drainage process, ψ_* value in the soil profile changes in the range of 0 to -1/ξ. According to the result derived from Figures 8.3 through 8.6, it is expected that $D_*(-\eta/\xi)$ is closely related to D_{a*} when η is equal to 0.75. In Figure 8.7, the relationship between $D_*(-0.75/\xi)$ and D_{a*} obtained for 50 different parameter sets (ξ, σ) is shown using a logarithmic scale. Values of σ were 0.25, 0.5, 1.0, 1.5, 2.0, and 2.5. Values of ξ were 0.2 and over for each σ value. Equation (8.27) was used to compute $D_*(-0.75/\xi)$ for each parameter set. Value of D_{a*} for each parameter set was derived by (8.26) using a_* value obtained by the numerical simulation of the drainage process using the same parameter set. The initial and boundary conditions for the numerical simulation were as described in Section 8.3. Value of a_* was defined as the absolute value of the slope of the $\ln(q_{out*})$-t_* curve when the rate of change of the common logarithm of the slope with respect to t_* became smaller than 10^{-5}. Figure 8.7 shows that there is a positive correlation between $D_*(-0.75/\xi)$ and D_{a*} except for the points for the parameter sets (ξ, σ) of (0.2, 0.25) and (0.3, 0.25). That is, $D_*(-0.75/\xi)$ can be used as an index of D_{a*} which describes the slope of the dimensionless recession hydrograph. Most of the points are plotted on a straight line with a unit gradient, which was fitted by eye. The relationship between $D_*(-0.75/\xi)$ and D_{a*} expressed by the fitted line is

$$D_{a*} = 3.5D_*(-0.75/\xi) \tag{8.29}$$

Since D_{a*} and $D_*(-0.75/\xi)$ are transformed into D_a and $D(-0.75L)$ by (8.23) and (8.28), respectively, (8.29) indicates that D_a for the soil profile with the vertical length of L has the positive correlation with $D(-0.75L)$. As a result, $D(-0.75L)$ can be successfully used as an index of the slope of the recession hydrograph in the vertical drainage process in surface soil. While $D_*(-0.75/\xi)$ continues to decrease as ξ decreases, the dimensionless recession hydrographs with different small ξ values resemble each other as shown in Figure 8.1. This is the reason that the points for the parameter sets (ξ, σ) of (0.2, 0.25) and (0.3, 0.25) are not plotted on the straight line in Figure 8.7. For these parameter sets, the recession hydrographs are not expressed as (8.25).

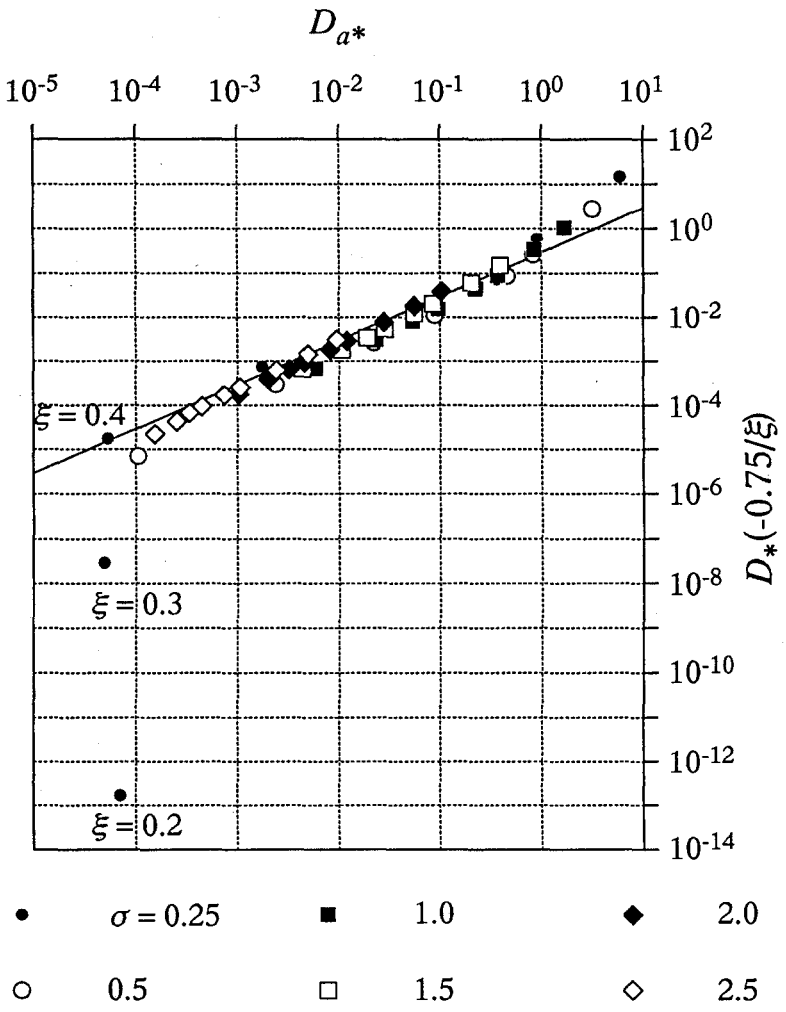

Figure 8.7 Relationship between $D_*(-0.75/\xi)$ and D_{a*} obtained for 50 different parameter sets (ξ, σ). Values of ξ were from 0.2 to 1.5 for σ value of 0.25, from 0.2 to 2.0 for σ value of 0.5, from 0.2 to 4.0 for σ values of 1.0 and 1.5, and from 0.2 to 8.0 for σ values of 2.0 and 2.5.

8.4.4 Effects of the Soil Pore Radius Distribution on the Recession Hydrograph

Figures 8.8a, 8.8b, 8.8c, and 8.8d are coordinate systems with ψ_m on the abscissa and σ on the ordinate showing the constant $\log(D(-0.75L))$ lines (D in cm^2/sec) with the L values of 150, 100, 50, and 25 cm, respectively. The constant $\log(D(-0.75L))$ lines were derived by (8.21). As shown in the figures, $D(-0.75L)$ decreases as ψ_m increases regardless of σ value. The rate of change of $D(-0.75L)$ with respect to ψ_m is large when σ is small, and is small with a large σ value. With a large ψ_m value, $D(-0.75L)$ becomes

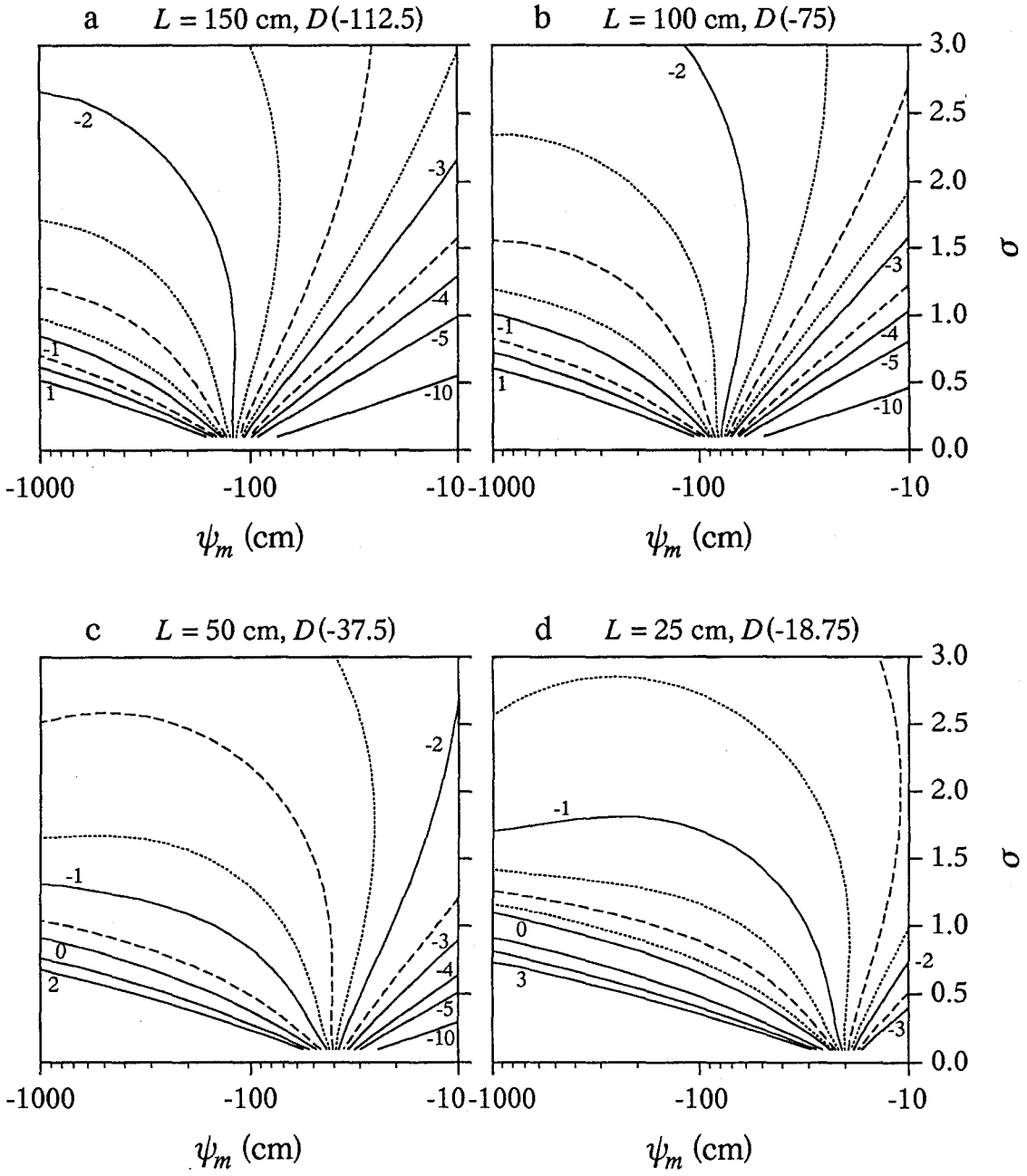

Figure 8.8 Coordinate systems with ψ_m on the abscissa and σ on the ordinate, showing the constant $\log(D(-0.75L))$ lines (D in cm^2/sec) with the L values of (a) 150, (b) 100, (c) 50, and (d) 25 cm. The constant $\log(D(-0.75L))$ lines were generated by (8.21).

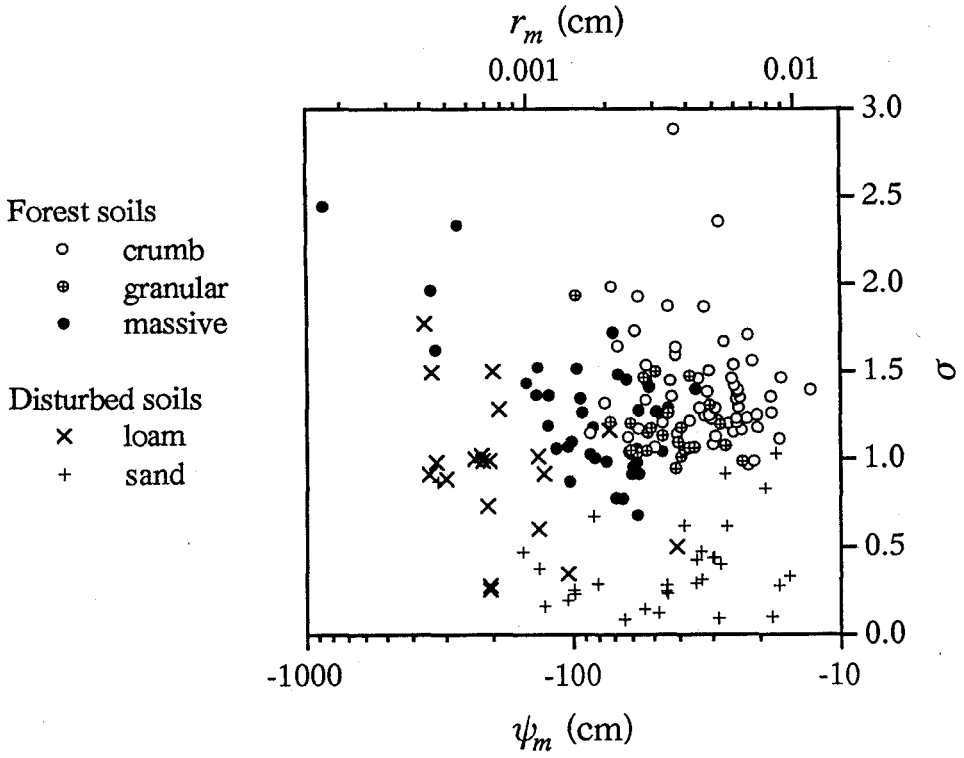

Figure 8.9 Relationship between ψ_m and σ estimated for the undisturbed forest soils (circles), and for the disturbed loamy and sandy soils (crosses and pluses). Each plot symbol represents the soil structure for the forest soils. Figure shows the same plots shown in Figure 5.3. Value of r_m is related to ψ_m by (3.2).

great as σ increases. When ψ_m is small, $D(-0.75L)$ becomes small as σ increases. This critical ψ_m value increases as L decreases.

As shown in the previous subsection, there is a positive correlation between $D(-0.75L)$ and the absolute value of the slope of the recession hydrograph. Consequently, Figures 8.8a through 8.8d can be used to evaluate the effect of parameters ψ_m and σ on the recession hydrograph. Parameter ψ_m is directly related to the median of the pore radius distribution $g(r)$ by the capillary pressure function, and σ represents the width of $g(r)$. Figure 8.8 clearly shows that the recession hydrograph in the vertical drainage process in surface soil becomes gradual as the median of $g(r)$ becomes great. For the surface soil with a relatively large median of $g(r)$, the recession hydrograph becomes steep as the width of $g(r)$ becomes great. When the median of $g(r)$ of the surface soil is relatively small, the hydrograph has more gradual decreases in recession flow as the

width of $g(r)$ becomes great. This critical value of the median of $g(r)$ increases as the length of surface soil becomes small.

Figure 8.9 shows the relationship between ψ_m and σ obtained for the undisturbed forest soils and the disturbed loamy and sandy soils (the same plots shown in Figure 5.3). Value of r_m (that is, the median of $g(r)$) is also shown in the figure. Values of ψ_m for the forest soils are greater than those for the disturbed loamy soils. Figure 8.8 indicates that the forest soil hydrograph has smaller decreases in recession flow than the loamy soil hydrograph. That is, forest soil yields greater amount of recession flow in the vertical drainage process in surface soil, and is more effective to increase baseflow than loamy soil. Values of ψ_m for most of the forest soils and the disturbed sandy soils are in the range of -100 to -20 cm, while σ values for the former are greater than those for the latter (see Figure 8.9). Figure 8.8a shows that the sandy soil hydrograph has smaller decreases in recession flow than the forest soil hydrograph when the surface soil length is 150 cm. Figure 8.8d indicates that forest soil yields greater amount of recession flow than sandy soil when the surface soil length is 25 cm.

As shown in Figure 8.9, many crumb-structure forest soils have greater ψ_m values than the granular-structure forest soils, and ψ_m values for massive forest soils are smaller than those for the crumb and granular-structure soils. That is, the hydrograph from crumb-structure soil generally has smaller decreases in recession flow than that from granular-structure soil. The recession hydrograph from massive soil is steeper than the recession hydrographs from crumb and granular-structure soils. It was shown in Chapter 5 that the process of the change of the soil pore radius distribution affected by the forest ecosystem can be regarded as the increasing process of the median of the distribution. Hence, it can be concluded that the well-developed forest soil, which has the greatest median of the pore radius distribution, produces the greatest amount of recession flow in the vertical drainage process in surface soil, and is most effective to increase baseflow from forestal hillslope.

8.5 SUMMARY AND CONCLUSIONS

In this chapter, one-dimensional, vertical flow equation for soil water (the Richards' equation) was solved numerically by using a Crank-Nicholson finite different scheme. The combined water-retention-hydraulic-conductivity model developed in Chapter 7 (the C-LN2 model) was applied to clarify the effect of soil pore radius distribution on the phenomena of water discharge from forestal hillslope.

The discharge phenomena from forestal hillslope can be regarded as the combination of two different processes: the vertical drainage process in surface soil and the downslope drainage process in subsurface soil. The hydrograph in the vertical drainage process is regarded as an input for the downslope drainage process. Hence, the vertical drainage process in surface soil, as well as the downslope drainage process in subsurface soil, is

important to analyze the hydrograph from forestal hillslope. Because the changes of soil pore radius distribution and hydraulic properties affected by forest ecosystem (forest plants and animals) are more significant in the surface soil than in the subsurface soil, the effect of the soil pore radius distribution on the vertical drainage process in surface soil was discussed in this chapter.

The vertical drainage process in surface soil was simulated by using observed rainfall data as inputs for the water flux at the soil surface and assuming the constant water table at the bottom of soil profile. Results showed that the increase in the vertical soil length makes the slope of the recession hydrograph gradual. Under the same soil length condition, the recession hydrograph becomes gradual as the median of the soil pore radius distribution $g(r)$ becomes great. For the surface soil with a relatively large median of $g(r)$, the recession hydrograph becomes steep as the width of $g(r)$ becomes great. When the median of $g(r)$ of the surface soil is relatively small, the hydrograph has more gradual decreases in recession flow as the width of $g(r)$ becomes great. This critical value of the median of $g(r)$ increases as the length of surface soil becomes small. The relationship between the soil pore radius distribution and the recession hydrograph was evaluated based on the analytical solution of the one-dimensional vertical flow equation. The result was that, in the vertical drainage process in the surface soil of length L, the soil water diffusivity at the capillary pressure value of $-0.75 \times L$ (that is, $D(-0.75L)$) can be used as an index of the slope of the recession hydrograph: the absolute value of the slope of the recession hydrograph becomes smaller as $D(-0.75L)$ value for the soil becomes smaller.

As shown in Chapter 5, the median of $g(r)$ for forest soil is greater than that for disturbed loamy soil. It was concluded that forest soil yields greater amount of recession flow in the vertical drainage process in surface soil than loamy soil. The width of $g(r)$ for forest soil is greater than that for disturbed sandy soil. Consequently, the sandy soil hydrograph has smaller decreases in recession flow than the forest soil hydrograph when the surface soil length is relatively large (about 150 cm). Forest soil yields greater amount of recession flow than sandy soil when the surface soil length is relatively short (about 25 cm). Crumb-structure forest soil has the greater median of $g(r)$ than the granular-structure forest soil, and the median of $g(r)$ for massive forest soil is smaller than those for crumb and granular-structure soils. That is, the hydrograph from crumb-structure soil has smaller decreases in recession flow than that from granular-structure soil. The recession hydrograph from massive soil is steeper than the recession hydrographs from the crumb and granular-structure soils.

In Chapter 5, it was shown that the process of the change of the soil pore radius distribution affected by the forest ecosystem can be regarded as the increasing process of the median of the distribution. As shown in Chapter 7, the saturated hydraulic conductivity becomes larger as the median of the soil pore radius distribution becomes greater. The large saturated hydraulic conductivity of soil decreases surface flow and increases the amount of water which infiltrates into the soil profile. Moreover, it was

shown in this chapter that the soil profile with a greater median of the pore radius distribution yields greater amount of recession flow in the vertical drainage process in surface soil. As a result, the well-developed forest soil, which has a great median of the pore radius distribution, is most effective as the surface soil to increase baseflow from forestal hillslope.

REFERENCES

Arimitsu, K., M. Araki, K. Miyakawa, S. Kobayashi, and M. Kato, Water holding capacities estimated by soil pore capacities of Takaragawa Experiment Station: Comparison of No. 1 and No. 2 experimental watersheds (in Japanese with English summary), *Jpn. J. For. Environment, 37*, 49-58, 1995.

Brooks, R. H., and A. T. Corey, Hydraulic properties of porous media, *Hydrol. Pap. 3*, Civil Eng. Dept., Colo. State Univ., Fort Collins, 1964.

Fujioka, Y., and T. Kitamura, Approximate solution of a vertical drainage problem, *J. Geophys. Res., 69*, 5249-5255, 1964.

Gardner, W. R., Approximate solution of a non-steady-state drainage problem, *Soil Sci. Soc. Am. Proc., 26*, 129-132, 1962.

Hino, M., T. Ohta, K. Sunada, and K. Watanabe, *Numerical Forecast of Floods: A First Step* (in Japanese), Morikita, Tokyo, Japan, 1989.

Kato, M., and I. Hotta, Estimation of the water holding capacity of the catchments by the runoff analysis (in Japanese with English summary), *Jpn. J. For. Environment, 37*, 77-88, 1995.

Kirkby, M. J., *Hillslope Hydrology*, John Wiley, New York, 1978.

Klute, A., and D. F. Heermann, Soil water profile development under a periodic boundary condition, *Soil Sci., 117*, 265-271, 1974.

Kubota, J., Y. Fukushima, and M. Suzuki, Observation and modeling of the runoff process on a hillslope (in Japanese with English Summary), *J. Jpn. For. Soc., 69*, 258-269, 1987.

Kutílek, M., and D. R. Nielsen, *Soil Hydrology*, Catena Verlag, Cremlingen, Germany, 1994.

Leibenzon, L. S., *Flow of Natural Liquids and Gases in Porous Medium* (in Russian), Gostekhizdat, Moscow, 1947.

Ohta, T., Y. Fukushima, and M. Suzuki, Research on runoff from hillsides by one-dimensional transient saturated-unsaturated flow (in Japanese with English Summary), *J. Jpn. For. Soc., 65*, 125-134, 1983.

Ohte, N., *Studies on Pore Structure and Hydraulic Properties of Forest Soils* (in Japanese*), A doctor thesis, Kyoto Univ., 1992.

Sammori, T., and Y. Tsuboyama, Study on method of slope stability considering infiltration phenomenon (in Japanese with English Summary), *J. Jpn. Soc. Erosion Control Eng., 43*(4), 14-21, 1990.

Seguchi, M., K. Tanaka, and S. Shikasho, Baseflow recession curve of small mountain river and its physical significances (in Japanese with English summary), *Trans. JSIDRE, 97*, 1-8, 1982.

Shiozawa, S., and M. Nakano, The mechanism of groundwater recharge as drainage process of unsaturated zone (in Japanese with English summary), *Trans. JSIDRE, 92*, 35-42, 1981.

Suzuki, M., The properties of a base-flow recession on small mountainous watersheds, I, Numerical analysis using the saturated-unsaturated flow model (in Japanese with English

summary), *J. Jpn. For. Soc.*, *66*, 174-182, 1984.

Swartzendruber, D., The flow of water in unsaturated soils, in *Flow through Porous Media*, edited by R. J. M. De Wiest, 215-292, Academic Press, New York, 1969.

Takeshita, K., Some considerations on the relation between forest soil and control function to river discharge (in Japanese), *Jpn. J. For. Environment*, *27*(2), 19-26, 1985.

Tani, M., The properties of a water-table rise produced by a one-dimensional, vertical, unsaturated flow (in Japanese with English summary), *J. Jpn. For. Soc.*, *64*, 409-418, 1982.

Tani, M., Analysis of one-dimensional, vertical, unsaturated flow in consideration of runoff properties of a mountainous watershed (in Japanese with English summary), *J. Jpn. For. Soc.*, *67*, 449-460, 1985.

Tsuboyama, Y., and T. Sammori, Numerical simulation of seepage in a forested hillslope by finite element method (in Japanese with English Summary), *J. Jpn. Soc. Hydrol. Water Resour.*, *2*(2), 49-56, 1989.

Tsukamoto, Y., *Forest Hydrology* (in Japanese*), Buneido, Tokyo, Japan, 1992.

van Genuchten, M. Th., A closed-form equation for predicting the hydraulic conductivity of unsaturated soils, *Soil Sci. Soc. Am. J.*, *44*(5), 892-898, 1980.

* The title is tentative translation from the original Japanese title by the author of this thesis.

CHAPTER 9

CONCLUSIONS

Forestal hillslope is covered with forest soils which have peculiar pore radius distribution and hydraulic properties. Unsaturated water flow in forest soils plays a significant role in the water circulation process in forestal watersheds. The hydraulic properties of unsaturated soil are represented by the relationship between the volumetric water content θ and the soil capillary pressure ψ (the water retention characteristic) and the relationship between the hydraulic conductivity K and ψ. Both relationships are closely related to the soil pore radius distribution. The objectives of this study were (a) to propose for soil water retention a general model which performs as well as any existing empirical model and which was developed by applying a distribution law available in general probability theory, (b) to derive a model for hydraulic conductivity from the proposed retention model, (c) to characterize the pore radius distribution and hydraulic properties of forest soils by application of the proposed models, and (d) to evaluate the effects of the pore radius distribution of forest soil on the water movement phenomena on forestal hillslope.

Chapter 2 summarized three water retention models, all of which have been used widely by soil scientists and hydrologists. According to the model suggested by *Brooks and Corey* [1964] (the BC model), the effective saturation S_e is expressed as a power function with respect to the capillary pressure. *Van Genuchten*'s [1980] model (the VG model) was transformed to include the capillary pressure at the inflection point on the θ-ψ curve. The retention model suggested by *Tani* [1982] was modified to include the bubbling pressure. The derived model was referred to as the TA model. By comparison of the parameters of the three water retention models, it was shown that the VG, BC, and TA models all have two parameters other than the saturated and residual water contents. The VG model does not use the bubbling pressure, the BC model does not use the capillary pressure at the inflection point, and the TA model does not use a dimensionless parameter which is related to the width of the pore radius distribution. Three different analytical expressions for the hydraulic conductivity, which were derived by combining the VG, BC, and TA models with *Mualem*'s [1976] model for predicting the hydraulic conductivity, were reviewed.

In Chapter 3, the water capacity function was regarded as the pore capillary pressure

distribution function $f(\psi)$, which is related to the pore radius distribution function $g(r)$ (where r is the pore radius) by the capillary pressure function. By application of a three-parameter lognormal distribution to $g(r)$, an expression for $f(\psi)$ which has an alternative three-parameter lognormal distribution form was obtained. A new expression for soil water retention (the LN model) was then derived which contains three parameters. These three parameters are the bubbling pressure ψ_c, the mode (ψ_0) of $f(\psi)$ (identical to the capillary pressure at the inflection point on the θ-ψ curve), and the standard deviation σ (dimensionless, $\sigma > 0$) of transformed $f(\psi)$, which describes the effective saturation S_e at the inflection point and is related to the width of the pore radius distribution.

The accuracies of the LN model as well as the VG, BC, and TA models were tested for 50 sets of observed retention data for various soils. Results showed the LN model to be very flexible. By comparing the estimated parameters of the LN model with those of the existing models, it was shown that the VG model is analogous to the LN model under the restriction $\psi_c = 0$, the BC model is similar to the LN model when $\psi_c \rightarrow \psi_0$, and the TA model is analogous to the LN model when σ is restricted to $\sigma \approx 0.62$. As a result, it was concluded that the three parameters corresponding to ψ_c, ψ_0, and σ must be included in a general retention model.

In Chapter 4, retention data sets of 24 forest soils, 16 undeveloped field soils, 20 disturbed loamy soils, and 40 disturbed sandy soils were analyzed using the LN model. Results showed that the LN model produces acceptable matches for retention data sets of the forest soils and the undeveloped field soils as well as for data sets of the disturbed loamy and sandy soils.

Using the average values of the estimated parameters, typical θ-ψ curves of forest soil, loamy soil, and sandy soil were generated. The typical θ-ψ curve of forest soil has a rather narrow air entry region. Because of large ψ_0 and σ values, the inflection point on the θ-ψ curve is close to the end of the air entry region. As a result, the typical θ-ψ curve of forest soil has rapid decreases in θ when $\psi > -30$ cm. The typical θ-ψ curve of loamy soil has a wide air entry region and a gradual decrease in θ at the inflection point. The typical θ-ψ curve of sandy soil has more rapid decreases in θ around the inflection point than the typical θ-ψ curve of loamy soil. The θ-ψ curves of five types of forest soils resemble each other, whereas the θ-ψ curves of three types of undeveloped field soils were different from each other.

By using parameters of the LN model, the standard deviation σ_ψ and the median ψ_m of the pore capillary pressure distribution function $f(\psi)$ were computed for each retention data set. Parameter σ_ψ represents the width of $f(\psi)$ and ψ_m is related to the median of the pore radius distribution. Results showed that the forest soils have larger $f(\psi)$ widths than the sandy soils and have greater ψ_m values (that is, medians of the pore radius distribution are greater) than the loamy soils. The undeveloped field soils have smaller ψ_m values than the forest soils.

In Chapter 5, the LN model was modified to have a relatively simple functional form. The resulting water retention model (the LN2 model) contains two parameters ψ_m and σ both of which have physical significance on the θ-ψ curve and are related directly to the statistics of the soil pore radius distribution $g(r)$. Parameter ψ_m is the capillary pressure when the effective saturation S_e is equal to 0.5. The pore radius r_m, which is related to ψ_m by the capillary pressure function, is identical to the median and the geometric mean of $g(r)$. Dimensionless parameter σ determines the effective saturation at the inflection point on the θ-ψ curve and describes the slope of the curve. Value of σ is equal to the standard deviation of the distribution of $\ln(r)$, and related to the width of $g(r)$.

The observed retention data sets of 282 undisturbed forest soils were analyzed using the LN2 model, and it was shown that the model performs fairly well for every retention data set. Using the estimated parameters ψ_m and σ, the effects of forest soil structure, texture, type, and horizon on the soil pore radius distribution and the soil moisture characteristic were analyzed. Results showed that many crumb-structure soils have greater median of $g(r)$ than the granular-structure soils, and the width of $g(r)$ for many crumb-structure soils are greater than those for the granular-structure soils. The massive soils have smaller median of $g(r)$ than the crumb and granular-structure soils. The disturbed loamy soils have smaller median of $g(r)$ than many of the forest soils and the disturbed sandy soils have smaller $g(r)$ width than the forest soils. It was concluded that the water retention characteristics of the undisturbed forest soils are related to the soil structure more closely than to the soil texture. The process of the change of $g(r)$ affected by the forest ecosystem (forest plants and animals) can be regarded as the increasing process of the median of the distribution. The brawn forest soils taken from A-horizon generally have the greater median of $g(r)$ than the brown forest soils taken from B-horizon. Some of the brown forest soils have the greater width of $g(r)$ than the black soils. The median of $g(r)$ of brown forest soil taken from A-horizon generally becomes greater as the soil moisture condition becomes wet.

Chapter 6 proposed soil pore ratios α, β, and γ based on the widely used soil pore classification systems. Here, α, β, and γ represent ratios of the fine capillary porosity, coarse capillary porosity, and non-capillary porosity to the effective porosity, respectively. The parameters ψ_m and σ of the LN2 model were correlated with the pore ratios α, β, and γ.

Most of the crumb and granular-structure forest soils have the non-capillary pore ratio γ greater than 0.4 and the coarse capillary pore ratio β smaller than 0.5. Values of γ estimated for the massive forest soils are smaller than 0.6, and those for the disturbed loamy soils are smaller than 0.25. Values of fine capillary pore ratio α estimated for the disturbed sandy soils were nearly equal to zero. As a result, it was concluded that the triangle diagram representing the soil pore ratios α, β, and γ is effectively used to evaluate the soil pore radius distribution. A coordinate system with ψ_m on the abscissa and σ on the ordinate, which represents the constant α, β, and γ lines, was proposed as

the new diagram to evaluate the soil pore radius distribution in connection with the soil water retention characteristic.

The method was suggested to estimate ψ_m and σ from measured soil pore ratios by using the statistical table which shows percentage points of the normal distribution. The simple means to estimate the parameters of the LN2 model from a small number of measured (θ, ψ) points were also proposed.

In Chapter 7, the LN2 model was combined with *Mualem*'s [1976] model for the purpose of deriving an analytical expression for the relative hydraulic conductivity K_r which is defined as the ratio of the unsaturated hydraulic conductivity to the saturated hydraulic conductivity. The accuracy of the resulting combined water-retention-hydraulic-conductivity model (the C-LN2 model) was verified for observed data sets for five soils. Results showed that the C-LN2 model produces adequate predictions of relative hydraulic conductivities.

Observed values of the saturated hydraulic conductivity K_s of the forest soils were correlated with the soil pore radius distributions using both the coordinate system with ψ_m on the abscissa and σ on the ordinate, and the triangle diagram showing the soil pore ratios α, β, and γ. Results showed that K_s is higher for the soil with a greater median of the pore radius distribution. There was the trend that the soil with a greater width of the pore radius distribution has a higher K_s value under the same median condition. Value of K_s increases as the non-capillary pore ratio γ becomes greater and as the coarse capillary pore ratio β becomes smaller. Analytical curves derived from *Mualem*'s [1976] model generally succeeded to reproduce the relationship between K_s and the parameters ψ_m and σ, and the relationship between K_s and the ratios α, β, and γ.

By combining the functional relationship between K_s and the parameters ψ_m and σ with the model for K_r, expressions of the hydraulic conductivity K with respect to S_e and with respect to ψ were developed. The derived model for the K-ψ curve succeeded to reproduce observed K-ψ curves of undisturbed forest soils. As a result, the soil hydraulic conductivity as well as the soil water retention curve was characterized by the two parameters ψ_m and σ by application of the C-LN2 model.

In Chapter 8, one-dimensional, vertical flow equation for soil water was solved numerically. The C-LN2 model was applied to clarify the effect of the pore radius distribution of forest soil on the vertical drainage process in surface soil.

Results showed that the increase in the vertical soil length makes the slope of the recession hydrograph gradual. Under the same soil length condition, the recession hydrograph becomes gradual as the median of the soil pore radius distribution $g(r)$ becomes great. For the surface soil with a relatively large median of $g(r)$, the recession hydrograph becomes steep as the width of $g(r)$ becomes great. When the median of $g(r)$ of the surface soil is relatively small, the hydrograph has more gradual decreases in recession flow as the width of $g(r)$ becomes great. This critical value of the median of $g(r)$

increases as the length of surface soil becomes small.

Because the median of $g(r)$ for forest soil is greater than that for disturbed loamy soil, it was concluded that forest soil yields greater amount of recession flow in the vertical drainage process in surface soil than loamy soil. The width of $g(r)$ for forest soil is greater than that for disturbed sandy soil. It was shown that the sandy soil hydrograph has smaller decreases in recession flow than the forest soil hydrograph when the surface soil length is relatively large (about 150 cm). Forest soil yields greater amount of recession flow than sandy soil when the surface soil length is relatively short (about 25 cm). Crumb-structure forest soil has the greater median of $g(r)$ than the granular-structure forest soil, and the median of $g(r)$ for massive forest soil is smaller than those for crumb and granular-structure soils. Consequently, the hydrograph from crumb-structure soil has smaller decreases in recession flow than that from granular-structure soil. The recession hydrograph from massive soil is steeper than the recession hydrographs from the crumb and granular-structure soils.

As shown in Chapter 5, the process of the change of the soil pore radius distribution affected by the forest ecosystem can be regarded as the increasing process of the median of the distribution. The results derived in Chapter 7 indicated that the saturated hydraulic conductivity becomes larger as the median of the soil pore radius distribution becomes greater. The large saturated hydraulic conductivity of soil decreases surface flow and increases the amount of water which infiltrates into the soil profile. Moreover, it was shown in Chapter 8 that the soil profile with a greater median of the pore radius distribution yields greater amount of recession flow in the vertical drainage process in surface soil. As a result, the well-developed forest soil, which has a great median of the pore radius distribution, is most effective as the surface soil to increase baseflow from forestal hillslope.

In summary, this study proposed an expression for soil water retention which performs as well as any existing empirical model by applying a theoretical probability law. The proposed LN model produces acceptable results, and its parameters are closely related to the statistics of the pore capillary pressure distribution function. By application of the C-LN2 model, which was developed by combining the modified LN model (the LN2 model) with *Mualem*'s [1976] model for predicting hydraulic conductivity, soil hydraulic properties are characterized by the two parameters both of which are related directly to the statistics of the soil pore radius distribution. The LN, LN2, and C-LN2 models and their parameters should be analyzed in future research connected to hysteretic phenomena in water retention, spatial variability of soil hydraulic properties, and physical analyses of various types of water movement occur in soils.

REFERENCES

Brooks, R. H., and A. T. Corey, Hydraulic properties of porous media, *Hydrol. Pap. 3*, Civil Eng. Dept., Colo. State Univ., Fort Collins, 1964.

Mualem, Y., A new model for predicting the hydraulic conductivity of unsaturated porous media, *Water Resour. Res.*, *12*(3), 513-522, 1976.

Tani, M., The properties of a water-table rise produced by a one-dimensional, vertical, unsaturated flow (in Japanese with English summary), *J. Jpn. For. Soc.*, *64*, 409-418, 1982.

van Genuchten, M. Th., A closed-form equation for predicting the hydraulic conductivity of unsaturated soils, *Soil Sci. Soc. Am. J.*, *44*(5), 892-898, 1980.

LIST OF SYMBOLS

LOWERCASE ARABIC

a	absolute value of slope of recession hydrograph plotted using a semi-logarithmic scale
a_*	absolute value of slope of dimensionless recession hydrograph plotted using a semi-logarithmic scale
b	constant in (8.16)
b_*	constant in (8.24)
erfc	complementary error function
$f(\psi)$	pore capillary pressure distribution function (identical to water capacity function)
g	acceleration of gravity
$g(r)$	pore radius distribution function
l	exponent in tortuosity factor of the Mualem model
m	dimensionless parameter of the van Genuchten model (= 1 - 1/n)
m_K	dimensionless parameter of the proposed VK model
n	dimensionless parameter of the van Genuchten model (= 1/(1 - m))
pF	common logarithm of $\|\psi\|$
q	vertical soil water flux
q_*	dimensionless vertical soil water flux
q_{out}	water discharge
q_{out*}	dimensionless water discharge
r	soil pore radius (= A/ψ)
r_a	mean of $g(r)$ based on the proposed LN2 model
r_m	median of $g(r)$ based on the proposed LN2 model (= A/ψ_m)
$r_{\max}$	maximum pore radius based on the proposed LN model (= A/ψ_c)
r_{mode}	mode of $g(r)$ based on the proposed LN2 model
r_0	soil pore radius related to ψ_0 by the capillary pressure function (= A/ψ_0)
t	time
t_*	dimensionless time
z	vertical distance taken positive upward
z_*	dimensionless vertical distance taken positive upward

UPPERCASE ARABIC

A constant in the capillary pressure function expressed as (3.2) (= -0.149 cm^2)
B constant in (7.14) (= $10^{0.4}$ cm^3/sec)
B' constant in (7.14) (= 114 $cm^{-1}sec^{-1}$)
C soil water capacity
C_* dimensionless soil water capacity (= $C(-\psi_m)/(\theta_s - \theta_r)$)
D soil water diffusivity
D_* dimensionless soil water diffusivity (= $D(\theta_s - \theta_r)/K_s(-\psi_m)$)
D_a mean soil water diffusivity
D_{a*} dimensionless mean soil water diffusivity (= $D_a(\theta_s - \theta_r)/K_s(-\psi_m)$)
K unsaturated soil hydraulic conductivity
K_r relative hydraulic conductivity (= K/K_s)
K_s saturated soil hydraulic conductivity
L vertical soil length
Q complementary normal distribution function
S_e effective saturation (= $(\theta - \theta_r)/(\theta_s - \theta_r)$)

LOWERCASE GREEK

α fine capillary pore ratio expressed as (6.1)
α_V parameter of the van Genuchten model
β coarse capillary pore ratio expressed as (6.2)
β_c contact angle
γ non-capillary pore ratio expressed as (6.3)
γ_w surface tension between water and air
ζ ratio of ψ_c to ψ_0
η constant to relate soil water diffusivity to mean soil water diffusivity
θ volumetric soil water content
$\theta_{pF1.8}$ volumetric soil water content at pF 1.8
$\theta_{pF2.7}$ volumetric soil water content at pF 2.7
θ_r residual soil water content
θ_s saturated soil water content
λ dimensionless parameter of the Brooks and Corey model
μ mean of transformed $g(r)$ based on the proposed LN model
ξ ratio of $-\psi_m$ to L
ϱ_w density of water
σ dimensionless parameter of the proposed LN and LN2 models
σ_ψ standard deviation of $f(\psi)$ based on the proposed LN model
ψ soil capillary pressure

ψ^* ratio of ψ to ψ_0

ψ_* dimensionless soil capillary pressure (= $-\psi/\psi_m$)

ψ_a mean of $f(\psi)$ based on the proposed LN model

ψ_{aB} mean of $f(\psi)$ based on the Brooks and Corey model

ψ_c bubbling pressure of the proposed LN model

ψ_{cB} bubbling pressure of the Brooks and Corey model

ψ_{cK} bubbling pressure of the proposed VK model

ψ_{cT} bubbling pressure of the modified Tani model

ψ_m median of $f(\psi)$ based on the proposed LN and LN2 models (identical to capillary pressure at $S_e = 0.5$)

ψ_{mB} median of $f(\psi)$ based on the Brooks and Corey model (identical to capillary pressure at $S_e = 0.5$)

ψ_{mV} median of $f(\psi)$ based on the van Genuchten model (identical to capillary pressure at $S_e = 0.5$)

ψ_0 mode of $f(\psi)$ based on the proposed LN and LN2 models (identical to capillary pressure at inflection point on θ-ψ curve)

ψ_{0K} mode of $f(\psi)$ based on the proposed VK model (identical to capillary pressure at inflection point on θ-ψ curve)

ψ_{0T} mode of $f(\psi)$ based on the modified Tani model (identical to capillary pressure at inflection point on θ-ψ curve)

ψ_{0V} mode of $f(\psi)$ based on the van Genuchten model (identical to capillary pressure at inflection point on θ-ψ curve)